Spring 2013

Effects of machining parameters and cooling strategies on cutting forces and surface integrity in high-speed slot end-milling of titanium alloy

Emenike Chukwuma

Department:

EFFECTS OF MACHINING PARAMETERS AND COOLING STRATEGIES ON CUTTING FORCES AND SURFACE INTEGRITY IN HIGH-SPEED SLOT END-MILLING OF TITANIUM ALLOY

by

EMENIKE NICK CHUKWUMA

A Thesis

PRESENTED TO THE FACULTY OF THE GRADUATE SCHOOL OF

Missouri University of Science and Technology

In Partial Fulfillment of the Requirements for the Degree

MASTER OF SCIENCE IN MECHANICAL ENGINEERING

2013

Approved by

A.C. Okafor, Advisor

K. Chandrashekhara

D. Grow

PUBLICATION THESIS OPTION

This thesis has been prepared in the publication option format as two separate papers for publication. Paper 1, comprising pages 3 through 82, is to be submitted for publication in the *International Journal of Machine Tools and Manufacture,* under the title, "Effects of Machining Parameters and Cooling Strategies on Cutting Forces, Cutting Temperature, and Tool Wear in High-Speed End-Milling of Titanium Alloy Ti-6Al-4V." Paper 2, comprising pages 83 through 147, is to be submitted for publication in the *Journal of Materials Processing Technology*, under the title, "Effects of Machining Parameters, MQL, and LN_2 Cooling Strategies on Surface Roughness and Residual Stresses in High-Speed Slot End-Milling of Titanium Alloy Ti-6Al-4V."

ABSTRACT

Paper 1 presents the results of the investigations of the effects of cooling strategies [Emulsion cooling, Minimum Quantity Lubrication (MQL) and Liquid Nitrogen (LN_2)] and machining parameters (feed rate and spindle speed) on cutting force components, cutting temperature and tool wear during slot end-milling of titanium Ti-6Al-4V workpiece. All machining experiments were conducted using four-flute 0.5 inch diameter uncoated solid carbide end-mill on Cincinnati Milacron, Sabre 750 vertical machining center equipped with Acramatic 2100 controller. Cutting force components were acquired and tool wear was indirectly measured from maximum cutting force variation per slot from the first pass to the eighth pass. The experimental results show that spindle speed and cooling strategies are the most significant factors that reduce cutting forces and tool wear, while cryogenic cooling, low spindle speed and high feed rate reduce cutting temperature. In paper 2, the results of the investigations on the effects of cooling strategies and machining parameters on surface roughness and residual stresses during slot end-milling of titanium alloy workpiece are presented. From the results obtained, combination of MQL and LN2 (MQL+LN_2) was best in reducing surface roughness both on the web and on the rib. The combination of MQL and LN_2 was the best in producing the most compressive residual stresses on the surface of the left rib while LN_2 cooling strategy alone was the worst with high tensile residual stress on the surface of the left rib.

Keywords: Slot end-milling; Cutting forces; Minimum Quantity Lubrication; cryogenic cooling; Machining parameters; Titanium alloy.

ACKNOWLEDGEMENTS

First I want to express my heartfelt appreciation and indebtedness to my research and academic advisor, Dr. Anthony Chukwujekwu Okafor for his encouragements, understanding, contributions, financial and moral support, and fatherly advice before and during my pursuit of this MS degree program. I would also like to thank Dr. K Chandrashekhara and Dr. David Grow for considering it worthwhile to serve as members of my thesis committee.

I wish to use this medium to thank my dad of blessed memory for always believing in me and motivating me till the last hour. I also wish to specially recognize the role played by my mom (Apo Chukwuma JP), siblings (Onyeka, Engr. Arize, Surv. Ndubuisi, and Chinelo) and friends (Ozgur Kilicay and Hilary Onyishi) in this MS pursuit, their words of wisdom and encouragement were priceless.

May I furthermore thank ITW Rocol for loaning us an Acculube MQL box applicator, Mitchell Cottrell, Lewis Randall, Bob Hribar and all the guys in the workshop for all their technical support and willingness to assist during the course of this research.

Finally, the financial assistance provided to me in the form of Graduate Research Assistantship by my Advisor, Dr. A. C. Okafor through his grants from the National Science Foundation, and the Graduate Teaching Assistantship from the Department of Mechanical and Aerospace Engineering are gratefully acknowledged.

TABLE OF CONTENTS

Page

LIST OF ILLUSTRATIONS

Figure

PAPER I Page

LIST OF TABLES

1. INTRODUCTION

Titanium alloy (Ti-6Al-4V) is an attractive material in aerospace and defense manufacturing industries, as well as in automotive and biomedical industries, due to its excellent combination of high strength-to-weight ratio maintained at high temperature, as well as its outstanding resistance to corrosion and fracture. They are classified as difficult-to-cut materials due to their low thermal conductivity, low modulus of elasticity, and high chemical reactivity. The applications of titanium are mainly in jet engines/airframe components, and pipelines that are subject to high temperature and pressure respectively. With the fast improvement in today's high-speed milling industry, particularly in the aerospace industries, the cutting forces generated during part machining, the surface roughness of the machined parts and residual stress analyses are very important in evaluating tool life and overall parts quality. The adoption of the end milling process in manufacturing is because of its versatility and efficiency and also because it may be used for the rough and finish machining of such features as slots, pockets, peripheries, and faces of components. Increase in cutting forces, cutter breakage, generation of finished part surface which does not conform to product design specifications and process instability are some of the problems which may arise from end milling process. It may result to shank or tool breakage if the level of cutting force applied is in excess. The stability of the end milling process is also dependent on the cutting force system and its interaction with the dynamics of the machining system.

However, it could be worse with the machining of titanium and its alloys because of several inherent properties of the material. Much greater metal removal rates at reduced cutting forces and increased spindle speed are possible with good combination of

cutting tool materials, wedge geometry, tool coating, machining parameters, cooling, lubrication and milling strategies. Titanium is very chemically reactive therefore has the tendency of welding to the cutting tool during machining thus, leading to premature tool failure. Its low thermal conductivity increases the temperature at the tool-work interface thus, affecting the tool life adversely.

In CNC industrial machining process, milling is a basic machining operation with end-milling as the most commonly used metal removal operation process encountered. Because of its wide use in machining delicate to machine parts, such as found in aerospace and automotive sectors, the quality cannot be over-emphasized. Surface roughness plays a very important role in functional attributes of parts such as; reduction of surface friction, wearing, light reflection, heat transmission, ability to distribute and hold lubricants, coating and resistance to fatigue. Residual stresses also play important roles in the performance of machined components in engineering applications. Cutting force is proportional to residual stresses; therefore, their effects in metals and alloys include but not limited to tool life, surface finish, fatigue life, corrosion resistance, and part distortion. The performance of machined components can be enhanced or impaired by cutting forces and residual stresses. Because of this, understanding the cutting forces and residual stress imparted by machining is essential in understanding machining and general part quality.

PAPER

I. EFFECTS OF COOLING STRATEGIES AND MACHINING PARAMETERS ON CUTTING FORCES, CUTTING TEMPERATURE, AND TOOL WEAR IN END-MILLING OF TI-6AL-4V USING DESIGN OF EXPERIMENT

A. Chukwujekwu Okafor and Emenike Chukwuma
Laboratory for Industrial Automation and Flexible Manufacturing
Department of Mechanical and Aerospace Engineering
Missouri University of Science and Technology
327 Toomey Hall, 1870 Miner Circle, Rolla, MO 65409-0050, USA
E-mails: okafor@mst.edu, encwdf@mst.edu

ABSTRACT

This paper presents the results of experimental investigation of the effects of cooling strategies (Emulsion, Minimum Quantity Lubrication (MQL), and cryogenic cooling-Liquid Nitrogen (LN2)), spindle speed and feed rate on cutting forces (F_x, F_y and F_z), cutting temperature, and tool wear in slot end-milling of Titanium alloy Ti-6Al-4V using design of experiment and analysis of variance. A one-third fractional factorial design of experiment was used to study the effects of the three factors at three levels.

End-milling experiments were conducted using four-flute 0.5 inch diameter uncoated solid carbide end-mill on Cincinnati Milacron, Sabre 750 vertical machining center equipped with Acramatic 2100 controller. An ungrounded K-type thermocouple probe of 0.125 inch diameter was inserted into drilled holes in the workpiece to measure the workpiece temperature. A nozzle was designed to regulate the flow and temperature of cryogenic liquid flown to the cutting zone, while an MQL applicator was simultaneously used to supply micro droplets of vegetable oil to the cutting zone for optimum cooling and lubrication at optimum cutting speed and feed rate.

Cutting force components were acquired by a Kistler 9272 4-component force dynamometer on which had the workpiece mounted and screwed tight to avoid the effects of vibrations from experimental process from affecting the values of the acquired forces. Tool wear was indirectly measured from maximum cutting force variation on each slot from the first pass to the eighth pass. Analysis of variance shows that cooling strategy, spindle speed, and feed-rate all have significant effects on cutting force components F_x, F_y and F_z while the interaction effects of cooling strategy and speed has significant effect only on F_x component. Among the three cooling strategies investigated (conventional emulsion, MQL and LN_2, environmentally friendly MQL from vegetable oil was found to be the best lubrication strategy that gave the lowest cutting force followed by LN_2 while emulsion gave the highest cutting force components. Cryogenic cooling by LN_2 was found to be the best cooling strategy for reducing workpiece temperature and improving tool life during slot end-milling of titanium alloy Ti-6Al-4V.

Minimum Quantity Lubrication (MQL), high spindle speed of 2000 rpm, and low feed-rate of 6 ipm are the optimum cooling strategy and machining parameters that gave the lowest cutting force components F_x, F_y and F_z for slot end-milling of Ti-6Al-4V.

Main effects of cooling strategy are the dominant and statistically significant factor on workpiece temperature, followed by main effect of feed-rate. Cryogenic Liquid Nitrogen (LN_2) cooling, low spindle speed of 1000 rpm and high feed rate of 18 ipm are, the optimum cooling strategy and machining parameter that gave the lowest maximum workpiece/cutting temperature. The cutting force component in the feed direction F_y (feed force) is more sensitive to tool wear and increases more rapidly than the other cutting force components F_x and F_z, thus this is recommended to be used for indirect

monitoring of tool wear. Cryogenic Liquid Nitrogen (LN_2) cooling, high spindle speed of 2000 rpm, and low feed rate of 6 ipm are the optimum cooling strategy and machining parameters that gave the lowest tool wear results.

Keywords: Minimum Quantity Lubrication, Cryogenic Machining, end-milling, fractional factorial design of experiment, cutting force components, Titanium alloy Ti-6Al-4V

1. INTRODUCTION/LITERATURE REVIEW

Titanium alloy (Ti-6Al-4V) is an attractive material in aerospace and defense manufacturing industries, as well as in automotive and biomedical industries, due to its excellent combination of high strength-to-weight ratio maintained at high temperature, and their excellent resistance to corrosion and fracture; but they are classified as difficult-to-cut materials due to their low thermal conductivity, low modulus of elasticity, and high chemical reactivity. The applications of titanium are mainly in jet engines/airframe components, and pipelines that are subject to high temperature and pressure respectively. Titanium alloys and nickel-based super alloys, such as Hastelloy C2000 and Inconel 718 are both classified as difficult-to-cut metals but widely used in the industries due to their exceptional corrosion resistance, high strength-to-weight ratio, and ability to retain their mechanical properties under high operating temperatures of over 700^0C [1, 2]. Nickel-chromium-molybdenum alloys are the most versatile nickel alloys as they contain molybdenum which protect against corrosion under reducing conditions, and chromium which resists corrosion under oxidizing conditions [3], but titanium alloy grade 5 (Ti-6Al-4V) is preferred in engineering applications because nickel-based alloys have higher mass-volume ratio. However titanium and nickel alloys are difficult-to-machine materials because of their low thermal conductivity, high work-hardening characteristics, abrasiveness, gumminess and strong tendency to weld to the tool and form a built-up edge, the high heat generated in the cutting zone by friction and cutting forces stays there, and build up to extreme values, and thus softening the cutting tool material [4, 5, 6, 7]. High cutting temperature and machining parameters strongly affect cutting forces, tool wear, tool life, chip formation mechanism and contribute to the thermal deformation of

the cutting tool in machining titanium alloy [8, 9, and 10]. Machining titanium alloys thus require a machine tool that is rigid. Solid carbide tools with positive rake angle and corner radius and effective cooling/lubrication system can guarantee effective machining output.

Currently water-based emulsion cooling is used in industry and it is not effective for machining difficult-to-cut metals, and moreover, it is not environmentally friendly. Based on the review of published literature, not much work has been done to investigate the influence of machining parameters in high speed end-milling of titanium alloy Ti-6Al-4V, and the influence of cooling/lubrication system for improving their machinability. Cryogenic coolant-Liquid Nitrogen (LN_2) and Minimum Quantity Lubrication (MQL) are emerging and environmentally friendly cooling and lubrication strategies with great potential for improving the machinability of difficult-to-cut materials and is investigated in the current research.

Milling is the most versatile cutting process for non-rotational machining process using multi-tooth tools called milling cutters. End-milling is a kind of vertical axis milling with a solid multi-tooth cutter called an endmill and is most commonly used for metal removal process in aerospace and automotive industries for making prismatic and monolithic parts. The reason for its popularity is because it can be used for rough and finish machining of such features as slots, pockets, peripheries and faces of components. Cutter breakage, heat generation, and process instability are the major problems experienced with end-milling process. Application of lubricants and coolants in the cutting processes play very important roles in increasing tool life and dimensional accuracy, reducing cutting temperature, improving surface quality, and reduction in

cutting force/power consumed during machining [11]. It is thus important to use coolants and lubricants in machining operations especially for difficult-to-cut high strength alloys. Conventional water-based emulsion coolants, hereafter referred to as conventional cooling, are more costly, ineffective and create some techno-environmental problems such as, environmental pollution due to chemical dissociation or break up due to high cutting temperature.

Cryogenic machining is considered a viable option to machining with conventional cooling, and for this purpose, liquid nitrogen as a cryogenic coolant has been identified as environmentally sound, best in chip-tool interface temperature reduction, tool wear reduction and tool life improvement, cutting force reduction, and surface integrity improvement [11]. With this method of cooling, there is no need for mist collection and/or filtration, no contaminated workpiece or need for disposal costs, and it supports power saving without all the pumps, fans and drives that go into handling conventional coolant.

MQL systems apply very light spray of an oil/air mixture to the cutting area to lubricate the tool as it cuts. The current study reported in the paper investigated MQL cooling strategy independently and also in combination with LN_2 cooling strategy for high-speed end-milling of titanium Ti-6Al-4V. From experimental runs, it was observed that the heat generated during machining titanium Ti-6Al-4V with MQL strategy burns off much of the oil, leaving a nearly dry part and nearly dry chips. Most researchers focused on the optimization of cutting parameters in conventional cooling conditions with fewer considerations on the effect of different cooling/lubrication strategies.

The current industrial standard for machining titanium, here after referred to as baseline parameters, are spindle speed of 382 rpm (50 fpm) for roughing and spindle speed of 2037 rpm (400 fpm) for finishing using solid carbide. Therefore any speed above this baseline parameter for titanium is regarded as High Speed Machining HSM. HSM is an emerging technology that offers significant potential for fabricating large structural components and hardened materials faster and more accurately, especially for the aerospace industry. It results in greater material removal rates, lower cutting forces, especially when enhanced with an effective cooling and lubrication strategy thus will result in significant improvement in productivity. Much greater metal removal rates are possible with good combination of cutting tool materials, wedge geometry, tool coating, machining parameters, cooling, lubrication and milling strategies [12]. However a lot of HSM and cooling issues are not well understood by airframe and automotive manufacturers. Tool life models were developed using small central composite design (CCD) for the optimization of cutting speed, axial depth of cut and feed rate. Flank wear was considered as the criterion for tool failure and it was reported that cutting speed has the most significant effects on tool life while feed has the most significant effect on surface roughness [13]. Milling force and temperature acquired under different cutting conditions and tool wear status were used to study surface roughness and residual stress on machined parts during endmilling of high strength titanium alloy TA15, and an empirical equation of tool life from multi-element regression analysis was generated. Cutting force component (F_x) perpendicular to the feed direction, F_y, was reported to be fairly larger than the other cutting force components, F_y and F_z and that tool-wear increases with cutting speed and cutting temperature [14]. Adhesion, diffusion,

dissolution, and oxidation were major mechanism of tool wear at high cutting speed, compared with adhesion at lower cutting speed [15]. Cutting force component in the feed direction Fy has a positive correlation with the tool wear propagation, which can be used as a variable to monitor the cutting process [16]. Shane et al [17] passed minimum amount of LN_2 through a dual micro-nozzle to the chip-tool interface at the point of highest temperature to reduce cutting force and eliminate workpiece pre-cooling. They reported improved tool life compared to dry cutting and emulsion cutting. Ke et al. [18] used nitrogen gas at a pressure of 0.7 MPa to inhibit chips burning during high-speed cutting of Ti-6Al-4V they reported high speed flowing of nitrogen gas speeds up the chips leaving the cutting zone and prevents the chips from burning, thereby reducing cutting force and temperature increment of the finished surface to about 5^oC.

Although few studies have investigated the feasibility of MQL and some form of cryogenic cooling, individually, there is no comprehensive and comparative evaluation of the main effects of conventional emulsion cooling, cryogenic cooling, MQL, and machining parameters-feeds and speeds on cutting forces, cutting temperature, and tool wear, and their interaction effects. There is also no comprehensive report as to repeatability of the method of cryogenic application at the cutting zone and also, there is no report on how the cryogenic temperature of LN_2 (-196 degree centigrade) has been controlled to a temperature within the working range of 0 to -15 degree centigrade. Therefore, the main objective of this research is to investigate the main effects and interaction effects of cooling strategies (conventional emulsion cooling, MQL and cryogenic cooling at -15 degree centigrade by LN_2) and machining parameters (cutting speed and feed rate) on cutting force components (F_x, F_y, and F_z), workpiece temperature

and tool wear; and the identification of optimum machining parameters and cooling strategies using fractional factorial design of experiment and analysis of variance (ANOVA). The second objective is to conduct comparative evaluation of MQL, LN_2, and the combination of MQL and LN_2 cooling strategies using the identified optimum machining parameters. The third objective is to reduce cutting forces, cutting temperature, tool wear, residual stresses and surface roughness in slot endmilling using bull-nosed end-mills.

Due to low thermal conductivity of Ti-6Al-4V alloy, high cutting temperature at the tool-chip contact zone are close to the cutting edge, and Ti-6Al-4V alloy has high chemical reactivity with most cutting tool materials at high temperature. Moreover, at high temperature and high contact stresses, the titanium chip maintains a very intimate contact with the tool on the tool rake surface and flank surface through an interfacial layer. Therefore, tool wear in cutting titanium alloys is much more intense due to high temperature and contact stresses at the tool-chip interface [16]. An efficient way to control temperatures when machining titanium is the use of cryogenic cooling; however, it leads to higher cutting forces at very low/cryogenic temperature because of the increased mechanical strength (hardness) of the material at very low temperature [19]. It was reported that in turning Ti-6Al-4V with uncoated solid carbide tools and liquid nitrogen cooling, fivefold tool life could be reached compared to conventional flood cooling [20].

2. THE OVERVIEW OF CURRENT RESEARCH

2.1 CRYOGENIC COOLING (LN_2) AND MINIMUM QUANTITY LUBRICATION STRATEGIES

The overview of current research plan for investigating the effects of cooling/lubrication strategies for high-speed machining of difficult-to-cut metals (nickel alloy, titanium alloy, and Hastelloy) is shown in Figure 1. Conventional emulsion cooling, MQL, Cryogenic cooling (LN_2), and LN_2 + MQL are investigated under varying machining parameters of cutting speed and feed rate using solid carbide end mills.

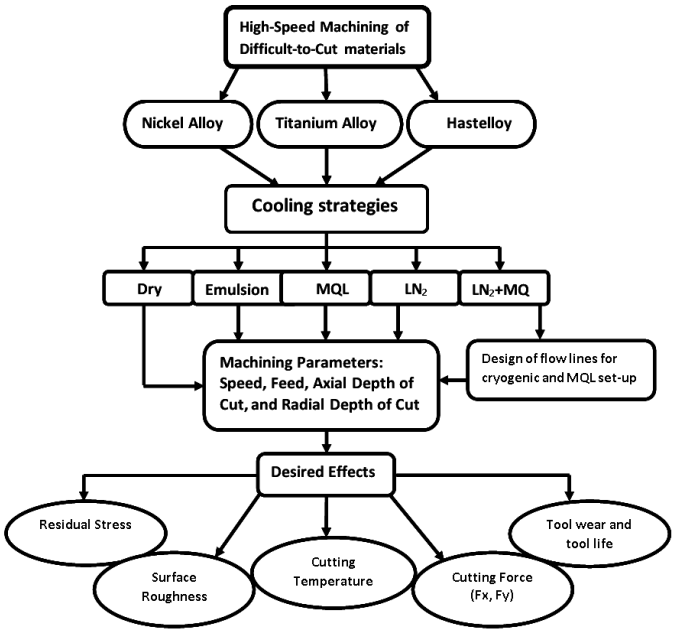

Fig 1. OVERVIEW OF CURRENT RESEARCH PLAN FOR INVESTIGATING THE EFFECTS OF COOLING/LUBRICATION STRATEGIES FOR HIGH-SPEED MACHINING OF DIFFICULT-TO-CUT METALS

2.1.1 DESIGN AND ASSEMBLY OF CRYOGENIC FLOW LINE

This is required to control a super chilled liquid nitrogen (LN_2) temperature of -196^{o}C to a temperature in the range of 0^{o}C to -15^{o}C (cold air). This was done using pipe couplings, valves and flexible cryogenic hose to connect the LN_2 tank to an in-house designed and fabricated nozzle for mixing LN_2 with shop air to supply cold air at a predetermined temperature to the cutting zone; and also mixing this controlled LN_2 with MQL and simultaneously flowing both through their different nozzles to the cutting zone. The pressure of LN2 flowing from the cryogenic (LN_2) cylinder was determined using a pressure gauge, however, this pressure gage measured LN2 pressure indirectly using a 0.25 inch Swagelok pipe fitting which was connected to 0.25 inch Tee and linked up to a 0.25 inch pigtail pipe as shown in Figure 2: Schematic diagram of experimental set-up showing cutting force data acquisition system, cryogenic and MQL flow lines. This design was to prevent the flowing LN2 from getting in contact with the pressure gauge in order not to destroy it. A 1.5 inch outer diameter (OD) and 1.375 inch inner diameter (ID) nozzles with an orifice of 1/16 inch was designed to help increase LN2 temperature from cryogenic temperature value of -196 ^{o}C to -15^{o}C. A 230 psi pressure relief valve was used on the cryogenic flow line to take care of pressure build up due to flow control of liquid nitrogen which expands at a very high rate when it changes from liquid to gas.

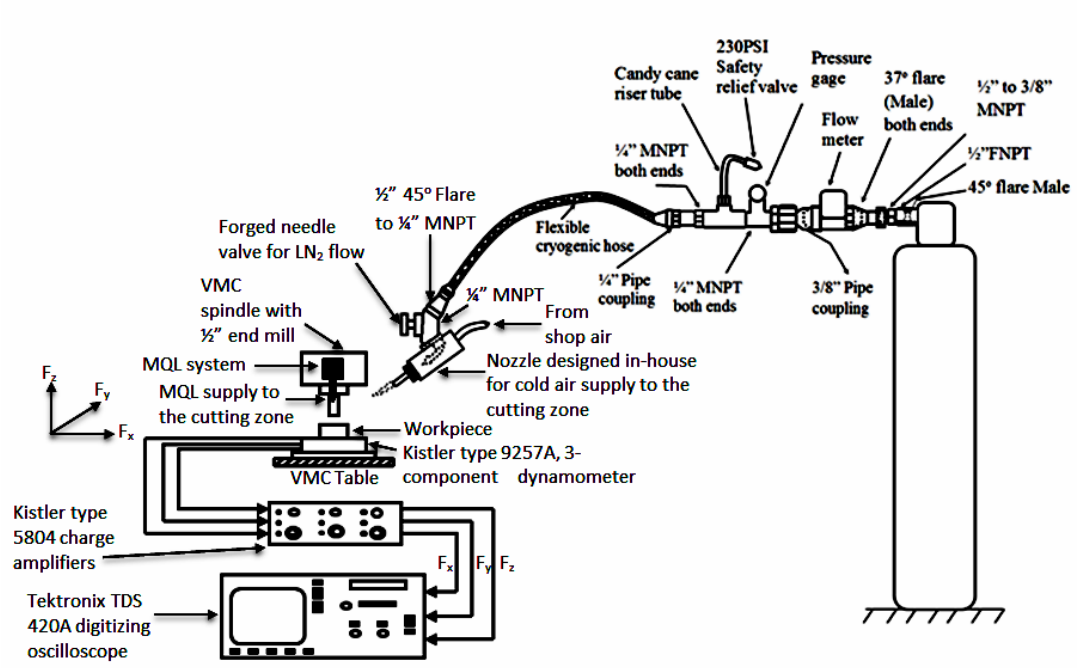

2a.VMC DATA ACQUISITION SYSTEM AND CRYOGENIC FLOW LINE

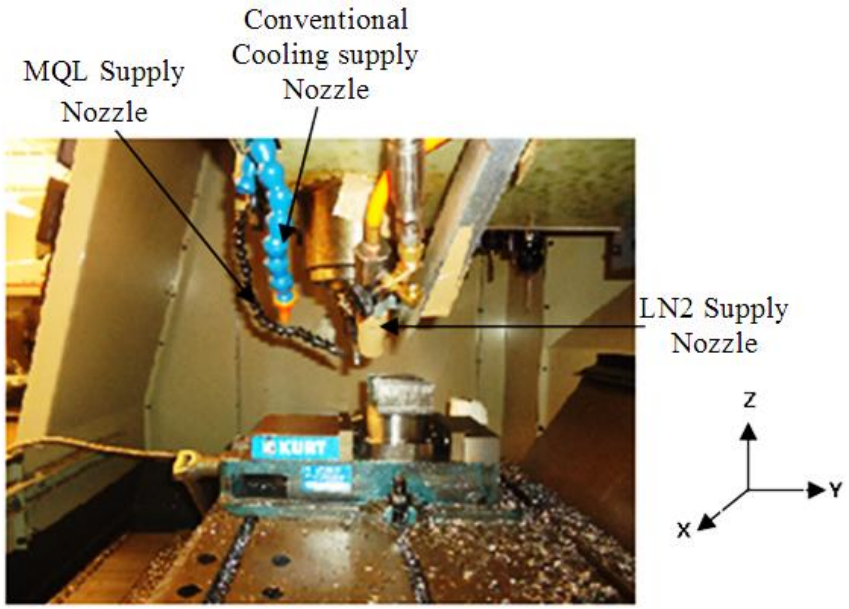

2b. MQL, LN2 AND CONVENTIONAL COOLING SUPPLIED TO THE CUTTING ZONE

Figure 2. SCHEMATIC DIAGRAM OF EXPERIMENTAL SET-UP SHOWING CUTTING FORCE DATA ACQUISITION SYSTEM, CRYOGENIC AND MQL FLOW LINES

2.1.2 CRYOGENIC FLOW LINE CALIBRATION

In an experiment, when two or more variables are related, it is of interest to model the relationship between these variables. In regression analyses, models have both dependent or response variables and independent or regressor variables. The relationship between the dependent and independent variables is called a regression model. Regression analysis is mostly used to analyze data from experiments that might arise from observation of uncontrolled phenomena. Multiple regression analysis is a flexible method of data analysis that may be appropriate whenever the dependent variable is to be examined in correlation to the independent variables in linear or nonlinear relationships. These analyses were conducted at a significance level of 0.05. Below are some of the results from analyzing 1 dependent variable of temperature and 2 independent variables of LN2 pressure and shop air pressure.

The general regression model is given below as:

$$Y = \beta_0 + X_1\beta_1 + X_2\beta_2 + \varepsilon \qquad 1$$

Where Y is the dependent variable (nozzle temperature) and X_1 & X_2 are the LN_2 pressure and air pressure respectively and β_1 and β_2 are the regression coefficients, ε is the error.

Experimental tests were conducted with combination of LN2 and shop air supplied to the cutting zone at varying flow pressure. The flow pressure for shop air and LN2 were independently recorded and STATSTICA^{TM} software from STATSOFT^{R} was used to obtain a regression model used for the calibration of the cryogenic flow line in order to accurately get a -15^{o}C cooling air temperature at the cutting zone. The calibration process was conducted by placing the thermocouple inside the nozzle for cold

air supply housing and taped in place, and flowing liquid nitrogen from the liquid nozzle of the LN_2 cylinder at a pressure of 70 psi for about 15 minutes until the whole length of the flow line is completely chilled up to the point where you can observe the white ice formed on the periphery of the entire length of the flow line, ensuring that Nitrogen in liquid phase is maintained in the line. At this point, LN2 pressure remained steady, then the pressure of LN2 is gradually reduced to 50 psi, and at that point it was still steady even without turning on the shop air pressure. Shop air of 5 psi is gradually added, but the rate at which it takes to attain steady state seemed too slow and may waste a lot of LN_2, so the shop air pressure is increased until the temperature slope/gradient on the computer was approximately zero. The point where the slope was almost zero was at 20 psi shop air, at this point, the temperature measured by the thermocouple probe is recorded. Table 1 shows the cryogenic flow line calibration data. The first nozzle temperature recorded, -10.5 ^{o}C, as described was for the combination of LN2 temperature at 50 psi and shop air temperature at 20 psi. The next nozzle temperature value recorded -20.5^{o} C, as described above was for combination of LN2 temperature at 60 psi and shop air temperature at 27.5 psi, for the next nozzle temperature of -52.5 ^{o} C, the pressure of shop air was kept constant while LN2 pressure was varied. This process continued with the rest of the other nozzle temperature data acquired, keeping LN_2 pressure constant at one point and varying shop air pressure and at another point; varying LN_2 pressure and keeping shop air pressure constant as can be seen from the 5th and 6th data points for constant LN_2 pressure and the 7th and 8th data points. The reason for this approach was that at continuous flow of about an hour of LN_2 flow through the cryogenic flow line at a temperature not low enough to chill the entire length of the flow line, there's fluctuation

of LN_2 pressure in the flow line and the thermocouple temperature recorded from the computer, this makes one always on the watch to monitor the pressure of LN_2 flowing through the line thereby making the process a flaw. It initially was very difficult to set LN_2 pressure at a predetermined value, but success was achieved following the above stated procedure and the flow line was successfully calibrated and used to run the experiments with confidence that it will remain at a set pressure point until it is changed.

Table 1. CRYOGENIC FLOW LINE CALIBRATION DATA

Calibration	LN2	Shop Air	Temperature
1	50	20	-10.5
2	60	27.5	-20.5
3	72.5	27.5	-52.5
4	75	35	-44.3
5	85	35	-56.5
6	85	45	-47.5
7	100	45	-70.5
8	100	50	-64.8

A simple least square model fitting technique was applied to the calibration data of Table 1 using the STATISTICA^{TM} software from STATSOFT^{R}.

Table 2 shows the regression analysis summary for nozzle cold air supply temperature; the embedded table shows an R^2 value of 0.96744821 with a P-level of <0.00019. The P-level which is the probability of obtaining a test statistic at least as extreme as the one that was actually observed when the null hypothesis is true. One often rejects the null hypothesis when the p-value is less than the significance level α which is

0.05 in this case. Since 0.00019 is less than 0.05, the null hypothesis is rejected, the result is therefore said to be statistically significant. From Table 2 it can be seen that the p-level of the intercept, LN2 pressure, and shop air pressure shows that the analysis was statistically significant. The regression model can be seen on the B column where 51.91926 is the intercept of the model, while -1.89403 and 1.42473 are the coefficients of X_1 (LN_2 pressure) and X_2 (shop air pressure) respectively.

Table 2. REGRESSION SUMMARY FOR DEPENDENT VARIABLE: TEMPERATURE, T

N=8	Regression Summary for Dependent Variable: Temperature (Deg C) R= .98358945 R²= .96744821 Adjusted R²= .95442749 F(2,5)=74.301 p<.00019 Std.Error of estimate: 4.4354					
	Beta	Std.Err. of Beta	B	Std.Err. of B	t(5)	p-level
Intercept			51.91926	8.298837	6.25621	0.001530
LN2 Pressure (PSI)	-1.62041	0.230626	-1.89403	0.269570	-7.02610	0.000901
Air Pressure (PSI)	0.71422	0.230626	1.42473	0.460054	3.09688	0.026948

This therefore yields a regression equation as shown in equation 2;

$$T = Y = 51.91926 - 1.89403X_1 + 1.42473\ X_2, \qquad R^2 = 0.96744821 \qquad 2$$

Forward stepwise regression was used in order to have the independent variables of LN2 pressure X_1 and shop air pressure X_2 to be added or removed from the model at 57.16415 and 9.959068 respectively until the best regression was obtained as shown in Table 3. Table 3 is the ANOVA table with the all the sums of squares, mean squares, degrees of freedom, F-ratio and P-level represented. As stated earlier, this regression analysis based on 0.05 significant level shows that the data collected from the calibration test is statistically significant.

Table 3. SUMMARY OF STEPWISE REGRESSION

Variable	Summary of Stepwise Regression; DV: Temperature (Deg C) (Spreadsheet1)						
	Step +in/-out	Multiple R	Multiple R-square	R-square change	F - to entr/rem	p-level	Variables included
LN2 Pressure (PSI)	1	0.951320	0.905009	0.905009	57.16415	0.000278	1
Air Pressure (PSI)	2	0.983589	0.967448	0.062439	9.59068	0.026948	2

The graph in Figure 3a below shows a 3D surface plot for the 3 variables with shop air pressure and LN2 pressure are along the y and x axes respectively while the z axis is the response variable, i.e. temperature in degree centigrade. From the surface plot, it can be seen that as the pressure of LN2 increases with a decrease in shop air pressure, the temperature response decreases, while as the shop air pressure increases and the LN2 pressure decreases the temperature response increases.

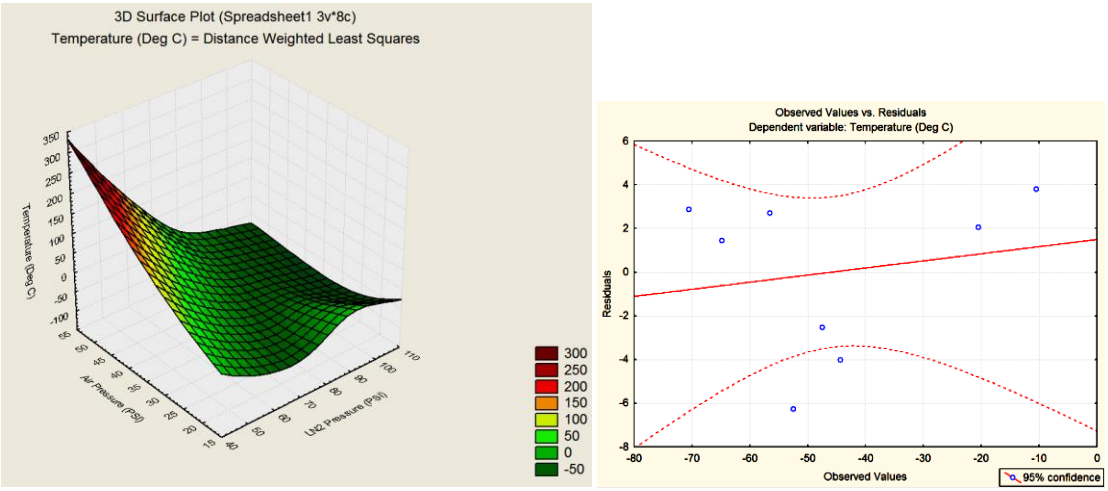

3a. Surface Plot for Nozzle Cold Air Temp 3b Plot of observed values vs residuals

Figure 3. SURFACE PLOT OF RESPONSE VARIABLE-TEMPERATURE VS LN2 AND SHOP AIR PRESSURE

Figure 3b shows the plot of observed values vs residuals which can be used to detect the outliers or group of observations that are consistently over predicted or under predicted which confirms the adequacy of the regression model. It is used to display how

well the entire set of observed values for observation points ties with the solution data. The values of desired output nozzle cold temperature and LN2 pressure were entered in the derived regression equation 2 to generate the values of shop air pressure to be used for the cryogenic slot end-milling experiments as seen in Table 4. This explains the reason why the resolution of the values in the shop air pressure column is very low, up to 8 decimal places.

Table 4. TABLE OF OBTAINED VALUES USING REGRESSION MODEL OF EQUATION 2

Y (temp in Deg C)	**Intercept**	**LN2 (PSI)**	**Shop Air (PSI)**
-10	51.91926	50	23.00944039
-15	**51.91926**	**55**	**26.14698224**
-20	51.91926	60	29.28452409

2.1.3 MQL COOLING/LUBRICATION STRATEGY-SET-UP

Acculube MQL Box precision pump box applicator automatic on/off with 18 inch copper nozzle was used. The applicator is a positive displacement lubrication system for MQL that regulates the amount of lubricant applied to the tool cutting edge in exact quantities. When the unit is switched on, it is supplied with compressed air at (80psi) and lubricant at 0.5 bars. The lubricant is supplied from the reservoir, flowing through the base to the volumetric pneumatic micro pumps. The delivery frequency of the micro pump used was four strokes per second and can be adjusted anytime with the pneumatic pulse generator, which is controlled via the control unit on the system. The flow rate of

the micro pump was set with a thumb wheel. The micro pump delivers a metered quantity of lubricant, which goes through the inner channel of the base to the coaxial outlet port then into the capillary tube of the coaxial line. Air was supplied from a compressed shop air network. The air inlet is controlled with a solenoid valve. The compressed air also flows through the base and is divided in two ways. Some compressed air is supplied to the micro pump to actuate it and the other part of the compressed air (called carrier air) is supplied to the coaxial outlet port and goes through the outer tube of the hose. The carrier air pressure of the outlet can be adjusted with a pressure regulator. The low-pressure carrier air and the lubricant are simultaneously transported via the coaxial hose to the nozzle. The carrier air is swirled in the nozzle. As a result, the metered quantity of lubricant is broken down into micro droplets, which are transported by the carrier air to the friction point without causing any mist. The micro droplet size (200 – 600 μm) ensures a perfect lubricant coating without atomization.

2.2. DESIGN OF EXPERIMENT

2.2.1 FRACTIONAL FACTORIAL DESIGN OF EXPERIMENT

A fraction of the total set of all treatment combinations is selected for the experiment. A three factor at three level, 3^3, full factorial experimental design requires that 27 experimental runs be conducted. With replication, this full factorial design will require 54 experimental runs. Therefore, the number of runs required may outgrow the resources required to carry out the experiment. In fractional factorial design, it is assumed that certain higher order interactions are negligible. This statistical method becomes necessary when there are insufficient resources to conduct experiments, as higher order experimental interactions reproduce initial results. Therefore a fraction of a complete factorial design of experiment will suffice. In this study, 1/3 fractional factorial design of experiment is used to reduce the number of experimental runs and cost, which requires 9 experimental runs or treatment combinations, each run was replicated resulting to 18 total runs in order to minimize the noise effect in the data obtained and allow the estimation of experimental error. Each replicate is divided into 3 blocks of 9 treatment combinations.

2.2.2 SELECTION OF PARAMETER AND THEIR LEVELS

The objectives of this experiment are to investigate the effects of cooling strategies and machining parameters on cutting forces, cutting temperature, and tool wear in slot end-milling and detect optimum machining parameters and cooling strategies to reduce cutting forces generated during end-milling of titanium alloy, reduce cutting tool-workpiece temperature, tool wear, improve residual stresses and surface finish during end-milling of Ti-6Al-4V using uncoated solid carbide endmill. Spindle speed at three

levels of (1000, 1500, and 2000 rpm), feed rate at 3 levels (6, 12 and 18 ipm) and cooling strategies at three levels (conventional emulsion, MQL and LN_2) were the three factors (parameters) selected for evaluation as shown in Table 5. Axial and radial depths of cut are kept constant at 0.125 inch and 0.5 inch respectively, also corner radius of 0.3 inch was kept constant for all the bull-nosed end-mills used throughout the experiments. These machining parameters chosen are based on optimum machining conditions in a previous work done by Okafor and Aramalla [21].

Table 5: SELECTION OF PARAMETER AND THEIR LEVELS

Table 5a: Experimental factors and levels

Level	Factors		
	Cooling Methods	Speed (RPM)	Feed (IPM)
0	Emulsion	1000	6
1	MQL	1500	12
2	LN2	2000	18

Table 5b. Design of experimental runs for the principal block

1	000	4	101	+	101	202	7	101	+	021	122
2	**012**	5	012	+	012	**021**	8	012	+	202	**211**
3	**101**	6	101	+	012	**110**	9	021	+	202	**220**

Each factor is investigated at three levels to determine the optimum setting for the end-milling process. A 3^3 full factorial experiment requires 27 treatment combinations. In

this experimental case, higher order interaction is aligned with the mean; this higher order interaction together with blocks is used to obtain $1/3^k$ fraction of a S^n experiment, where (n) is the number of factors and (S) is the level of each factor. This case uses $K = 1$, $S = 3$ and $n = 3$, which allows the construction of three blocks with each block having $3^{3-1} = 9$ treatment. The treatment combination (1, 1, 1) is chosen for higher order interactions. Let AB^2C^2 be the generator of the fraction that will be confounded with blocks.

The defining contrast is given in equation 3;

$$L = X_1 + 2X_2 + 2X_3 \qquad 3$$

From the defining contrast above, it is easy to verify that the treatment combinations, 000, 012, and 101 belong to the principal block and the remaining experimental runs in the principal block generated as shown in Table 5b. In Table 5b, the figures in bold prints are the runs generated for the principal block and it is this principal block that is chosen as the one-third fraction of the 27 treatment combinations as shown in Table 6.

In Table 6, the column designated as treatment combination is the runs generated for the principal block and it is the one-third fraction of the 27 treatment combinations.

Table 6: 1/3 FRACTIONAL FACTORIAL EXPERIMENTAL DESIGN

Experimental Runs	Treatment Combinations	3 Factors at 3 Levels		
		Cooling Methods	Speed (RPM)	Feed (RPM)
1	(0,0,0)	Emulsion	1000	6
2	(0.1.2)	Emulsion	1500	18
3	(1,0,1)	MQL	1000	12
4	(2,0,2)	LN2	1000	18
5	(0,2,1)	Emulsion	2000	12
6	(1,1,0)	MQL	1500	6
7	(1,2,2)	MQL	2000	18
8	(2,1,1)	LN2	1500	12
9	(2,2,0)	LN2	2000	6

2.2.3 ANALYSIS OF VARIANCE

Analysis of variance (ANOVA) was used to test the significant differences between the means for each factor. ANOVA can determine if the variation in the result of the variable is due to the changing of each factor from one level to another, or if the variation is attributed to random error. It can also quantify the contribution of each cutting parameter to the total variation in the dependent variable quality characteristics. The columns of the ANOVA tables are the sources (factors), degrees of freedom (df), sum of square (SS), means square (MS), variance factor (F), and the P-values for the factors. The variance can be separated into effect or error, by analyzing the sum of squares of the variation (SS). Taking into account, the SS for each factor, interaction, and error, and dividing by the number of degrees of freedom, the mean square effect and mean square error are obtained. The variance ratio, F, is the variance ratio of the mean square effect to the mean square error. The larger the variance ratio for a given factor, the more significant that factor's effect is on the total variance. P-values are the significance

level of the test. A factor is said to have significant effect on the response variable if the P-value for that factor is less than the significance (α) level of the test.

2.2.4 MARGINAL MEANS

Marginal means plots in this experimental runs were used to visually represent the effects of each factor on the dependent variable: cutting force components, tool wear, and cutting temperature. The marginal means of a factor at a particular level are calculated as the mean of the dependent variable with the factor set at that level. The marginal means presented in the results are for all three levels and are calculated as shown in equation 4 below;

$$\overline{X}_1 = \frac{\sum_{i=1}^{N1} X1}{N_1} \qquad 4$$

Where $\overline{X}$ = Marginal mean for every level
X_1 = value of dependent variable at level 1
N_1 = Number of measurements at level 1

2.2.5 PARETO CHART

Pareto chart of effects is a visual representation of the main effects and interaction that are calculated using ANOVA. The magnitude of each effect is represented by a shaded column and the dotted line crossing the column indicates the magnitude of each effect required for that effect to be statistically significant. The Pareto chart lists each effect in the order of significance.

3 EXPERIMENTAL SET-UP AND PROCEDURE

3.1 MACHINE TOOL, WORKPIECE MATERIAL, CUTTING TOOL AND CONDITIONS

A schematic diagram of the experimental set-up is shown in Figure 2. The slot end-milling experiments were conducted on Cincinnati Milacron, Sabre 750 Vertical Machining Center (VMC) with Acramatic 2100 controller. The workpiece material used are two rectangular blocks of Titanium alloy Ti-6Al-4V, 6 inches (152.4 mm) long x 3 inches (76.2 mm) wide x 1.5 inches (38.1 mm) thick. Two sets of experiments were conducted on each block. For the first block, Block A, all the experimental runs using conventional emulsion and MQL cooling strategies were carried out on it with 3 slots on one half of the block for conventional emulsion cooling (experimental runs 1, 2 and 5) and another 3 slots on the second half of the block for MQL cooling strategy (experimental runs 3, 6 and 7) all at different combinations of machining parameters as shown in Table 6. The second block, Block B, has the experimental runs (slots) for LN_2 cooling strategy (experimental runs 4, 8 and 9) on one half of the block and on the second half of the block 3 slots were machined for a comparative evaluation of MQL, LN_2 and MQL + LN_2 cooling strategies using the identified optimum machining parameters from the analysis of variance of fractional factorial design of experiments. The cutting tool used is a 4-flute uncoated solid carbide endmill of 0.5 inch (12.7 mm) diameter, 0.5 inch (12.7 mm) shank diameter, 1 inch (25.4 mm) flute length, 3 inch (76.2 mm) overall length, and 0.3 inch (0.76 mm) corner radius. A corner radius of 0.3 inch was chosen to give minimum cutting force values as reported by Okafor, and Aramalla [9]. A new endmill was used for each experimental run (slot) to eliminate the effect for tool wear and

a total of 12 endmills were used for all experiments. The range of cutting speed and feed rate were selected with the aim of suitably covering the recommended ranges of machining conditions for Titanium alloy while cooling strategies and cryogenic temperature of -15^{o}C were selected from recommendations from published literatures. The cutting conditions chosen for the experiments were; cutting speed 1000 rpm (39.9 m/min), 1500 rpm (59.85 m/min), 2000 rpm (79.8 m/min), feed rate 6 ipm (152.4 mm/min), 12 ipm (304.8 mm/min) 18 ipm (457.2 mm/min), axial depth of cut was 0.125 inch (3.175 mm) and radial depth of cut was 0.5 inch (12.7 mm). Figure 4 shows a pictorial view of the entire set-up with all the components labeled.

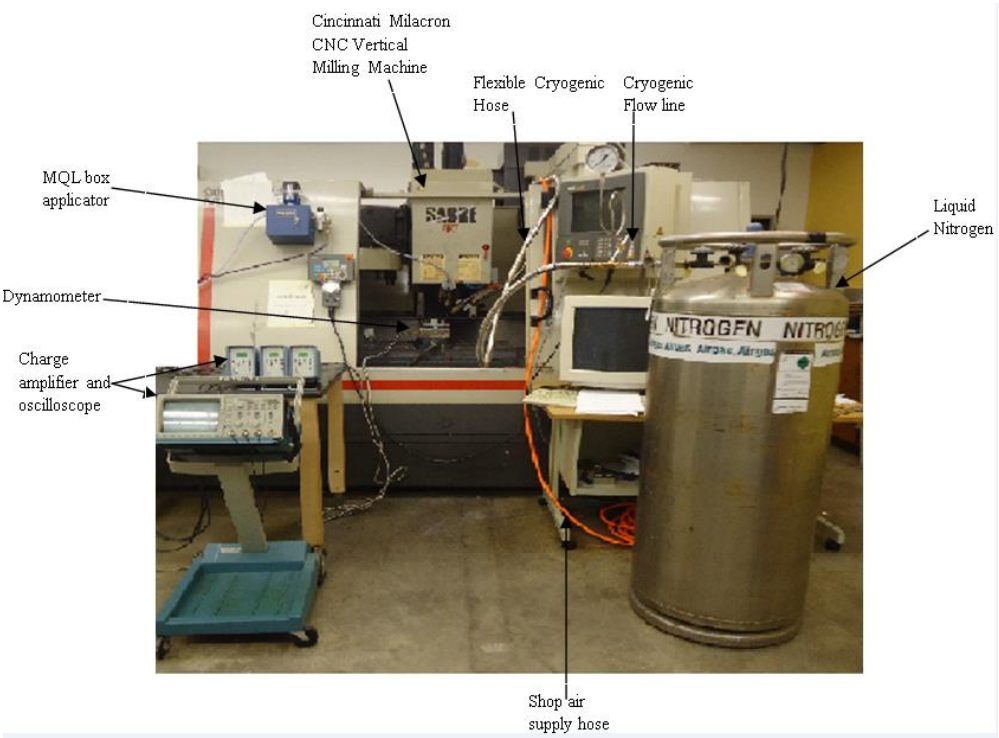

Figure 4. PHOTOGRAPH OF COMPLETE EXPERIMENTAL SET-UP SHOWING VMC, FORCE DATA ACQUISITION SYSTEM, MQL AND LN_2 COOLING SYSTEMS

The set-up for the cooling strategies investigated was made up of cryogenic liquid nitrogen (LN_2) flow line built in-house at Missouri University of Science and Technology for liquid nitrogen (LN_2) cooling, conventional emulsion coolant supplied from the VMC, and Acculube Minimum Quantity Lubricant precision box applicator for MQL cooling. The set-up for the comparative evaluation of MQL + LN_2 with MQL, LN_2 and conventional emulsion cooling strategies as shown in Figures 2 a, b and Figure 4, was used for comparison with the original three levels of cooling strategies. The cryogenic (LN_2) flow line is a nozzle designed to regulate the flow and temperature of both liquid nitrogen and a mixture of liquid nitrogen and shop air when flown directly on the cutting zone.

Before the slot endmilling tests, the workpiece materials were prepared by drilling two holes with two counter bores. The holes were tapped to allow tight clamping of the workpiece to the KISTLER force dynamometer with threaded bolts, and the dynamometer was tightened on the vice of the CNC machine bed. Clamping the workpiece on the dynamometer through threaded holes on the workpiece will prevent play and extraneous noise effects being superimposed on the acquired force and temperature signals.

3.2. EXPERIMENTAL PROCEDURE

The slot end-milling experimental runs were performed at cutting speeds of 1000 rpm, 1500 rpm, and 2000 rpm, feed rates at 6 ipm, 12 ipm and 18 ipm, and cooling strategies were emulsion cooling, cryogenic cooling at -15^{o}C, and minimum quantity lubrication at constant axial and radial depths of cut of 0.125" (3.175 mm) and 0.5" (12.7 mm) respectively were maintained. The feed direction of the workpiece/table was along the negative y-axis of the workpiece/table applying right-hand rule. A total of 8 machining passes were made for each machined slot, for the 1 inch (25.4 mm) deep slots. The CNC program containing the G & M codes for machining test run #1 (slot #1) in inch unit is given below;

```
:100 T1 M6
N10 G01 X0.375 Y-1 Z1 F50
N20 Z-0.25
N30 S1000 M03
N40 G01 Y3.7 F18
N50 G01 Z1 F50
N60 G01 X0.375 Y-1 F50
N70 G01 Z-0.375
N80 G01 Y3.7 F18
N90 G01 Z1 F50
N100 G01 X0.375 Y-1 F50
N110 G01 Z-0.5
N120 G01 Y3.7 F18
N130 G01 Z1 F50
N140 G01 X0.375 Y-1 F50
N150 G01 Z-0.625
N160 G01 Y3.7 F18
N170 G01 Z1 F50
N180 G01 X0.375 Y-1 F50
N190 G01 Z-0.75
N200 G01 Y3.7 F18
N210 G01 Z1 F50
N220 G01 X0.375 Y-1 F50
N230 G01 Z-0.875
N240 G01 Y3.7 F18
N250 G01 Z1 F50
N260 G01 X0.375 Y-1 F50
N270 G01 Z-1
N280 G01 Y3.7 F18
N290 G01 Z1 F50
N300 G01 X0.375 Y-1 F50
N310 M02
N320 M30
```

3.2.1 CUTTING FORCE ACQUISITION AND TOOL WEAR MEASUREMENT

For each machining session (slot end-milling), each workpiece was clamped on a Kystler 9272 4-component dynamometer that was clamped in the vice of the CNC machine bed. The voltage proportional signals obtained by the dynamometer were

separated via a Kystler type 5405A breakout junction box into three components of cutting force (F_x, F_y, F_z). Once separated, the three components of the cutting force signals (F_x, F_y, F_z) were passed through three separate Kistler Type 5010B dual mode amplifier. The amplified signals were passed through low pass filters set at 680 Hz to get rid of unwanted noise from the slot-endmilling process. These filtered signals were passed to a Tektronix TDS 420A digitizing oscilloscope where they were digitized at a 2.5 KHz sampling frequency, F_s, using 5000 sampling points (N) per signal, resulting in a time domain record length (T) of 2 seconds. The digitized signals were saved and transferred to a Pentium PC for further processing and analysis. The three cutting force components were acquired at every pass when the end-mill has progressed about 1 inch (25.4 mm) along the slot. A new end-mill was used per slot and forces acquired at passes number 1 & 2 were treated as replicates for purpose of analysis of variance and error estimation. Forces acquired for passes number 1, 2, 4, 5, 7 & 8 were used for indirect monitor of tool wear per machined slot and cooling strategy

3.2.2 WORKPIECE TEMPERATURE MEASUREMENTS

Eight 0.125 inch diameter, 1 inch deep holes were drilled on the front sides of all the Titanium Alloy Ti-6Al-4V materials at the middle of each slot. An ungrounded K-type thermocouple probe of 0.125 inch diameter was inserted into the drilled holes to ensure snug fit. The ungrounded thermocouple probe was used to reduce unwanted noise from the endmilling process. Thermal grease was applied at the tip of the thermocouple probe to ensure proper conduction and reduce convection heat transfer. The thermocouple probe was connected to a National Instrument NI USB-9211A Data Acquisition Device

(DAQ) for thermocouple and the DAQ device was connected to a Pentium computer. Temperature signals were acquired using Labview Signal Express 3.0. The maximum temperature experienced at the cutting tool-workpiece interface was recorded for every machining pass at every experimental run. The workpiece was allowed to cool for 24 hours before starting the next experimental run. Figure 5 shows the geometry of the workpiece design.

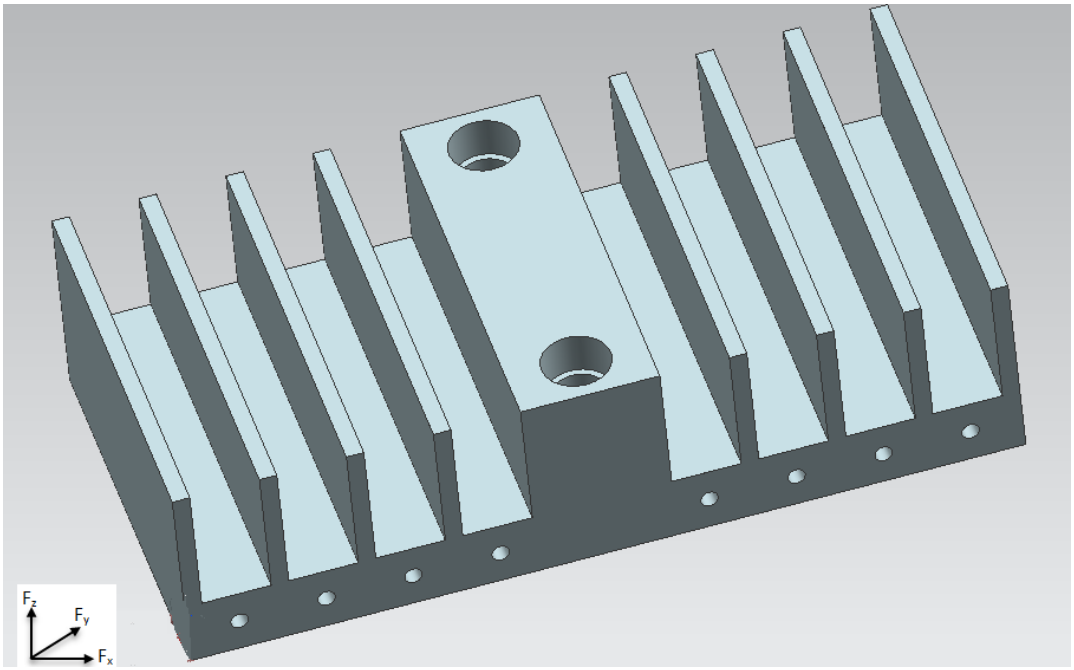

5a. 3D view of workpiece with machined 8 slots and 8 drilled thermocouple holes

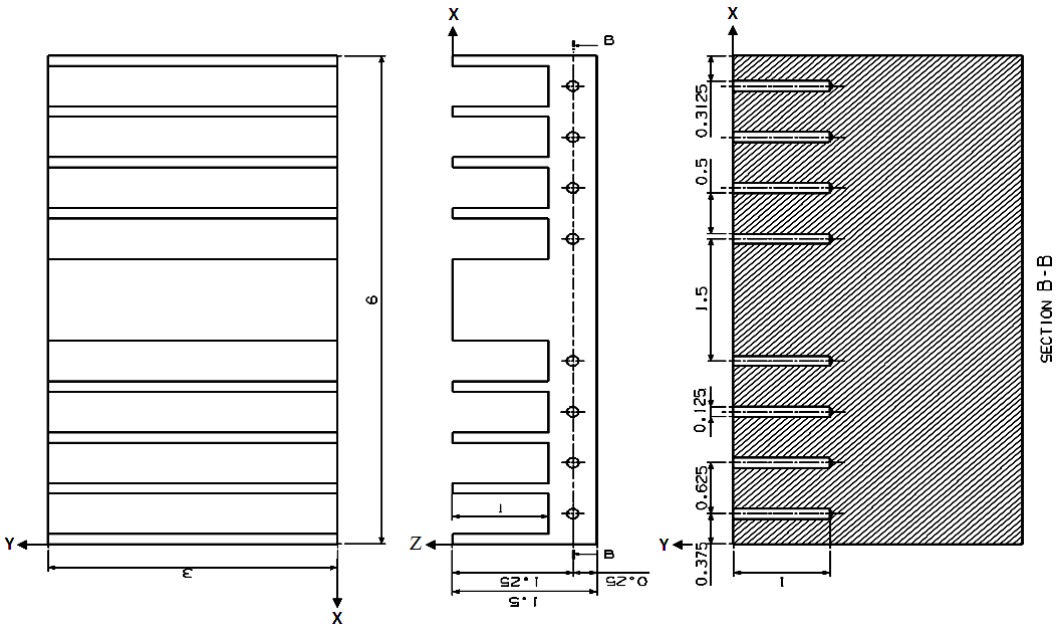

5b. Top and side views of workpiece with dimensions and hatched section

Figure 5. WORKPIECE DESIGN FOR SLOT END-MILLING EXPERIMENTS

4. RESULTS AND DISCUSSION

4.1 CUTTING FORCE AND WORKPIECE TEMPERATURE DATA PROCESSING AND ANALYSES

The acquired (measured) raw cutting force components signals (F_x, F_y, F_z) were processed using a 10-point moving average to post-filter out some of the random noise and bring out the major patterns in the time domain signal. Figure 6 shows the processed cutting force components (F_x, F_y, F_z) of 2 seconds record length for experimental run 3 [MQL]. Absolute values of the maximum measured values of the cutting force components were determined for each machining pass acquired force data. The absolute values of the maximum measured cutting force components for pass number 1 and pass number 2 as shown in Tables 7a and 7b were used as first and second replicates to perform Analysis of Variance (ANOVA), to identify statistically significant trends in the measured cutting force components data and temperature data to monitor indirect tool wear. The cutting force components data acquired at the 7^{th} and 8^{th} passes of each experimental run were measured to monitor indirect tool wear. The 7^{th} and 8^{th} passes are treated as first and second replicates respectively for indirect tool wear analysis using ANOVA.

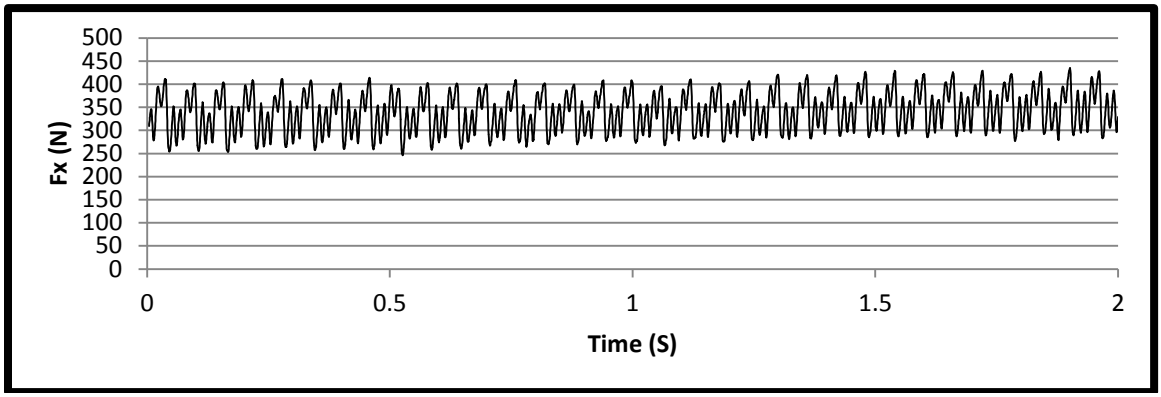

6a. Graph of cutting force component F_x for run 3 (MQL, n = 1000 rpm, F = 12 ipm)

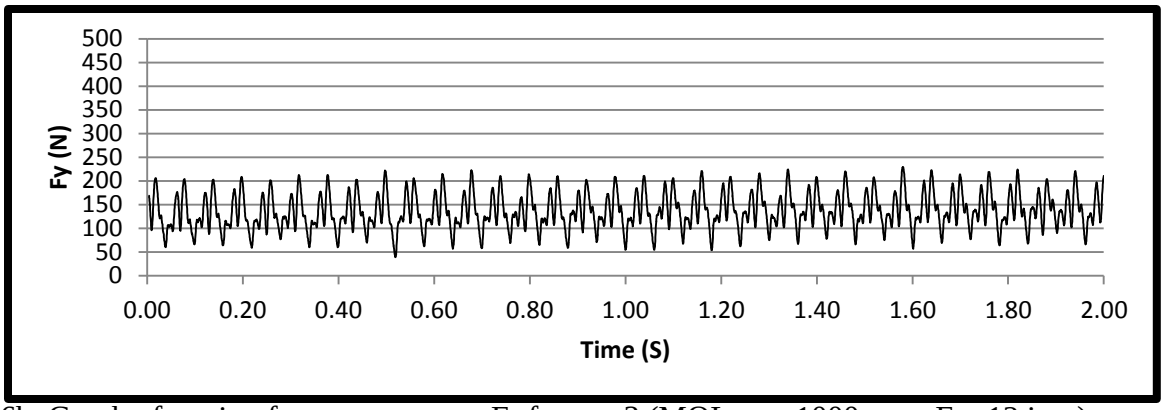

6b. Graph of cutting force component F_y for run 3 (MQL, n = 1000 rpm, F = 12 ipm)

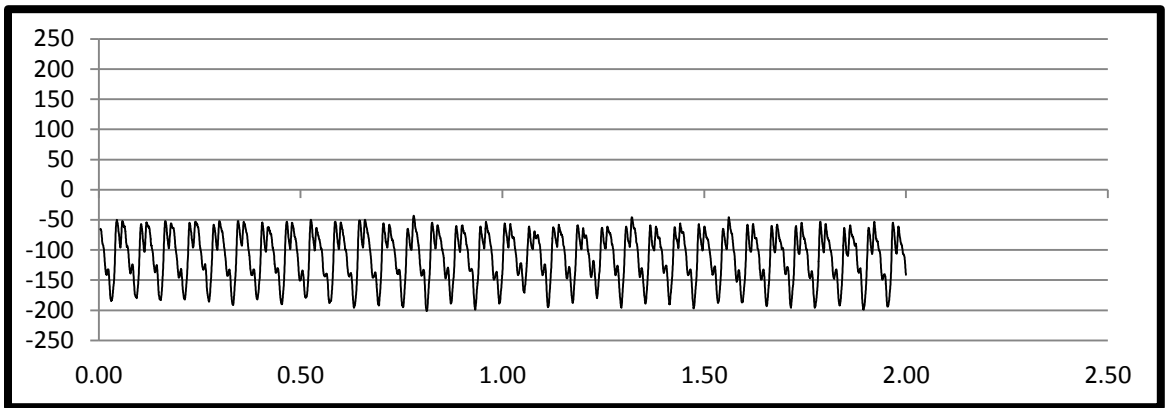

6c. Graph of cutting force component F_z for run 3 (MQL, n = 1000 rpm, F = 12 ipm)

Figure 6. MEASURED CUTTING FORCE COMPONENTS (F_X, F_Y, AND F_Z) FOR EXPERIMENTAL RUN #3 (MQL) @ N = 1000 RPM, F= 12 IPM

Table 7: CUTTING FORCE DATA PROCESSING AND ANALYSES

Table. 7a. Pass 1 with cutting forces for all experimental runs

Treatments Combination	Cooling Methods	Speed (RPM)	Feed (IPM)	Fx (N)	Fy N)	Fz (N)	Fr (N)
(0,0,0)	Emulsion	1000	6	375	308	130	485.2721
(0,1,2)	Emulsion	1500	18	669	536	244	857.238
(1,0,1)	MQL	1000	12	435	230	200	492.062
(2,0,2)	LN2	1000	18	1031	515	440	1152.47
(0,2,1)	Emulsion	2000	12	340	257	187	426.203
(1,1,0)	MQL	1500	6	198	168	63	259.669
(1,2,2)	MQL	2000	18	313	180	82	361.0665
(2,1,1)	LN2	1500	12	530	391	158	658.6205
(2,2,0)	LN2	2000	6	288	335	75	441.7794

Table. 7b. Pass 2 with cutting forces for all experimental runs

Treatment Combination	Cooling Methods	Speed (RPM)	Feed (IPM)	Fx (N)	Fy (N)	Fz	Fr
(0,0,0)	Emulsion	1000	6	400	320	137	512.2499
(0,1,2)	Emulsion	1500	18	720	596	265	934.6743
(1,0,1)	MQL	1000	12	594	352	288	690.4636
(2,0,2)	LN2	1000	18	949	525	305	1084.54
(0,2,1)	Emulsion	2000	12	349	320	140	473.4987
(1,1,0)	MQL	1500	6	92	108	52	141.8732
(1,2,2)	MQL	2000	18	317	156	115	353.3058
(2,1,1)	LN2	1500	12	681	470	265	827.4424
(2,2,0)	LN2	2000	6	300	321	64	439.3643

4.2 ANOVA SURFACE/CONTOUR DESIRABILITY PLOT AND PARETO CHART FOR CUTTING FORCE COMPONENTS (F_X, F_Y, AND F_Z)

ANOVA, Pareto chart, marginal plots, and surface/contour desirability plots were used to statistically analyze the main and interaction effects of machining parameters and cooling strategies on cutting force components data acquired from the experimental runs.

Tables 8a, b, c are the ANOVA table for the three components of the cutting force, (F_x, F_y, and F_z) respectively. **ANOVA**: The tables show the combined linear and quadratic main effects, and the measurable linear by linear two-factor interactions, the P-values (P) associated with each factor level and interactions along with the sum of square effects (SS), degree of freedom (DF), mean square (MS), and F-values (F). A low P-value (i.e. P-value < 0.05) indicates statistical significance for the factor (source) on the corresponding response. The 0.05 indicates 5% significant level.

Table 8: ANALYSIS OF VARIANCE (ANOVA) FOR CUTTING FORCE COMPONENTS

Table 8a. ANOVA for Cutting Force Component F_x

	ANOVA; Var.:Fx; R-sqr=.9679; Adj:.93936 (Spreadsheet21) 3 3-level factors, 1 Blocks, 18 Runs; MS Residual=3861.611 DV: Fx				
Factor	SS	df	MS	F	p
(1)Cooling L+Q	279088	2	139544.2	36.13627	0.000050
(2)Speed L+Q	293814	2	146907.1	38.04294	0.000041
(3)Feed L+Q	172909	2	86454.7	22.38824	0.000321
1*2	15109	2	7554.4	1.95628	0.197032
Error	34754	9	3861.6		
Total SS	1082588	17			

Table 8b. ANOVA for Cutting Force Component F_y

Factor	ANOVA; Var.:Fy; R-sqr=.95275; Adj:.91074 (Spreadsheet21 3 3-level factors, 1 Blocks, 18 Runs; MS Residual=1850.556 DV: Fy SS	df	MS	F	p
(1)Cooling L+Q	178478.8	2	89239.39	48.22303	0.000016
(2)Speed L+Q	53006.8	2	26503.39	14.32186	0.001598
(3)Feed L+Q	45989.4	2	22994.69	12.42583	0.002576
1*2	29398.8	2	14699.39	7.94323	0.010286
Error	16655.0	9	1850.56		
Total SS	352453.1	17			

Table 8c. ANOVA for Cutting Force Components F_z

Factor	ANOVA; Var.:Fz; R-sqr=.89015; Adj:.7925 3 3-level factors, 1 Blocks, 18 Runs; MS Residual=2302.667 DV: Fz SS	df	MS	F	p
(1)Cooling L+Q	21693.0	2	10846.50	4.71041	0.039829
(2)Speed L+Q	58513.0	2	29256.50	12.70549	0.002393
(3)Feed L+Q	23382.0	2	11691.00	5.07716	0.033411
1*2	8589.0	2	4294.50	1.86501	0.210068
Error	20724.0	9	2302.67		
Total SS	188650.0	17			

Pareto Charts: The corresponding Pareto charts are given in Figure 7 a, b& c for cutting force components F_x, F_y, and F_z. The effects are separated into linear and quadratic main effects, and linear by linear two factor interactions, with all effects listed in order of their significance. The ANOVA table for F_x, F_y, and F_z shows that the main effects of cooling strategies, spindle speed and feed rate all have significant effects on cutting force components F_x, F_y, and F_z. The interaction of cooling strategies with spindle speed has significant effects only on the F_y component of the cutting force which acts along the feed direction.

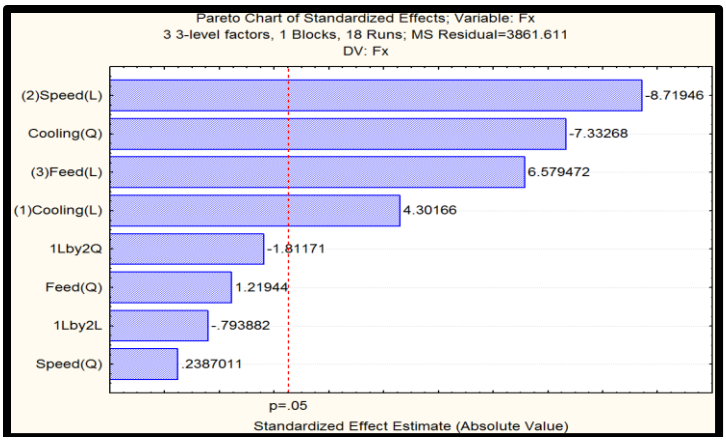

7a: Pareto Chart for F_x using force data for the First and Second Passes

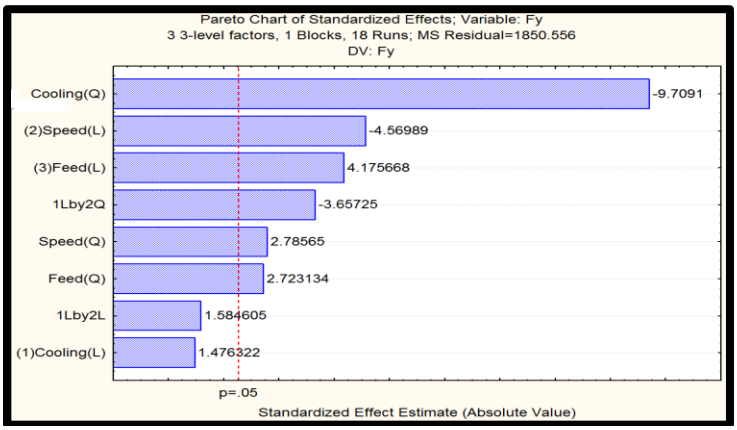

7b: Pareto Chart for F_y using force data for the First and Second Passes

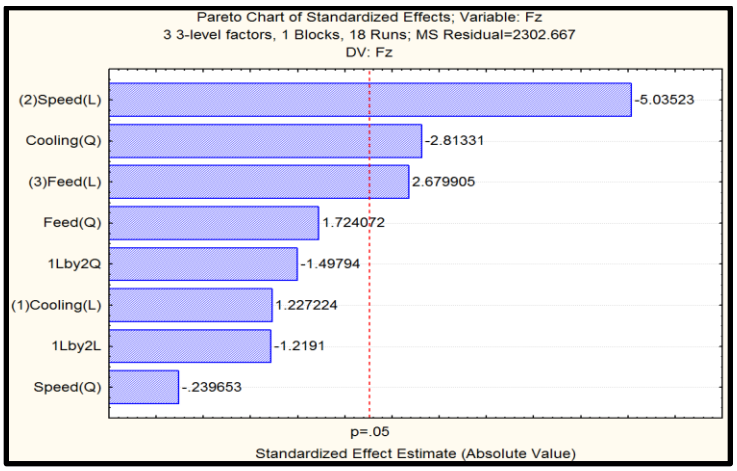

7c: Pareto Chart for F_z using force data for the First and Second Passes

Figure 7. PARETO CHARTS FOR CUTTING FORCE COMPONENTS (F_X, F_Y, AND F_Z)

Desirability surface/contour plot: The desirability surface/contour plots are shown in Figure 8 which shows which levels of the desirable and undesirable main effects of cooling strategies, spindle speed, and feed rate produce the most desirable responses on the cutting force components. The first plot of Figure 8 shows the desirable effects of cutting speed and cooling strategies on cutting force components. It is seen that desirable optimum cutting force components are produced by the levels of MQL cooling strategy and high spindle speed of 2000 rpm. The next plot of feed rate and cooling strategies shows that low feed level of 6 ipm using either cooling level of MQL or LN_2 is the optimum combination of feed rate and cooling strategies that produce the most desirable response on the cutting force components. The third plot shows the surface plot of feed rate and spindle speed. Optimum combination of feed rate and spindle speed was at low feed rate level of 6 ipm and high spindle speed of 2000 ipm.

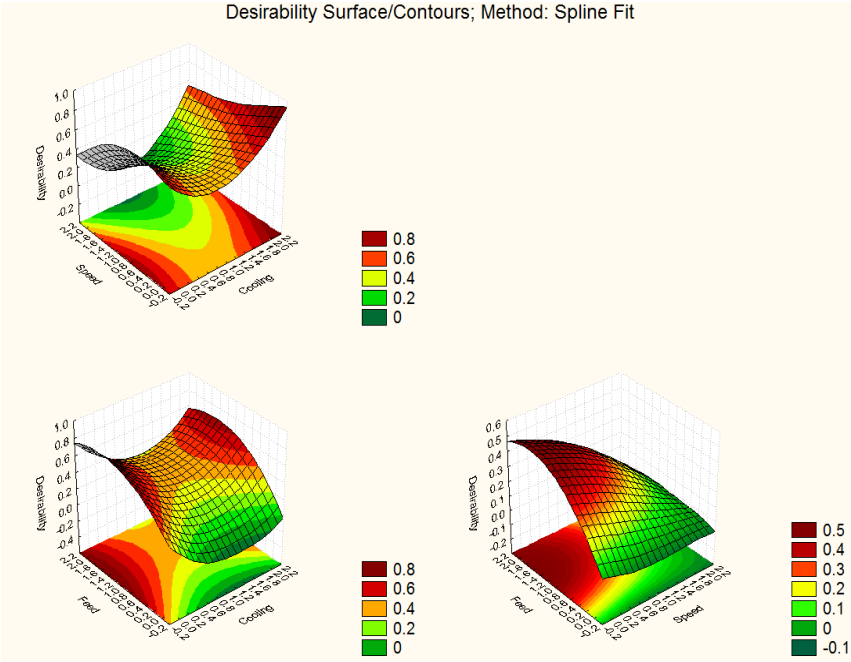

Figure 8. CUTTING FORCE COMPONENTS DESIRABILITY SURFACE/CONTOUR PLOTS

4.2.1 EFFECTS OF COOLING STRATEGIES AND MACHINING PARAMETERS ON CUTTING FORCE COMPONENT F_X

The Pareto chart in Figure 7a shows the effects of the experimental factors (cooling strategies, feed rates and spindle speeds) on cutting force in the X direction, which is the direction perpendicular to direction Y. The chart shows that the linear effect of cutting speed is the dominant and statistically highly significant parameter and has a decreasing effect on cutting force F_x with increase in cutting speed.

The second significant parameter is quadratic cooling strategy which also has a decreasing effect on cutting force with increase in cooling strategy going from emulsion to cryogenic LN_2 cooling. The chart indicates that factor 3-linear feed rate has increasing effects on cutting force F_x and it is the third statistically significant factor in this experiment. The forth statistically significant factor from the chart is linear cooling strategies which show an increasing linear effect on cutting force F_x going from emulsion to LN_2 cooling.

4.2.2 EFFECTS OF COOLING STRATEGIES AND MACHINING PARAMETERS ON CUTTING FORCE COMPONENT F_Y

The second chart in the Pareto chart of Figure 7b shows the effects of cooling strategies, feed rate and spindle speed on cutting force component in the Y direction, F_y. From the chart, it can be seen that factor 1, cooling strategies, has a quadratic and decreasing effect on cutting force F_y and it is the dominant and most statistically significant factor affecting cutting force F_y; also, factor 2, cutting speeds, shows a linear and decreasing effect on cutting force in y but at a significantly lower magnitude than the quadratic and decreasing effects of factor 1, cooling strategies.

Just as for cutting force in x direction, factor 3, feed rates has a linear and increasing effect on cutting force component F_y. The linear interaction of cooling strategies with quadratic effect of cutting speed shows a decreasing effect on cutting force component F_y. This effect is the fourth statistically significant in the Pareto chart of factors and factors interactions effects on cutting force in y. Quadratic effect of speed and feed on F_y are statistically significant but they are respectively 5^{th} and 6^{th} in the order of significance.

4.2.3 EFFECTS OF COOLING STRATEGIES AND MACHINING PARAMETERS ON CUTTING FORCE COMPONENT F_Z

For cutting force component in the axial direction, Z, F_z, the linear effect of spindle speed is the dominant and most statistically significant parameter with a decreasing effect on cutting force component, F_z.

The second statistically significant parameter is the quadratic effect of cooling strategies which also has a decreasing effect on F_z. Linear effect of feed-rate is the third and last statistically significant parameter with an increasing effect on F_z.

4.2.4 MARGINAL MEAN PLOT OF MAIN EFFECTS ON CUTTING FORCECOMPONENTS (F_X, F_Y, AND F_Z)

The marginal mean plots of all significant main effects of cooling strategies, spindle speed and feed rate and their contribution to the maximum cutting force are shown in Figure 9.

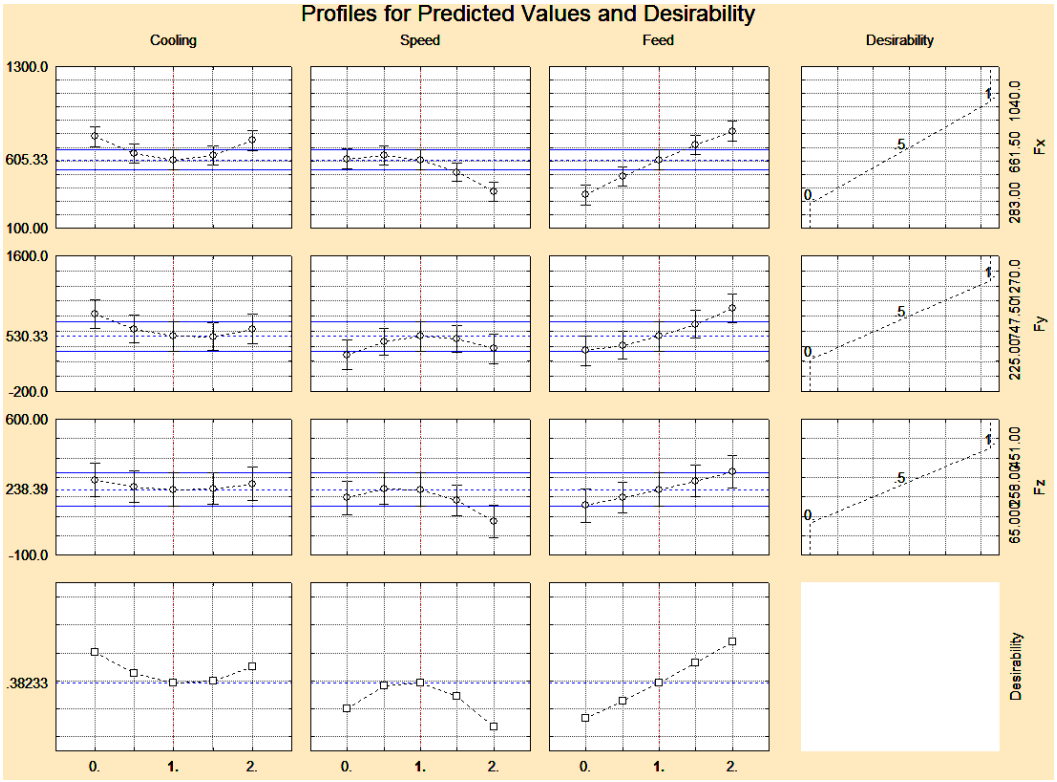

Figure 9. MARGINAL MEANS PLOT FOR CUTTING FORCE COMPONENT IN THE X, Y AND Z-AXES

4.2.4.1 EFFECT OF COOLING STRATEGY ON CUTTING FORCE COMPONENTS (F_X, F_Y, AND F_Z)

The first plot in the first row of Figure 9 shows the effects of cooling strategies on F_x. From the plot, it can be seen that MQL reduces cutting force component F_x better than emulsion cooling and LN_2 cooling. Plots on the second row show the effects of cooling strategies, cutting speed and feed rate on cutting force component in the feed direction F_y.

The first plot in the second row shows that MQL is best in reducing cutting force component in Y direction (feed force) F_y, followed by LN_2 while the plot indicates that emulsion cooling is the least preferred cooling strategy in reducing the feed force. The same trend was followed on the third row which shows effect of cooling strategies on cutting force component in the axial direction, F_z. The desirability plots are shown in

fourth row of Figure 8. From the desirability plot it can be seen that least (optimum) cutting force value for cooling was generated using MQL cooling approach.

4.2.4.2 EFFECT OF CUTTING/SPINDLE SPEED ON CUTTING FORCE COMPONENTS (F_X, F_Y, AND F_Z)

From Figure 9, it can be seen from the plot of the second column that low level of speed (1000 rpm) and medium speed level of 1500 rpm produced approximately 605 N cutting force value in the X direction while at high level cutting speed of 2000 rpm, the cutting force component F_x is reduced by about 50 percent. The second plot of the second column shows that low speed of 1000 rpm was the best in reducing feed force F_y while high spindle speed of 2000 rpm is next preferred cutting speed with a little feed force F_y margin higher than at low speed. Medium speed is also the least preferred as was for F_x.

For axial cutting force (in Z direction), F_z, high speed of 2000 rpm was the best followed by low spindle speed of 1000 rpm as second best in reducing cutting force F_z. Medium spindle speed of 1500 rpm was least preferred cutting force level on F_z.

4.2.4.3 EFFECT OF FEED RATE ON CUTTING FORCE COMPONENTS (F_X, F_Y, AND F_Z)

The third plot in the first row shows that low level feed rate of 6 ipm has the least cutting force value in the X direction F_x, and as the feed increases to 12 ipm and 18 ipm, the slope of the plot increases positively; showing that cutting force F_x increases in direct proportion with feed rate.

The third plot in the second row of Figure 9 shows the effect of feed rate on feed force F_y, it shows that low feed of 6 ipm is best in reducing feed force followed by medium feed rate of 12 ipm, then high feed. The feed plot shows that there's a slight

increase in the slope from medium feed of 12 ipm to high feed rate of 18 ipm, this shows that the feed force F_y increases more rapidly when the feed rate is increased from 12 ipm to 18 ipm in feed rate is highly significant to increase in feed force. The same trend was followed on the third row which has effects of these factors on cutting force component axial to the end-mill F_z.

4.2.5 EXPERIMENTAL RUNS/TREATMENT COMBINATIONS PRODUCING MINIMUM AND MAXIMUM CUTTING FORCES FOR EACH OF THE COOLING STRATEGIES FOR ALL 8 PASSES

From Figure 10, the effect of low cutting speed of 1000 rpm and low feed rate of 6 ipm using emulsion cooling strategy which represents experimental run 1 is seen. Emphases were on the effects of the stated cutting parameters on cutting forces in the X, Y and Z axes (F_x, F_y, F_z), and it shows that cutting force perpendicular to the feed direction, F_x was higher than the cutting force value in the feed direction F_y while cutting force in the Z, F_z remains the lowest generated cutting force at the cutting zone. The slope of these cutting force components (F_x, F_y, F_z) showed the rate which these force components increased with increase in cutting length at constant depth of cut of 0.125 inch (3.175 mm).

The cutting force components in the X and Y directions followed the same trend and with almost the same slope from the first cutting pass of 76.2 mm till the last pass of 609.6 mm. The cutting force component in the Z direction, F_z was the least magnitude among the three cutting force components, and previous publications have shown that cutting force components in Z directions do not have any significant effects during end-milling of titanium alloy, Ti-6Al-4V.

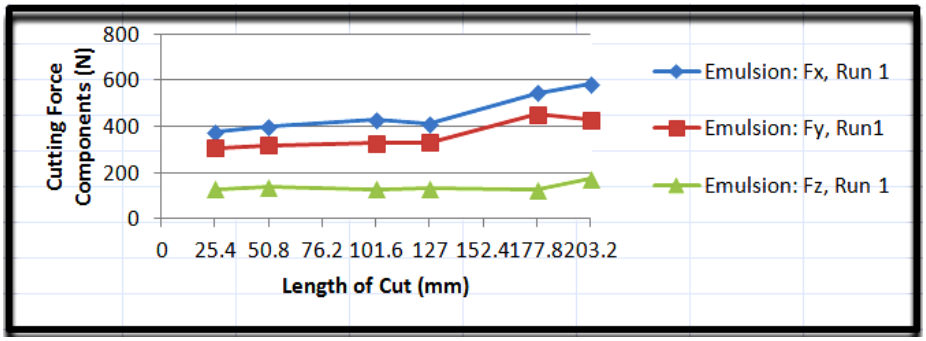

10a. Minimum cutting force components for run 1 (n = 1000rpm, F = 6 ipm)

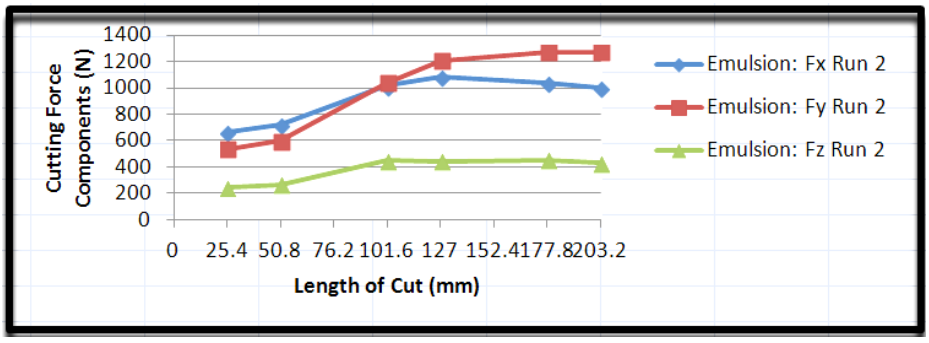

10b. Maximum cutting force components for run 1 (n = 1500rpm, F = 18 ipm)

Figure 10. MINIMUM AND MAXIMUM CUTTING FORCE COMPONENTS FOR EMULSION COOLING STRATEGY

The maximum cutting force components experienced by the tool at the cutting zone when the tool travels from a cutting length of 3 inches (76.2 mm) for pass #1 to a cutting length of 24 inches (609.6 mm) for a total of 8 passes were plotted. The second set graphs in Figure 10b show the effects of emulsion cooling using a cutting speed of 1500 rpm and feed rate of 18 ipm. From the graph, it can clearly be seen that the values of the cutting force components increased significantly, from approximately 700 N with cutting force in the feed direction, F_y to about 1100 N increasing above the component force F_x perpendicular to the feed direction at a point when the cutting length is 12 inches (304.8 mm) (4^{th} pass), then to about 1300 N at the 8^{th} pass. This shows how much effect feed rate could have on cutting forces during slot end-milling especially in the feed

direction. The axial force, F_z is the least force component and is fairly stable with increase in cutting length (machining pass) with maximum force below 500 N.

Figure 11 shows the plots of maximum cutting force components for MQL cooling strategy

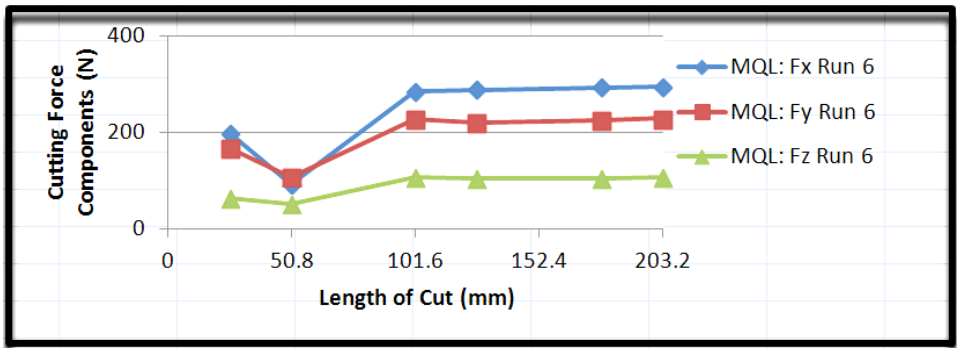

11a. Plot of minimum cutting force components, Experimental Run 6 (n = 1500rpm, F = 6 ipm)

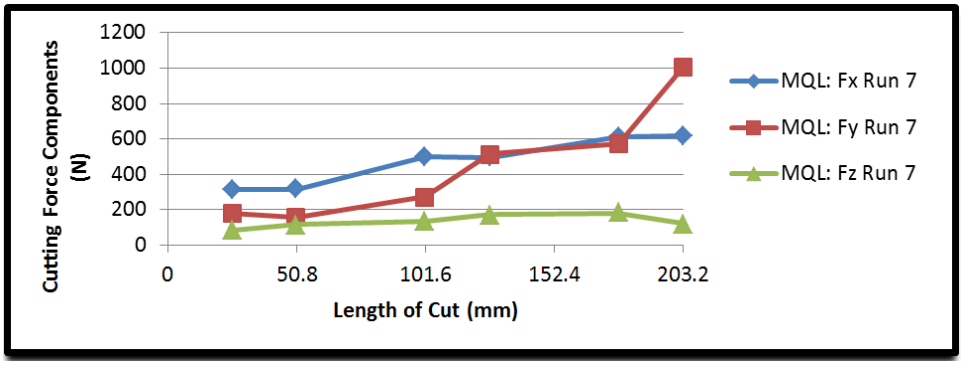

11b. Plot of maximum cutting force components, Experimental Run 7 (n = 2000rpm, F = 18 ipm)

Figure 11. PLOT OF MINIMUM AND MAXIMUM CUTTING FORCE COMPONENTS FOR MQL COOLING STRATEGY

The first set of graphs in Figure 11a shows the plots for cutting force components in slot end-milling of Ti-6Al-4V using MQL cooling/lubrication strategy at a cutting speed of 1500 rpm and a feed rate of 6. The magnitude of the cutting force components

can be seen to be significantly lower compared to the magnitude of cutting force components generated by emulsion cooling with F_x having a maximum value of about 300 N. The slope or the rate of increase in cutting force components especially in the X and Y axes, (F_x, and F_y) as the length of cut increases, as shown in the figure, did not show any significant changes from 76.2 mm length of cut to 609.6 mm length of cut. This shows that there was no significant effect on cutting force components at these cutting conditions and MQL cooling strategy thereby, causing the magnitude of cutting force to be low. The second plot in Figure 11b is a plot of the cutting force response when MQL cooling strategy was used, at cutting speed and feed rate of 2000 rpm and 18 ipm respectively. The plot shows low cutting force values of about 200 N and 300 N for F_y and F_x respectively at the first pass, but as the cut length (pass) increases, the cutting force component in the feed direction F_y increases beyond the cutting force component, F_x to about 1000 N. This justifies that feed rate has significant effect on cutting force components in the X and Y direction, particularly in the Y direction for this slot milling experiment. The force in the Z remained almost unchanged in almost all the cases and it's the least cutting force component generated at the cutting zone at any particular cutting force acquisition for the slot end-milling.

Figure 12 shows the plot of the minimum and maximum cutting force components for LN_2 cooling strategy. Figure 12a shows the plot of cutting force components using cryogenic cooling at cutting speed of 2000 rpm and feed rate of 6 ipm which gave the minimum cutting force components of all the three cryogenic (LN_2) conditions. The plot shows low cutting force values of about 300 N, 321 N, and 64 N for F_x, F_y, and F_z respectively for the first pass of 76.2 mm cutting length and cutting force values of 283

N, 349 N and 75 N for F_x, F_y, and F_z respectively for the last pass of 609.6 mm, this is a clear indication that LN_2 at low speed produced little or no significant variation in the cutting force components. It also shows that low feed rate has little effect on cutting force variations. Maximum values of the cutting force components for all the three axes (F_x, F_y, F_z) show that cutting forces were at their peak in the fifth cutting pass, that is, 381 mm cutting length.

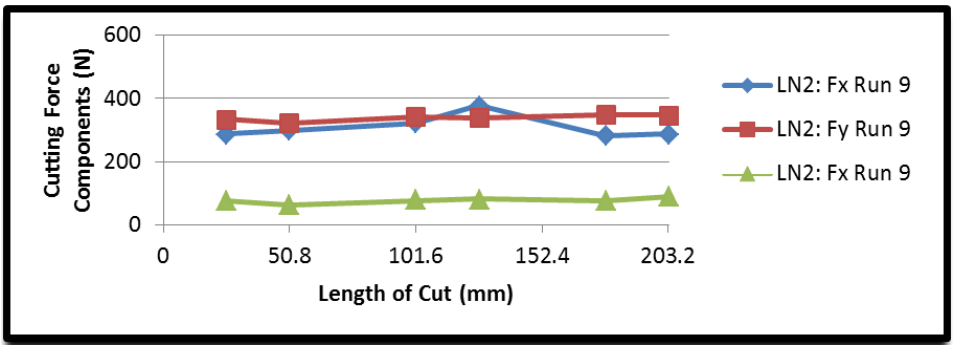

12a. Plot of minimum and maximum cutting force components, Experimental Run 9 (n = 2000rpm, F = 6 ipm)

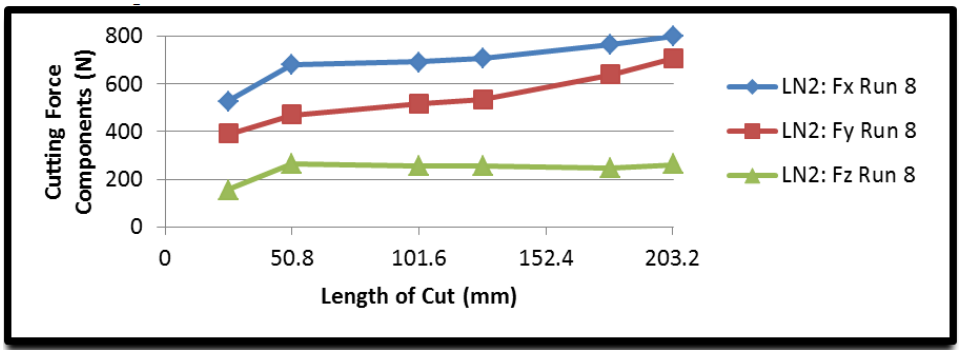

12b. Plot of minimum and maximum cutting force components, Experimental Run 8 (n = 1500rpm, F = 12 ipm)

Figure 12. PLOT OF MINIMUM AND MAXIMUM CUTTING FORCE COMPONENTS FOR LN_2 COOLING STRATEGY

The second plot, Figure 12b shows another condition of LN_2 cooling at 1500 rpm, and 12 ipm which gave the maximum cutting force components values for all the three cryogenic cooling (LN_2) conditions. The cutting forces response show that there are significant increases in cutting force components (F_x, F_y, F_z) from the first pass with 530 N, 391 N and 158 N recorded for F_x, F_y, and F_z respectively to 800 N, 708 N and 262 N for F_x, F_y, and F_z respectively for the last (8^{th}) pass. From careful inspection of the plot, it can be seen that cutting force component in the X direction, F_x dropped at the last pass or increased at a slower rate while the cutting force component in the feed direction, F_y was increasing/moving rapidly towards F_x at the last pass. This validates the claim that feed rate has a very significant effect on F_y as the end-mill progresses down the slot during slot end-milling of titanium alloy Ti-6Al-6V. The F_z component remained fairly stable throughout the passes at approximately 262 N.

Figure 13 shows a pictorial view Ti-6Al-4V with slots made using end-mills. The picture shows slots made using different machining parameters with conventional emulsion cooling used for slots on the left hand side and MQL cooling for slots on the right hand side

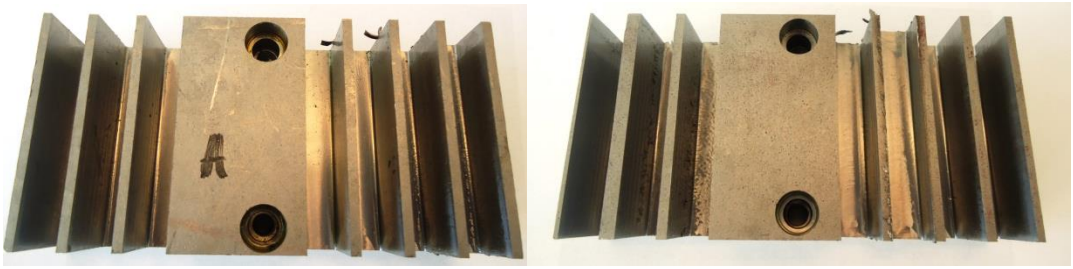

a) Block A b)Block B

Figure13: PHOTOGRAPHS OF MACHINED BLOCKS: A) USING EMULSION COOLING AND MQL (BLOCK A), B) USING CRYOGENIC COOLING (BLOCK B)

4.3 EFFECTS OF COOLING STRATEGIES AND MACHINING PARAMETERS ON WORK PIECE TEMPERATURE

Thermal effects is a significant cause of peak force variation in first cutting passes in most end-milling operations while tool wear propagation remains a significant factor for gradual increase of the mean peak force in successive cutting passes [21]. Slot end-milling operations is a cutting process where there may be fluctuation in the cutting edges. These variations may be as a result of the rate which the end-mill feeds into the workpiece or due to the cutting speed of the rotating end-mill. The fluctuation in cutting edges makes the machining process to experience fluctuating peak cutting forces and heats up the cutting tool mostly at entry and exit of the workpiece. The low thermal conductivity of Ti-6Al-4V alloy is the reason for the high cutting temperature at the tool-workpiece contact zone close to the cutting edge. The high chemical reactivity of titanium alloy Ti-6Al-4V with most tool materials at high temperature is another major cause of tool wear and increased temperature. During high-speed end-milling of titanium alloy Ti-6Al-4V, the high local temperature at the tool-workpiece interface and the concentration gradient of chemical constituents between the solid carbide end-mills and the titanium alloys Ti-6Al-4V simultaneously supports diffusion of cutting tool constituents (higher concentration) into the workpiece (lower concentration) and diffusion of workpiece material particles into the cutting tool at the cutting zone.

Figure 14 shows 2-D clustered bar chart of measured maximum workpiece temperature during slot end-milling of Ti-6Al-4V under the various cooling strategies and machining parameters. The horizontal scale of the chart shows the length of the machining passes in millimeter while the vertical scale represents the magnitudes of the thermocouple-measured workpiece temperature during slot end-milling. The charts are of

different colors which represent different experimental runs with varying cutting parameters and cooling strategies. From the chart, it can be seen that maximum temperature of the workpiece was at experimental run 6 which represents a cutting speed of 1,500 rpm and a feed rate of 6 ipm using MQL strategy. Maximum temperature was observed at all passes for this condition while experimental run 7 closely followed experimental run 6 but just for the first pass but the temperature gradient dropped significantly by the last pass (8^{th} pass). It could be seen that experimental run 7, produced the second highest maximum temperature for passes# 1, 2, 4, and 5 and dropped to 4^{th} and 5th highest values for the 7^{th} and the 8^{th} passes respectively but experimental run 9 (LN_2 at 2000 rpm and feed rate of 6 ipm) shows the lowest temperature value for the first pass but increased significantly at the last pass to become the second highest temperature value recorded during this experiment.

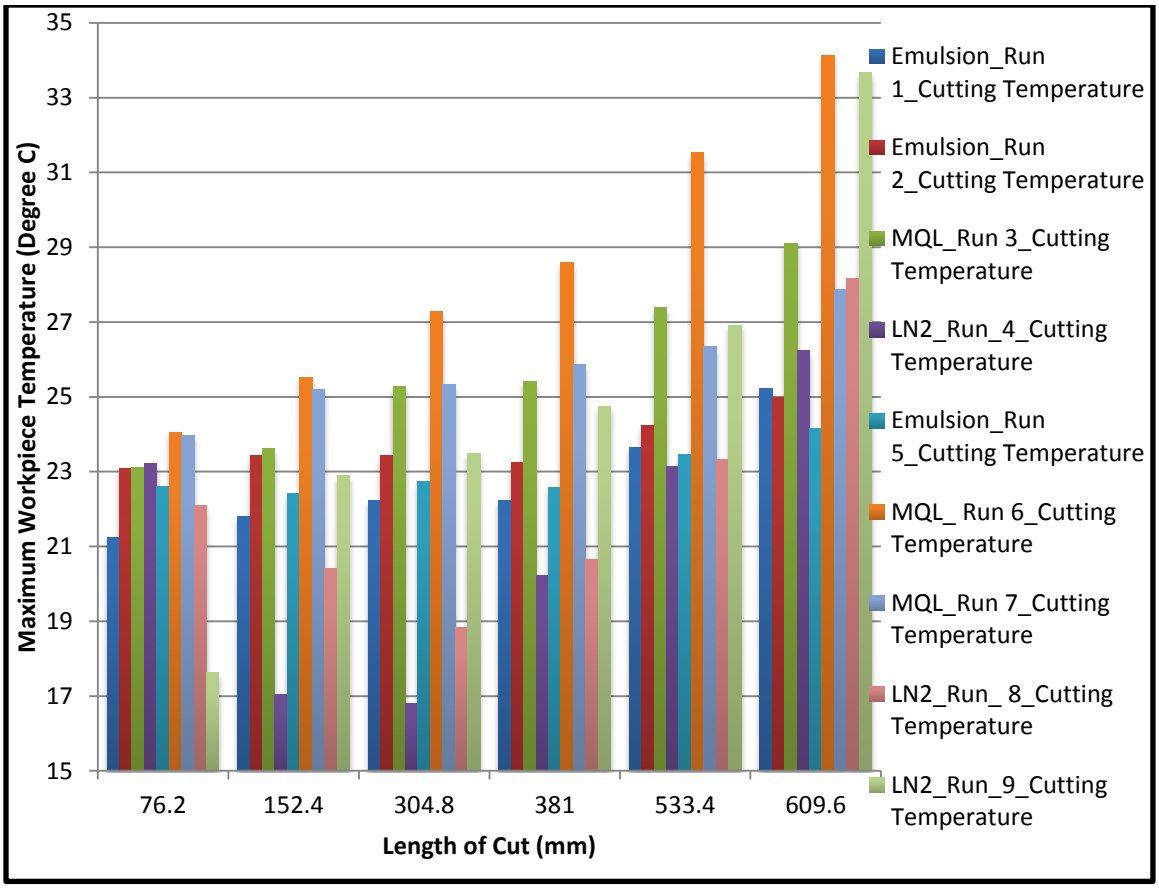

Figure 14. 2-D CLUSTERED BAR CHART WORK PIECE TEMPERATURE DURING SLOT END-MILLING OF TI-6AL-4V UNDER VARIOUS COOLING STRATEGIES AND MACHINING CONDITIONS

The lowest temperature at the last pass was with emulsion cooling using a cutting speed of 2000 rpm and a feed rate of 12 ipm.

ANOVA using maximum workpiece temperature measured during the first and second passes were performed. The ANOVA table for the maximum workpiece temperature is shown in Table 9 shows the main effects and interaction effects (factors). A 95% confidence interval of was used for the analysis.

Table 9. ANOVA FOR MEASURED MAXIMUM WORKPIECE/CUTTING TEMPERATURE

	ANOVA; Var.:Temp; R-sqr=.81835; Adj:.65689 3 3-level factors, 1 Blocks, 18 Runs; MS Residual=4.648261 DV: Temp				
Factor	SS	df	MS	F	p
(1)Cooling L+Q	80.7744	2	40.38722	8.68867	0.007917
(2)Speed L+Q	15.3729	2	7.68647	1.65362	0.244550
(3)Feed L+Q	50.1653	2	25.08263	5.39613	0.028831
1*2	21.2014	2	10.60072	2.28058	0.158036
Error	41.8343	9	4.64826		
Total SS	230.3078	17			

The ANOVA table for measured maximum workpiece/cutting temperature shows that the main effect of cooling strategy is the dominant and statistically significant parameters on cutting temperature followed by the main effect of feed rate.

Figure 15 shows the Pareto chart of the main effects of cooling strategies and machining parameters and the interaction effects on maximum workpiece temperature. The chart shows that the linear effect of feed-rate is the dominant and statistically significant parameter on slot end-milling of titanium alloy Ti-6Al-4V with a decreasing effect on temperature.

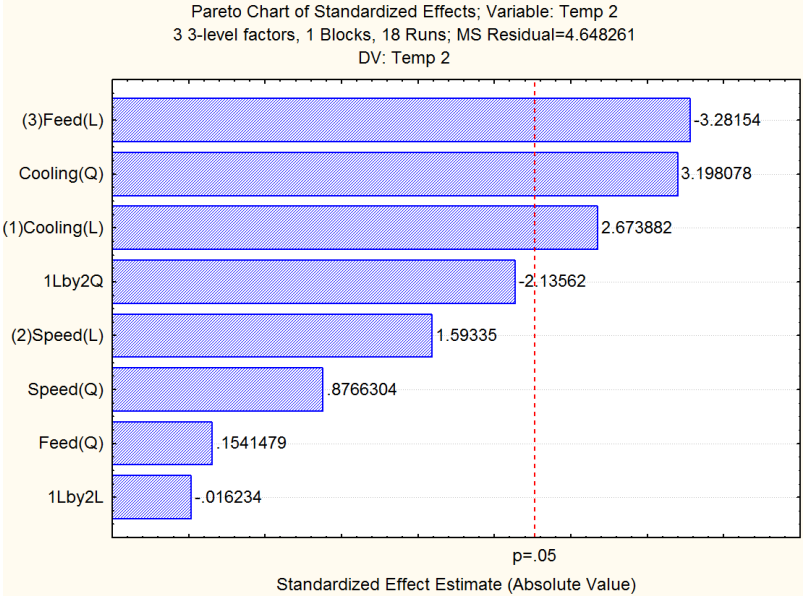

Figure 15. PARETO CHART FOR MAXIMUM WORKPIECE TEMPERATURE

The second statistically significant factor is the quadratic effect of cooling strategy which has an increasing effect on workpiece temperature. The 3rd statistically significant factor is the linear effect of cooling strategy with an increasing effect on workpiece temperature.

The marginal mean plots of all main effects of cooling strategies, spindle speed and feed-rate and their contribution to the maximum measure workpiece temperature are shown in Figure 16. The first plot in the first row of Figure 16 shows the effects of cooling strategies on maximum workpiece temperature T. From the plot it is seen that MQL produced the highest workpiece temperature while LN_2 cooling strategy produced the lowest workpiece maximum temperature, followed by emulsion cooling. The desirability plots are shown in the second row. From the desirability plot it can be seen that cryogenic cooling by LN_2 produced the lowest workpiece temperature followed by emulsion cooling while MQL produced the highest workpiece temperature among the

three cooling strategies. This explains why there was more burr formation at the exit of all the slots machined with MQL cooling strategy. There were fewer burr formation using Emulsion cooling and LN2 cooling. Cutting temperature drastically dropped when LN2 cooling was used as the highest cooling level for this experiment. The second plot on the top row of Figure 16 shows the effect of cutting speed at different levels ranging from 1000 rpm to 2000 rpm in an interval of 500 rpm. From the plot, it could be seen that low speed of 1000 rpm gave the lowest workpiece temperature which increases gradually to maximum value at a spindle speed of 1500 and 1550 rpm, after which the maximum workpiece temperature decreases slightly at 2000 rpm. The desirability plot shows the same trend/pattern. The third plot on the first row shows the effect of feed-rate on the temperature of the cutting tool and workpiece interface. The plot shows that low feed rate of 6 ipm gave the highest maximum workpiece temperature which can be because with lower feed rate, the tool spends more time during the milling process making conduction of heat generated at the cutting zone more effective. There is a linear decreasing trend (negative slope) of workpiece temperature as feed rate increases to mid feed rate level of 12 ipm. Maximum workpiece temperature decreased more when the highest feed rate level of 18 ipm is used, giving the lowest values of cutting temperature. The desirability plot also gave the same trend.

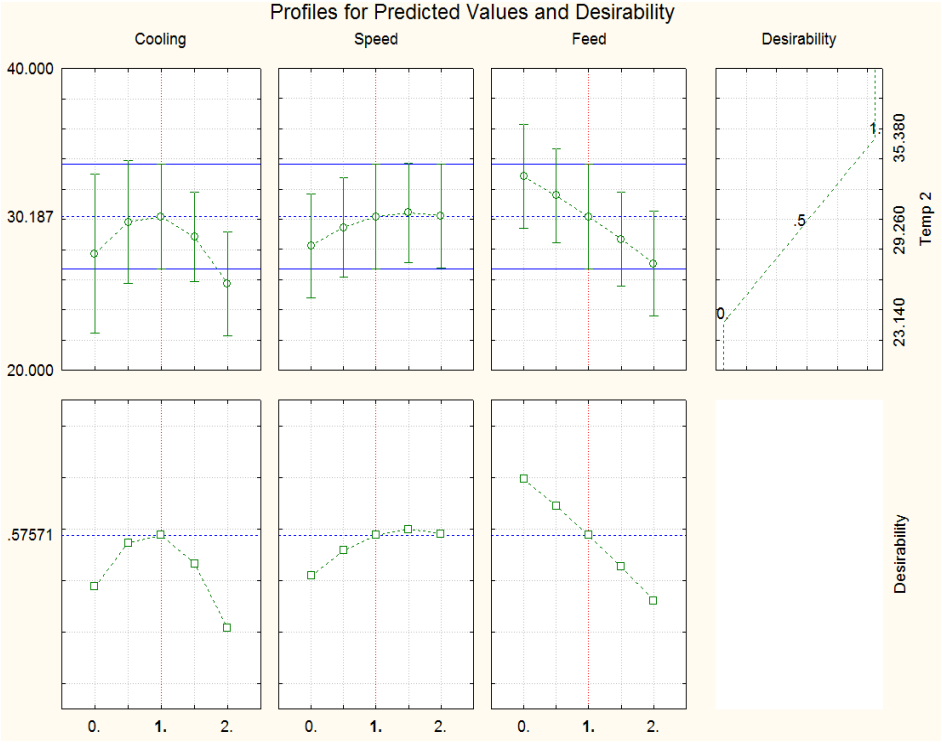

Figure 16. MARGINAL MEANS PLOT FOR MAXIMUM WORKPIECE TEMPERATURE USING PROFILES FOR PREDICTED VALUES AND DESIRABILITY PLOT

From the surface contour/desirability plots of workpiece temperature shown in Figure 17, it is seen from the first surface desirability plot against speed and cooling strategy that cryogenic cooling (LN2) gave the lowest cutting/workpiece temperature values for both low and high spindle speeds while the combination of intermediate speed of 1500 rpm and LN_2 gave the highest maximum workpiece temperature. The second desirability plot against feed and cooling strategy, cryogenic cooling by LN_2 gave lower workpiece maximum temperature at all feed levels. Emulsion cooling is next in choice when cooling and feed rate levels are combined for lower cutting temperature results. The third desirability plot against feed and speed show that low and high cutting speed also gave better (lower) cutting/workpiece maximum temperature values compared to mid

cutting speed values when combined with feed rate levels. It can be seen from the last plot that low feed of 6 ipm at either low speed of 1000 rpm or high speed of 2000 rpm is best machining parameter for reducing workpiece temperature.

The results from all the analyses of cutting force components and workpiece maximum cutting temperature (ANOVA, PARETO charts and marginal mean plots) were used to identify the optima machining parameters and cooling strategies for the main aim of evaluating cooling strategies. Cryogenic cooling has been identified as the most effective cooling strategy on cutting temperature while MQL has been identified as the most effective lubrication approach for end-milling of Ti-6Al-4V.

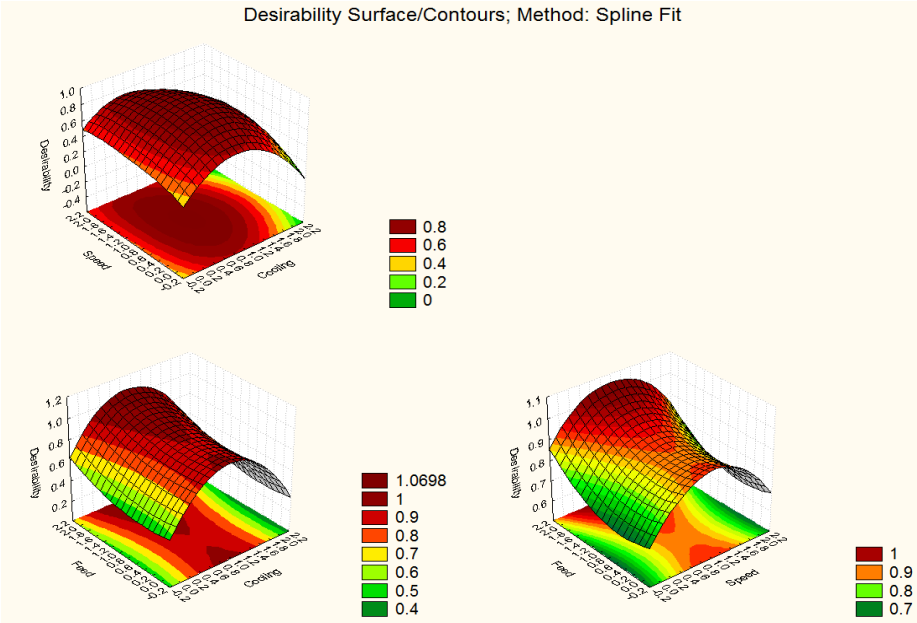

Figure 17. TEMPERATURE IN DEGREE C DESIRABILITY SURFACE/CONTOUR PLOTS

4.3.1 COMPARATIVE EVALUATION OF OPTIMA COOLING STRATEGIES AND MACHINING PARAMETERS CUTTING FORCE COMPONENTS, TOOL WEAR AND CUTTING TEMPERATURE

High cutting speed of 2000 rpm was also identified as best out of the three cutting speed levels. Low feed rate of 6 ipm was preferred to medium and high feed rate level of 12 and 18 ipm respectively because from analysis, it reduces cutting forces, tool wear and cutting temperature.

Figure 18 shows the plot for the comparative evaluation of MQL, LN_2 and MQL+LN_2 cooling strategies at the identified optimum feed (6 ipm) and speed (2000 rpm) respectively for thermocouple-measured workpiece temperature. The plot shows that the combination of MQL and LN_2 (i.e. MQL+LN_2) is best at the first pass and at the last (8^{th}) pass of 609.6 mm length of cutting. MQL produced the highest workpiece/cutting temperature at all passes with increase with the number of passes (length of cut) while LN_2 gave the lowest maximum workpiece temperature for the 2^{nd} and 4^{th} passes after which it increases rapidly at the 7^{th} and the 8^{th} passes to surpass the combination of MQL and LN_2 .

The cutting temperature is the key influencing factor of tool wear, although Ti-6Al-4V workpiece material has low thermal conductivity, the heat generation increases drastically at high cutting speed, therefore the temperature on the tool-chip and tool-workpiece contact area increases when there are no proper cooling and lubrication strategies, thus, this causes the increase in diffusion coefficient, and this is proportional to diffusion wear of the cutting tool.

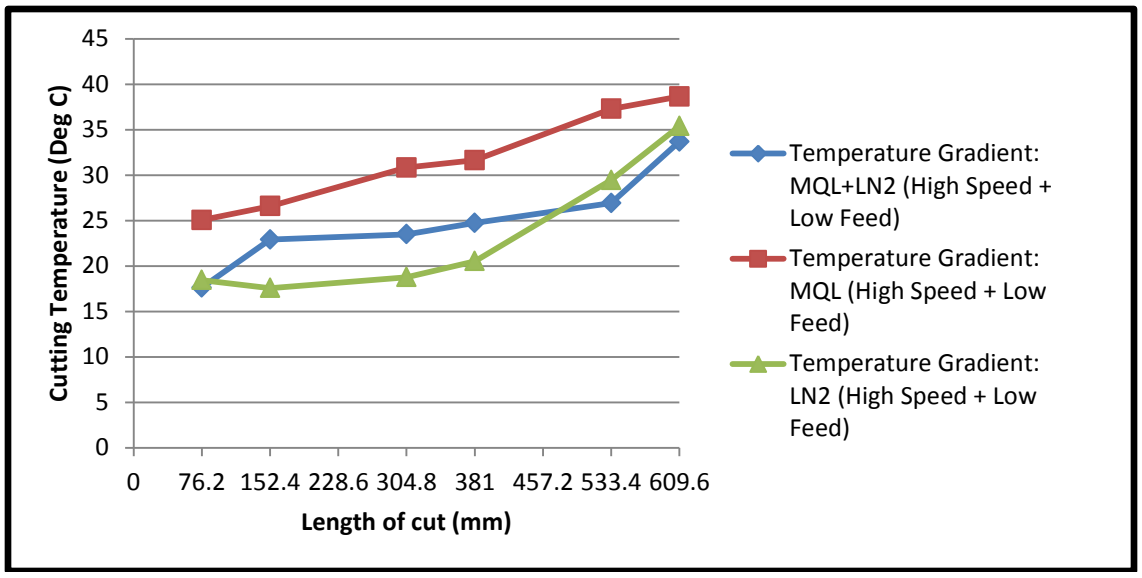

Figure 18. CUTTING/WORKPIECE TEMPERATURE VS LENGTH OF CUT FROM PASS 1 TO 8

4.4 EFFECTS OF COOLING STRATEGIES AND MACHINING PARAMETERS ON INDIRECT TOOL WEAR

In this study, maximum cutting force variations were used to indirectly investigate cutting tool wear propagation. Tool wear was analyzed by plotting the maximum cutting force variations for all the 9 experimental runs and their replications. Indirect tool wear measurement using maximum cutting force component values is adopted as indirect measure of tool wear where tool maker's microscope is not available or not functional.

The 7^{th} and the 8^{th} passes were used to perform analysis of variance (ANOVA), plot Pareto charts, surface contour desirability plot and marginal mean effect plots in order to evaluate the effects of cooling strategies and machining parameters on tool wear. It could be observed from the cutting forces plots of run 1 of 1000 rpm cutting speed and 6 ipm feed rate using emulsion cooling, shown in Figure 10 that F_x showed higher cutting force magnitude than F_y from the first pass to the last pass while F_z was the least cutting force component acquired in run 1 and all other runs. This is because previous research study has shown that cutting parameters and other cutting factors have no significant effects on F_z. In the same plot, it could be seen that the maximum forces recorded from the X and Y directions showed a linear slope from the first pass which was at a cutting distance of 76.2 mm to the fifth cutting pass which was at a distance of 381 mm, the slope of the recorded maximum forces started increasing on the 7^{th} and the 8^{th} pass when the cutting tool has significantly worn. The cutting force component Fy has a helpful correlation with the tool wear propagation, which can be used as a variable to monitor the cutting process [21]. Therefore, from the analysis of the first run, it can be seen that the tool wear in this experiment was not too obvious as variation in feed force F_y was not too high. The second plot in Figure 10 shows the how tool wear affects feed force. From the

plot, it can be observed that F_x was higher in the first and second passes 76.2 mm and 152.4 mm respectively, but significantly dropped in the 4th pass, 304.8 mm with feed force taking over. The increase in feed force F_y (i.e. slope/gradient) was highest between the 2nd and the 5th passes, 152.4 mm to 381 mm while it drops as it moves from the 5th pass to the last/8th pass, 609.6 mm. F_z as always, remained the least cutting force component acquired. The significant increase in F_y can be attributed to the increased feed rate and cutting speed because they were the only factors that changed at the second run. Figure 19 shows the plots of maximum cutting force components showing variation in cutting force for different passes for the three levels cooling strategies.

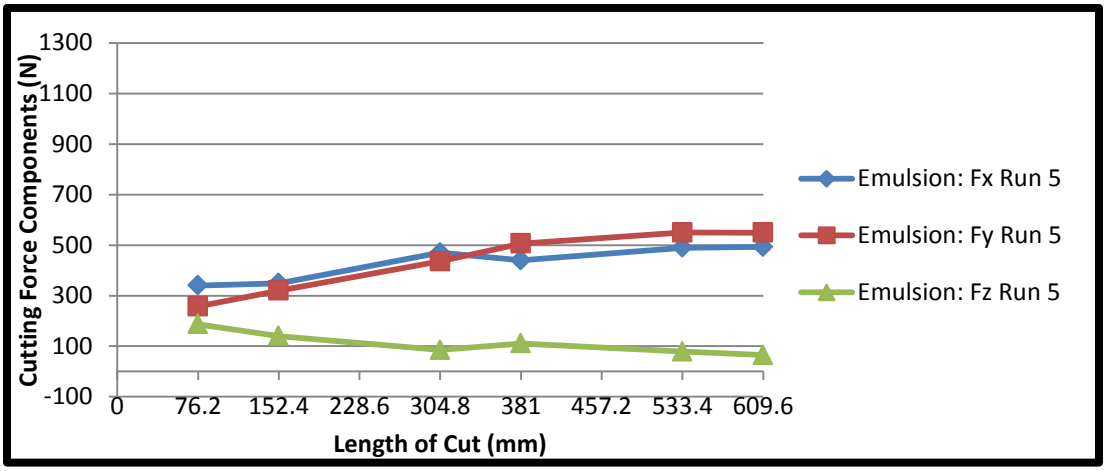

19a. Sample Plot of cutting force components for indirect tool wear measurement using emulsion cooling at n = 2000 rpm and F = 12 ipm

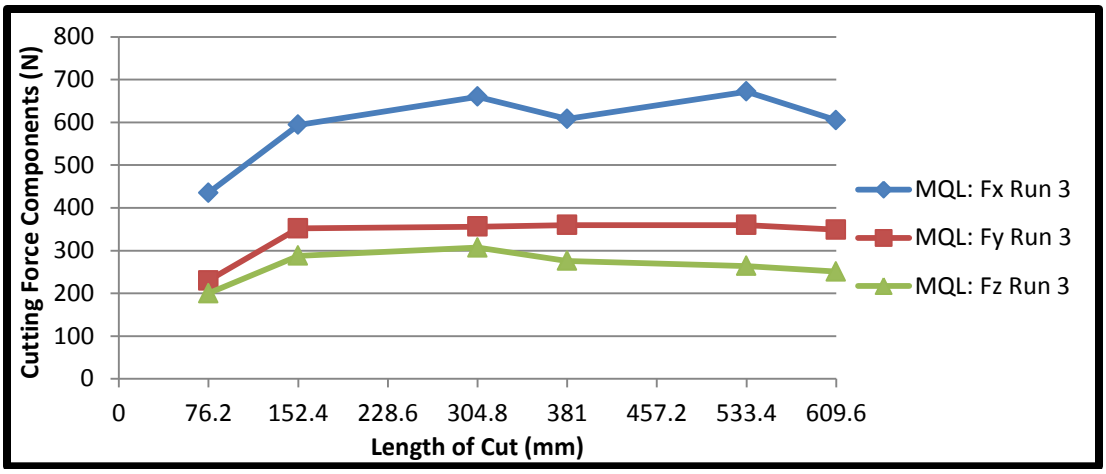

19b. Sample Plot of cutting force components for indirect tool wear measurement using MQL at n = 1000 rpm and F = 12 ipm

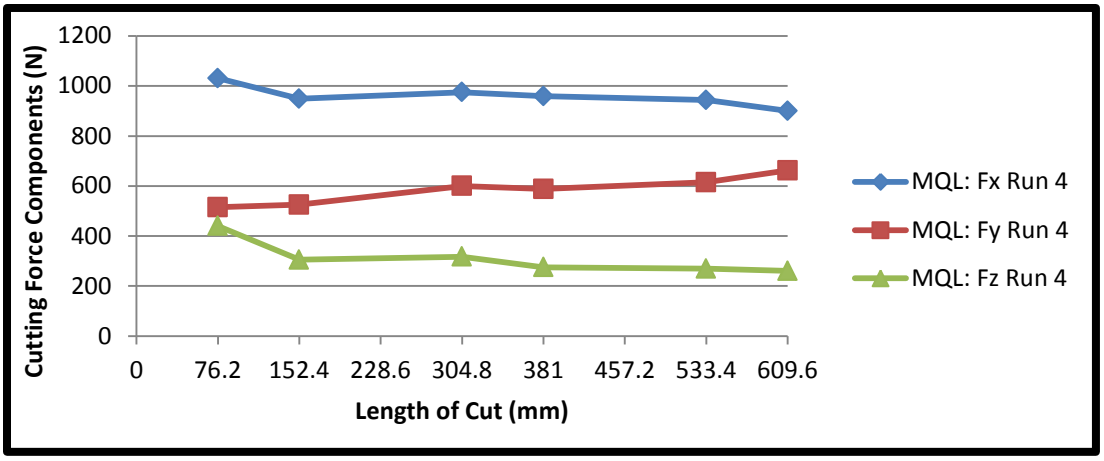

19c. Sample Plot of cutting force components for indirect tool wear measurement using LN_2 at n = 1000 rpm and F = 18 ipm

Figure 19. PLOTS OF MAXIMUM CUTTING FORCE COMPONENTS SHOWING VARIATION IN CUTTING FORCE FOR DIFFERENT PASSES FOR THE THREE LEVELS COOLING STRATEGIES

Figure 19a shows the plot for run 5 which represents the effect of feed rate of 12 ipm and a cutting speed of 2000 rpm using the conventional cooling condition (emulsion cooling). F_x was higher from the 1st pass of 76.2 mm but dropped at the 2nd pass of 152.4 mm and 4th pass of 304.8 mm. F_y increased above F_x just immediately after the 4th pass of 304.8 mm and continued the lead till the last pass of 609.6 mm. This again shows the

there's feed rate and cutting speed has some level of effects on tool wear. The effects of these factors will further be analyzed using STATISTICA in order to get the statistical significance of all the factors considered in this experiment on tool wear. Cutting force variations of run 6 shown in Figure 11 shows that there are no significant cutting force variations for all the cutting force components, also the magnitude of the maximum cutting forces are considerably too low compared to the magnitude of the maximum cutting forces values acquired for other runs. This experimental run is one with MQL cooling strategy with a feed rate of 6 ipm and a cutting speed of 1500 rpm. This further tells that low feed rate and medium speed could be recommended for lower cutting force components using MQL cooling strategy. The second plot in Figure 11 shows the plot of cutting force variation run 7 when MQL cooling strategy was kept constant while varying cutting speed and feed rate at 2000 rpm and 18 ipm respectively. The plot showed F_x with higher magnitude compared to F_y from the first pass to the fourth pass, but increase significantly at the fifth pass. The both forces were almost of the same magnitude between the fifth pass and the seventh pass but F_y increased significantly at the last pass. Run 3 of Figure 19 shows the variation in cutting forces using MQL cooling strategy at a cutting speed of 1000 rpm and a feed rate of 12 ipm, from the plot, it can be seen that there were no significant tool wear at between the seventh and the eight pass since this research focuses on the seventh and the eight pass for tool wear measurement as it is believed that after many passes, the tool would have worn out enough to clearly indicate tool wear effects from significant cutting force variations in the last pass. Although the slope of the cutting force values increase significantly between the first and the second pass, but not much significant increase was seen at subsequent passes, also the feed force

did not increase beyond F_x, this therefore shows that this condition has little effect on tool wear since it has been established that cutting force component F_y has a strong correlation with the tool wear propagation. In run 9 of Figure 12, cryogenic cooling (LN2) was used with a cutting speed of 2000 rpm and a feed rate of 6 ipm, the plot shows that there were no significant cutting force variation from the first to the last pass although there were very little indication that the feed force was more than the force perpendicular to the feed direction from the first pass to the last pass. This is an indication that there was minimal tool wear as can be seen from the cutting forces variation from the first to the last pass. The second plot in Figure 12 is the plot for run 8 which shows how cutting speed of 1500 rpm and a feed rate of 12 ipm affect cutting force components. This gave a higher cutting force magnitude for all the components with F_x more in magnitude than F_y from the first pass of 76.2 mm to the last pass of 609.6 mm.

Run 4 of Figure 19 displays the effect of 1000 rpm of cutting speed and 18 ipm of feed rate on cutting force components using cryogenic cooling (LN_2) strategy. From the plot, it can be seen that there were decreasing effect of this experimental run on F_x. The force might have been higher in the first pass as a result of the sharpness and newness of the cutting tool and the change in physical properties induced by the cold air used at -15 degree centigrade as this was the first experimental run using LN2.

However, the force in the feed direction showed a positive slope with a steady increase from the first to the last pass. This indicated there was tool wear in this experimental run which may be as a result of the feed rate used. F_x in this plot showed a negative slope as a result of high cutting force in the first pass. F_y remained below F_x in

all passes as a result of the low cutting speed level as it has been found that cutting speed increases tool wear [15].

4.4.1 ANOVA TABLES, SURFACE/CONTOUR DESIRABILITY PLOTS AND PARETO CHART FOR CUTTING FORCE COMPONENTS (FX, FY, AND FZ) FOR INDIRECT TOOL WEAR MEASUREMENT

ANOVA, Pareto chart, marginal plots and surface/contour desirability plots were used to statistically analyze the main and interaction effects of machining parameters and cooling strategies on cutting force components data acquired from the experimental runs. Tables 10 a, b, and c are the ANOVA table for the three components of the cutting force (F_x, F_y, and F_z) on the 7^{th} and 8^{th} passes used for indirect tool wear. The table shows the combined linear and quadratic main effects and the measurable linear by linear two-factor interactions, the P-values (P) associated with each factor level and interactions along with the sum of square effects (SS), degree of freedom (DF), mean square (MS) and F values (F). A low P-value (i.e. P-value < 0.05) indicates statistical significance for the factor (source) on the corresponding response. The 0.05 indicates 5% significant level. The corresponding Pareto charts are also shown below for cutting force components in F_x, F_y, and F_z at the 7^{th} and 8^{th} passes. The effects are separated into linear and quadratic main effects, and linear by linear two factor interactions, with all effects listed in order of their significance. The ANOVA table shows that the linear and quadratic main effects of cooling strategies, spindle speed and feed rate all have significant effects on cutting force components F_x, F_y, and F_z at the 7^{th} and 8^{th} passes used for tool wear measurement. The interaction of cooling strategies with spindle speed has significant effects on the all the three axes of the cutting force components F_x, F_y, and F_z. Table 11 shows the maximum

cutting force values for all experimental runs in the 7th and 8th passes which were used to perform ANOVA, and generate both Pareto charts and Marginal mean plots.

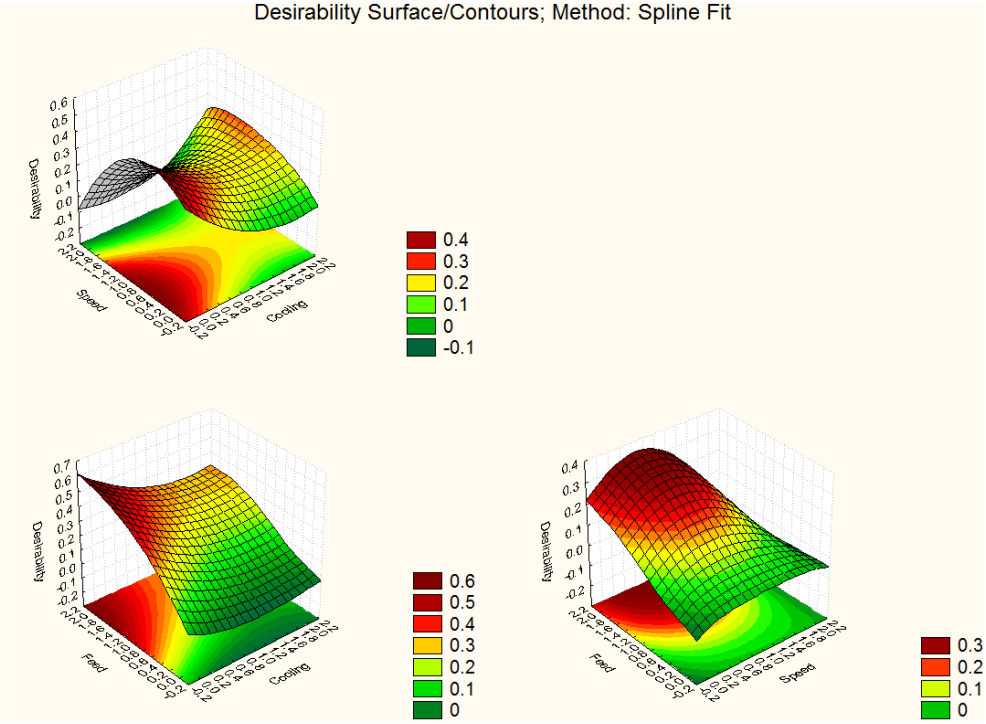

Figure 20. INDIRECT TOOL WEAR EVALUATION DESIRABILITY SURFACE/CONTOUR PLOTS

Figure 20 shows the effects of main effects of machining parameters and cooling strategies on the desirability of cutting forces.

From the first plot, it can be seen that the combination of speed and cooling shows that MQL is best at high speed while LN2 is good at low speed. The combination of feed rate and cooling shows that MQL and LN2 are best at low feed while emulsion is good at low feed rate. The combination of feed rate and speed tells us that low feed is best for cutting forces at both low and high cutting speed. From the plot, it can be seen that low feed is best for both MQL and LN2 cooling. The second plot of Figure 20 shows the effects of feed rate and cooling strategies. From the plot, it could be seen that MQL

cooling gave the lowest rate of tool wear in the X direction at the last pass while LN2 was next; emulsion cooling gave the highest F_x values. This shows how cooling strategies affect each experimental run after the tool has worn significantly. It can also be observed that cutting force component was greatly decreased when cutting speed was highest (2000 rpm) at a low feed rate of 6 ipm, also, cutting force components (F_x, F_y, F_z) were decreased at low feed rate of 6 ipm and low cutting speed of 1000 rpm; therefore, increased cutting speed is encouraged in order to reduce tool wear but increased feed rate for all speed levels (1000 rpm ,1500 rpm and 2000 rpm) increases tool wear as can be seen from the third plot of Figure 20.

Table 10: ANOVA TABLES FOR INDIRECT TOOL WEAR MEASUREMENT

Table 10a. ANOVA Table for Indirect Tool Wear on F_x

	ANOVA; Var.:Fx; R-sqr=.99496; Adj:.99047 3 3-level factors, 1 Blocks, 18 Runs; MS Residual=581.6111 DV: Fx				
Factor	SS	df	MS	F	p
(1)Cooling L+Q	107384	2	53692.2	92.3163	0.000001
(2)Speed L+Q	230154	2	115077.2	197.8593	0.000000
(3)Feed L+Q	470873	2	235436.3	404.8003	0.000000
1*2	27004	2	13502.0	23.2148	0.000280
Error	5234	9	581.6		
Total SS	1038007	17			

Table 10b. ANOVA Table for Indirect Tool Wear on F_y

	ANOVA; Var.:Fy; R-sqr=.94117; Adj:.88887 3 3-level factors, 1 Blocks, 18 Runs; MS Residual=10838.06 DV: Fy				
Factor	SS	df	MS	F	p
(1)Cooling L+Q	275430	2	137715.2	12.70663	0.002392
(2)Speed L+Q	187464	2	93732.2	8.64843	0.008026
(3)Feed L+Q	781517	2	390758.3	36.05428	0.000050
1*2	122508	2	61254.2	5.65177	0.025705
Error	97542	9	10838.1		
Total SS	1657971	17			

Table 10c. ANOVA Table for Indirect Tool Wear on F_z

Factor	SS	df	MS	F	p
ANOVA; Var.:Fz; R-sqr=.98402; Adj:.96981 3 3-level factors, 1 Blocks, 18 Runs; MS Residual=404.7222 DV: Fz					
(1)Cooling L+Q	7134.8	2	3567.39	8.8144	0.007586
(2)Speed L+Q	87811.1	2	43905.56	108.4832	0.000001
(3)Feed L+Q	82515.7	2	41257.86	101.9412	0.000001
1*2	39275.1	2	19637.56	48.5211	0.000015
Error	3642.5	9	404.72		
Total SS	227890.3	17			

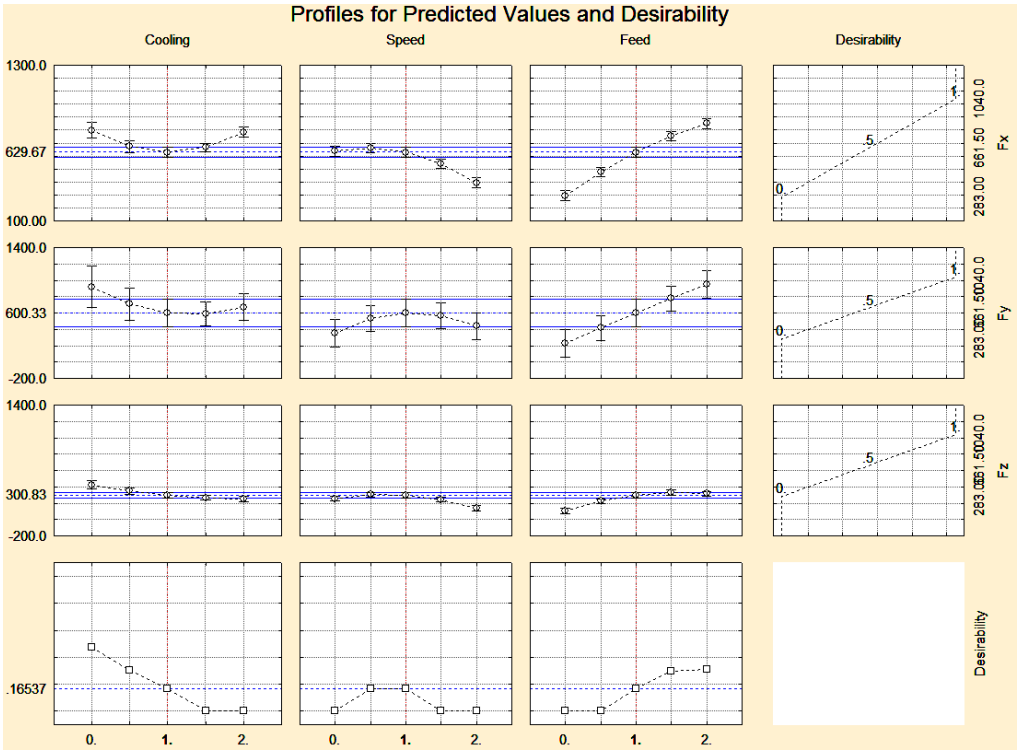

Figure 21. MARGINAL MEANS PLOT FOR TOOL WEAR IN THE X, Y AND Z CUTTING AXES

4.4.2 MARGINAL MEAN PLOT OF MAIN EFFECTS ON CUTTING FORCE COMPONENTS (F_X, F_Y, AND F_Z) ON THE 7TH AND 8TH PASSES USED FOR INDIRECT TOOL WEAR MEASUREMENT

The marginal mean plots of all significant main effects of cooling strategies, spindle speed and feed rate and their contribution to indirect tool wear are shown in Figure 21.

4.4.2.1 EFFECT OF COOLING STRATEGY ON INDIRECT TOOL WEAR

The positive slope from the marginal mean plot shown in the tool wear marginal mean plot summary of Figure 21shows that both Emulsion and LN2 cooling strategies are ineffective with tool wear propagation in F_x as both levels of cooling showed a significant increase in F_x compared to MQL cooling approach which showed the least F_x value. For cutting force component in the feed direction, F_y, the second plot in the first column of second row shows that conventional emulsion cooling gave the highest value of cutting force in the feed direction, F_y. The best cooling strategy on F_y from the plot is shown to also be MQL which is slightly better than LN_2 cooling strategy with almost an insignificant margin.

On the Z force (F_z), conventional emulsion cooling also gave the highest Z force (F_z) while LN_2 gave the lowest cutting force value in the Z direction (F_z), slightly followed by MQL with an insignificant margin. Figure 21 shows the marginal means plot for tool wear in the x, y and z cutting axes.

4.4.2.2 EFFECT OF SPINDLE/CUTTING SPEED ON INDIRECT TOOL WEAR

In Figure 21, the first plot on the second column of the first row, it can be seen that low and medium cutting/spindle speed 1000 rpm and 1500 rpm respectively are least preferred with 630 N of cutting force component in X axis (F_x) while high spindle speed of 2000 rpm reduced cutting force component in X axis F_x by about 50%. This shows that high spindle speed (2000 rpm) is very effective in reducing cutting force component F_x. The second plot on the second row of the second column shows that low speed of 1000 rpm and high speed of 2000 rpm are best in reducing cutting force component in Y axis F_y while medium speed of 1500 rpm is the least preferred. The third plot on the third

column of the second row shows that both low and medium speed are least preferred on F_z while high speed is shown to be best in cutting force component reduction on Z axis (F_z).

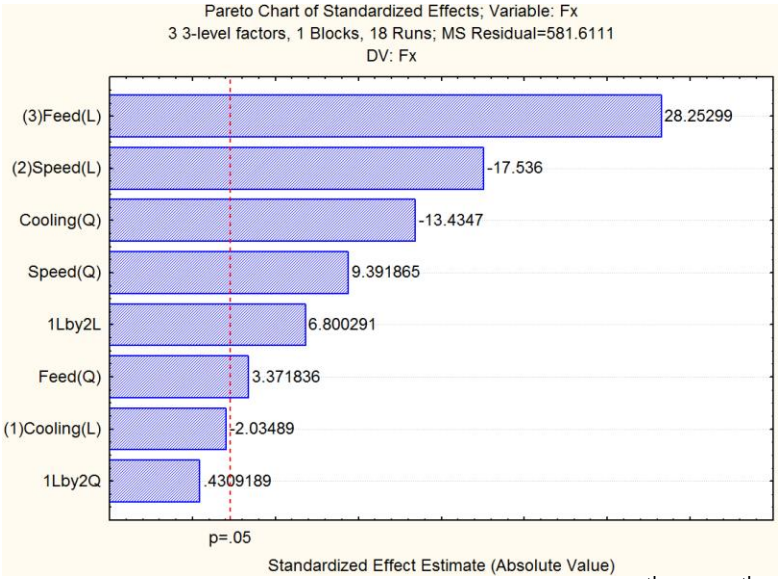

22a. Pareto Chart for F_x using Force Data for the 7th and 8th Passes

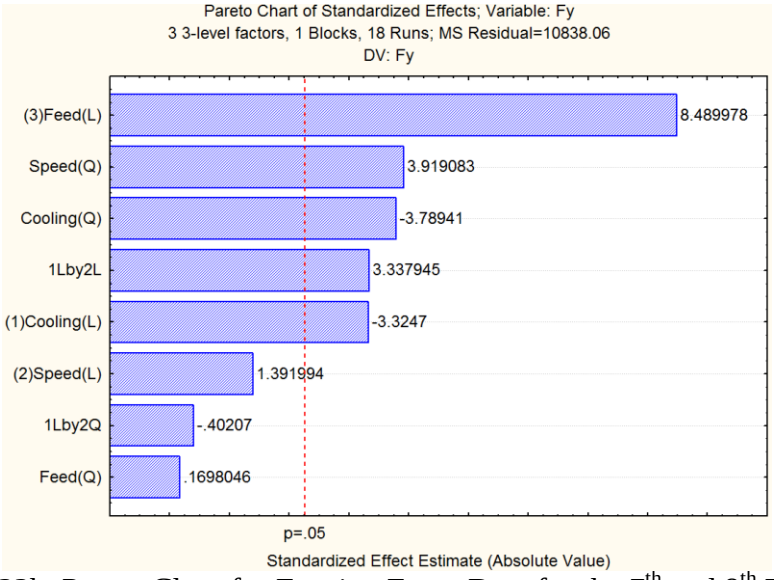

22b. Pareto Chart for F_y using Force Data for the 7th and 8th Passes

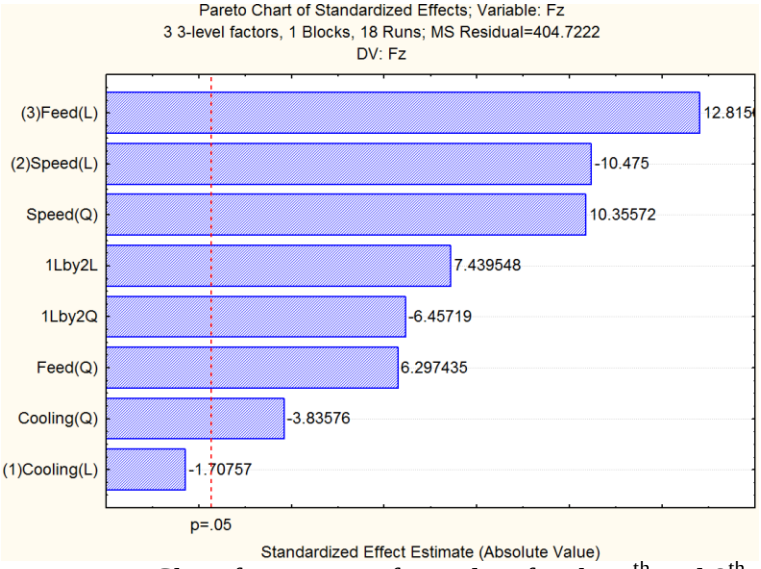

22c. Pareto Chart for F_z using force data for the 7th and 8th Passes

Figure 22. PARETO CHARTS FOR CUTTING FORCE COMPONENTS (F_X, F_Y, AND F_Z)

4.4.2.3 EFFECT OF FEED RATE ON INDIRECT TOOL WEAR

In Figure 21 the first plot on the third column shows that as feed rate increases, tool wear increases for F_x. The same trend is followed on the second plot (on the second row) on the third column for F_y. The trend changed a little bit on F_z although it can be seen that low feed rate of 6 ipm is still preferred as was seen in the other plots for F_x and F_y but on F_z, the plot shows that medium and high feed rate of 12 ipm and 18 ipm respectively produced approximately the same effect on cutting force component on Z axis.

The plots on the third column of Figure 21 therefore shows that low feed of 6 ipm is the optimum feed rate for reducing cutting force component on Z axis F_z for the last passes of 7 and 8 used for indirect tool wear measurement.

Table 11: INDIRECT TOOL WEAR DATA PROCESSING AND ANALYSES

Table 11a. Pass 7 with cutting forces for all experimental runs

Treatment Combination	Cooling Methods	Speed (RPM)	Feed (IPM)	Fx (N)	Fy (N)	Fz (N)	Fr (N)
(0,0,0)	Emulsion	1000	6	546	451	125	708.1786
(0,1,2)	Emulsion	1500	18	1040	1270	451	1641.493
(1,0,1)	MQL	1000	12	672	360	264	762.3542
(2,0,2)	LN2	1000	18	944	615	269	1126.659
(0,2,1)	Emulsion	2000	12	490	550	79	736.6139
(1,1,0)	MQL	1500	6	293	225	105	369.4239
(1,2,2)	MQL	2000	18	610	570	182	834.8653
(2,1,1)	LN2	1500	12	767	639	247	998.3036
(2,2,0)	LN2	2000	6	283	349	75	449.3217

Table 11b. Pass 8 with cutting forces for all experimental runs

Treatment Combination	Cooling Methods	Speed (RPM)	Feed (IPM)	Fx (N)	Fy (N)	Fz (N)	Fr (N)
(0,0,0)	Emulsion	1000	6	582	429	172	723.0249
(0,1,2)	Emulsion	1500	18	1001	1270	429	1617.066
(1,0,1)	MQL	1000	12	605	349	251	698.4454
(2,0,2)	LN2	1000	18	900	662	260	1117.248
(0,2,1)	Emulsion	2000	12	493	549	65	737.8686
(1,1,0)	MQL	1500	6	295	229	107	373.4515
(1,2,2)	MQL	2000	18	620	1003	121	1179.156
(2,1,1)	LN2	1500	12	800	708	262	1068.3
(2,2,0)	LN2	2000	6	288	347	89	450.9468

4.5 COMPARATIVE, FEED RATE AND SPINDLE SPEED ON INDIRECT TOOL WEAR EFFECTS OF OPTIMUM COOLING STRATEGIES

Figure 23a is the bar charts of the maximum cutting force components F_x, F_y and F_z for optimum cutting parameters (spindle speed of 2000 rpm, and feed rate of 6 ipm), optimum cooling strategy (MQL and LN_2) and combination of MQL and LN_2 for first and eighth passes during slot end-milling of Titanium alloy.

In figure 23a, the bar charts and graphs showing comparative analyses of effects of optima machining parameters and cooling strategies on cutting forces for indirect tool wear monitoring are shown.

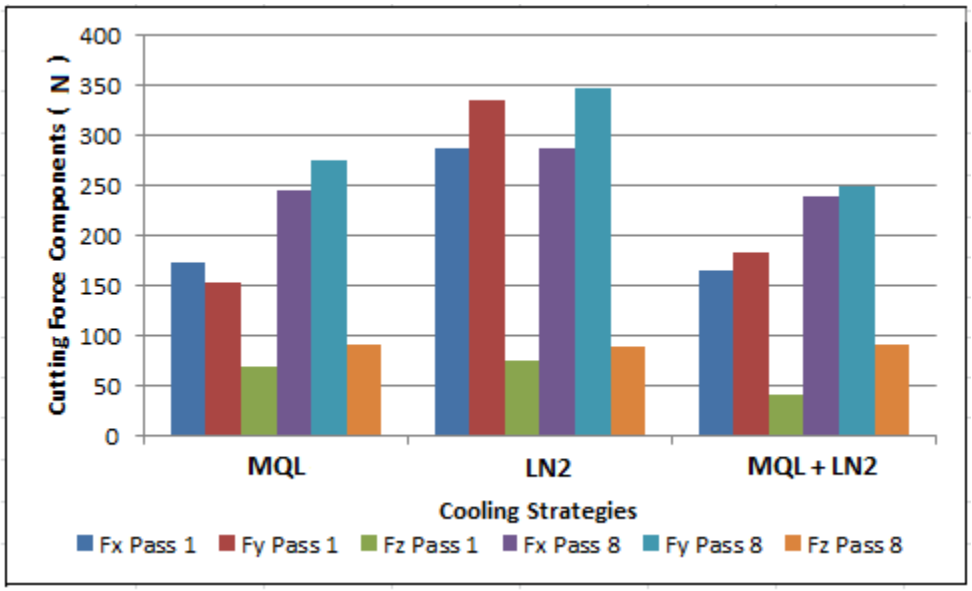

23a. Bar charts of the maximum cutting force components F_x, F_y and F_z for optimum machining parameters (spindle speed of 2000 rpm, and feed rate of 6 ipm), optimum cooling strategy (MQL and LN_2) and combination of MQL and LN_2 for first and eighth passes

The chart shows that LN_2 cooling strategy alone was the worst in reducing cutting forces and indirect tool wear in X, Y and Z axes (F_x, F_y and F_z), while MQL was next best in reducing cutting forces and indirect tool wear in X, Y and Z axes. Combination of

MQL and LN_2 was the best in reducing cutting forces in reducing cutting forces and tool wear in X, Y and Z axes and indirect tool wear. Figure 23 shows 3 different sets of graphs for comparative analyses of cutting forces on indirect tool wear. The first sets of graphs, i.e. Figure 23bi shows the plot for cutting force components using MQL at 2000 rpm and Feed Rate of 6 ipm. The plot shows the comparison cutting force components acquired at the cutting zone from a cutting length of 76.2 mm till 609.6 mm. The force component perpendicular to the feed direction F_x can be seen from the graph is highest at the first pass but by the cutting length of 381 mm, it drops slightly while the force component in the feed direction F_y increases at this same cutting length and is approximately the same cutting force value at this cutting length. F_y which is the major indicator for tool wear increases above F_x up till the last pass at 609.6 mm. This shows that tool wear increases significantly with increase in cutting length, this can be seen from the gradient of the F_y trend line. From Figure 23bii, spindle speed of 2000 rpm and feed rate of 6 ipm was used with a LN_2 cooling strategy; the plot shows variation in cutting force component perpendicular to feed direction F_x producing an approximately zero slope, showing that the rate of tool wear in X direction is very minimal, also F_y produced an almost horizontal trend line with an approximately zero slope indicating that tool wear using LN_2 cooling strategy was minimal as the slope of F_y is used as an indicator for tool wear. The same was followed for F_z which is the least cutting force component out of the three force components acquired during slot end-milling of Titanium alloy.

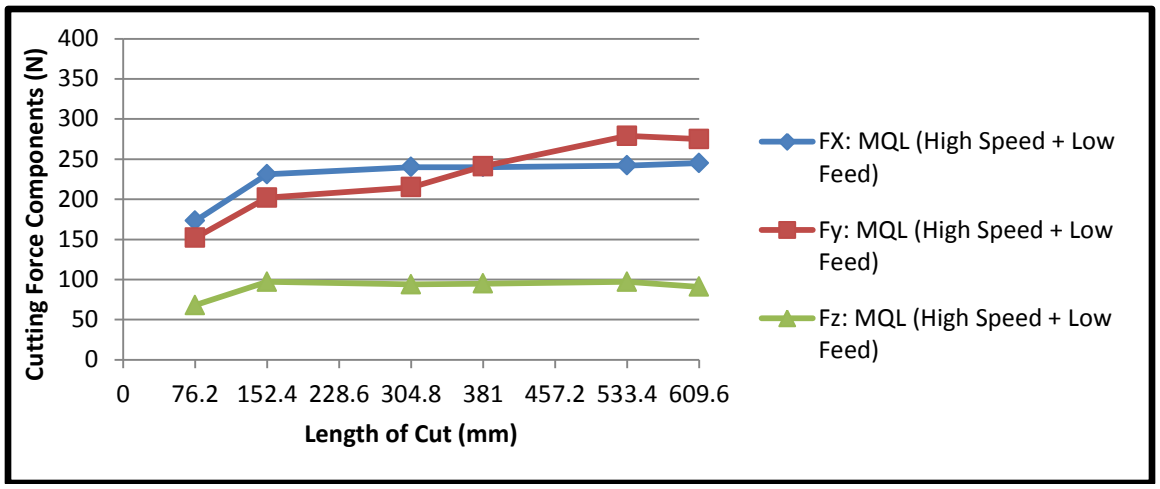

23bi. Plot of Cutting Force Components using MQL Cooling Strategies at Spindle Speed of 2000 rpm and Feed Rate of 6 ipm

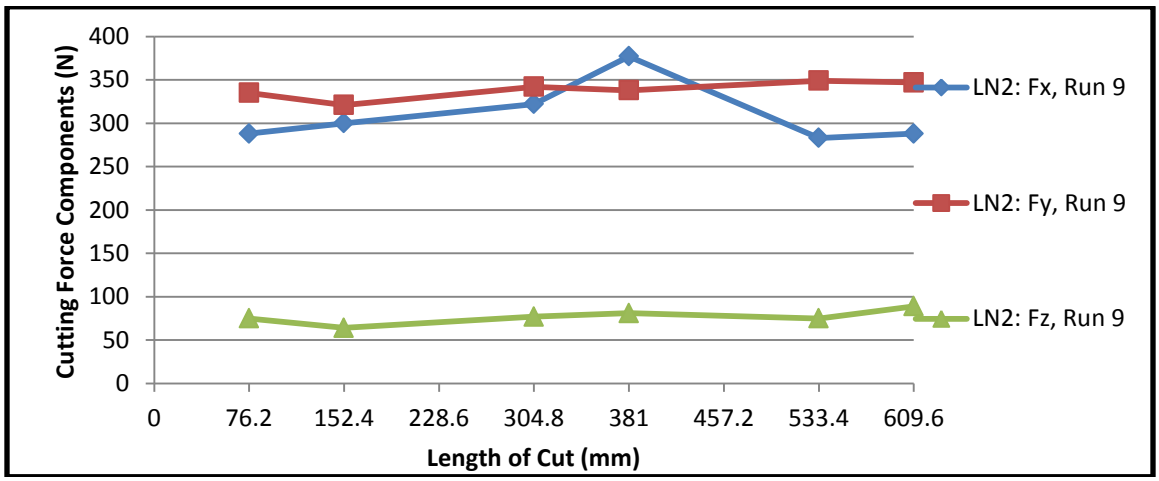

23bii. Plot of Cutting Force Components using LN_2 Cooling Strategies at Spindle Speed of 2000 rpm and Feed Rate of 6 ipm

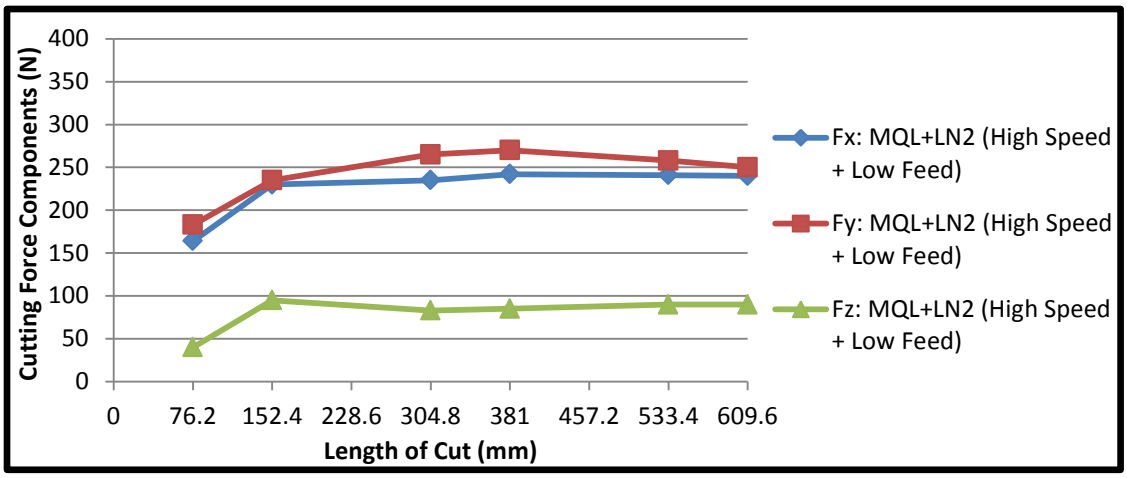

23biii. Plot of Cutting Force Components using MQL+LN_2 Cooling Strategies at Spindle Speed of 2000 rpm and Feed Rate of 6 ipm

Figure 23. BAR CHARTS AND GRAPHS SHOWING COMPARATIVE ANALYSES OF EFFECTS OF OPTIMA MACHINING PARAMETERS AND COOLING STRATEGIES ON CUTTING FORCES FOR INDIRECT TOOL WEAR MONITORING

Figure 23biii shows the effect of the combination of MQL and LN_2 on cutting forces and tool wear in order to compare the effects seen from Figures 23bi and 23bii, where the same cutting parameters of 2000 rpm spindle speed and 6 ipm feed rate but using combination of LN_2 and MQL cooling strategies. From the figure, it could be seen that lowest cutting forces were acquired when compared with the values of cutting forces acquired in Figure 23bi and 23bii. For tool wear, it could be seen that tool wear was highest when LN2 was used as the cooling method since maximum F_y acquired at a cutting length between 533.4 mm and 609.6 mm was slightly above 350 N compared with a maximum F_y of 275 N at a cutting length between 533.4 mm and 609.6 mm for MQL approach and a maximum of 265 N F_y at cutting length of 381 mm for the combination of MQL and LN_2. Therefore, it could also be seen that there are slightly higher forces when MQL was the cooling approach with the same cutting parameters than with combination of MQL and LN_2.

5. CONCLUSIONS

This research investigated the effects of machining parameters and cooling strategies on cutting force components, cutting temperature and indirect tool wear during slots end-milling of titanium alloy Ti-6Al-4V workpiece. From the results, the following conclusions are made:

1 A cryogenic flow line was designed, and in-house built and calibrated at Missouri University of Science and Technology for the regulation of the temperature of liquid nitrogen during end-milling of difficult-to-cut metals.

2 Analysis of variance shows that cooling strategy, spindle speed, and feed rate all have significant effects on cutting force components F_x, F_y and F_z, while the interaction effects of cooling strategy and speed has significant effect only on F_x component.

3 Among the three cooling strategies investigated (conventional emulsion, MQL and LN_2), environmentally friendly MQL from vegetable oil was found to be the best lubrication strategy that gave the lowest cutting force followed by LN_2, while emulsion gave the highest cutting force components. Cryogenic cooling by LN_2 was found to be the best cooling strategy for reducing workpiece temperature and improving tool life during slot end-milling of titanium alloy Ti-6Al-4V.

4 Minimum Quantity Lubrication (MQL), high spindle speed of 2000 rpm, and low feedrate of 6 ipm are the optimum cooling strategy and machining parameters that gave the lowest cutting force components F_x, F_y and F_z for slot end-milling of Ti-6Al-4V.

5 Cutting force component F_x perpendicular to the feed direction Y, was found to be larger than the other cutting force components F_y and F_z for the initial passes, while the axial force F_z is the least cutting force components and remains fairly stable for all cutting passes.

6 Main effects of cooling strategy are the dominant and statistically significant factor on workpiece temperature, followed by main effect of feedrate.

7 Cryogenic Liquid Nitrogen (LN_2) cooling, low spindle speed of 1000 rpm and high feedrate of 18 ipm are the optimum cooling strategy and machining parameter that gave the lowest maximum workpiece/cutting temperature.

8 The cutting force component in the feed direction F_y (feed force) is more sensitive to tool wear and increases more rapidly than the other cutting force components F_x and F_z, thus this is recommended to be used for indirect monitoring of tool wear.

9 Cryogenic Liquid Nitrogen (LN_2) cooling, high spindle speed of 2000 rpm, and low feed rate of 6 ipm are the optimum cooling strategy and machining parameters that gave the lowest tool wear results.

10 Comparative evaluation of MQL, LN_2 and MQL+LN_2 cooling strategies at optimum machining parameters of 2000 rpm and 6 ipm show that combination of MQL and LN_2 gave the lowest cutting force components for the first and last passes.

6. ACKNOWLEDGEMENTS

The financial support from the National Science Foundation (NSF) under grant no. CMMI 800871 and Intelligent Systems Center (ISC) of Missouri University of Science and Technology are gratefully acknowledged. The financial assistance provided in the form of Graduate Teaching Assistantship by the Department of Mechanical and Aerospace Engineering at Missouri University of Science and Technology is also gratefully acknowledged.

7. REFERENCES

[1] A. Devillez, F. Schneider, S. Dominiak, D. Dudzinski, D. Larrouquere, "Cutting forces and wear in dry machining of Inconel 718 with coated carbide tools," Wear, 2007, Vol.262, pp.931-942

[2] A. Jawaid, S. Koksal, S. Sharif, "Cutting performance and wear characteristics of PVD coated and uncoated carbide tools in face milling Inconel 718 aerospace alloy," Journal of Materials Processing Technology, 2001, Vol.116, pp.2-9

[3] Raul B.Rebak, "Effects of Metallurgical Variables on the corrosion of High-Nickel Alloys," ASM Handbook, 2005, Vol.13A, pp.279

[4] Z.Y. Wang, K.P. Rajurkar, J. Fan, S. Lei, Y.C. Shin, G. Petrescu, "Hybrid machining of Inconel 718, International Journal of Machine Tools & Manufacture," 2003, Vol.43, pp.1391-1396

[5] M. Alauddin, M.A. Mazid, M.A. El Baradi, M.S.J. Hashmi, "Cutting forces in the end milling of Inconel 718," Journal of Materials Processing Technology, 1998, Vol.77, pp.153-159

[6] P.K Wright, J.G. Chow, 1982, "Deformation Characteristics of Nickel Alloys during Machining," Transaction of ASME, Journal of Engineering Materials Technology. Vol. 104, 85-93

[7] Hanasaki, S., Fujiwara, J., 1994, "Ceramic Coated Cutting Tools. Key Engineering Materials," Vol. 96, pp 197-220

[8] A. Chukwujekwu Okafor, B. Oguejiofor, 2007, "Investigating the effects of cutting parameters on temperature in high speed end-milling of thin-walled titanium structure," Proceedings of the 10th CIRP international workshop on modeling of machining operations, Regio-Calabria, Italia pp 381-388

[9] A. Chukwujekwu Okafor, S. Aramalla, 2006," Modeling of Cutting Forces in High Speed End Milling of Titanium Alloys using Finite Element Analysis and Mechanistic Model," Proceedings of the 9th CIRP international workshop on modeling of machining operations, Ljubljana Slovenia, pp.219-226

[10] A. Chukwujekwu Okafor, Development of Virtual Computer Numerical Control Machine Tools and Web-based Machining Process Simulation and Learning – NSF Annual Report Year 3, May 31, 2011

[11] Yuan S.M., Yan L.T, Liu W.D. Liu Q., "Effects of Cooling Air Temperature on Cryogenic Machining of Ti-6Al-4V Alloy," Journal of Material Processing Technology (2010)

[12] Abele E. & Frohlich B., "High Speed Milling of Titanium Alloys" Advances in Production Engineering & Management 3 (2008) 3, 131-140

[13] Turnad L Ginta, A.K.M. Nurul Amin, A.N.M Karim, Anayet Patwari, M.A. Lajis, (2008), "Modeling and Optimization of Tool Life and Surface Roughness for End Milling Titanium Alloy Ti-6Al-4V Using Uncoated WC-Co Inserts," Curtin University of Technology Science and Engineering International Conference.

[14] G.S.Geng, J.H. Xu, Y.F. Ge and Y.C. Fu, (2004),"Experimental Study on the Milling of a High Strength Titanium Alloy," Material Science Forum Vols 471-472, pp 731-735.

[15] Xiaoqin Wang, Xing Ai, Jun Zhao and Tiantian Li, "Experimental Investigation on Cutting Force and Tool Wear of Carbide Tools in Ti6Al4V Turning" *Key Engineering Materials Vols. 375-376 (2008) pp 231-235*

[16] S. Zhang & J. F. Li & J. Sun & F. Jiang, "Tool wear and cutting forces variation in high-speed endmilling Ti-6Al-4V alloy" *International Journal of Advanced Manufacturing Technology (2010) vol. 46 pp 69–78*

[17] Shane Hong, Irel Markus, Woo-cheol Jeong, (2001), "New Cooling Approach and Tool Life Improvement in Cryogenic Machining of Titanium Alloy Ti-6Al-4V", International Journal of Machine Tools & Manufacture, 41, pp 2245-2260

[18] Ke Ying-lin, Dong Hui-yue, Liu Gang, Zhang Ming, "Use of Nitrogen Gas in High-Speed Milling of Ti-6Al-4V," *Trans Nonferrous Met Soc China vol. 19 (2009) pp 530-534*

[19] E.O. Ezugwu, J. Bonney, Y. Yamane, "An Overview of the Machinability of Aeroengine Alloys", Journal of Material Processing 134 (2004) pp 233-253

[20] Z.Y. Wang, K.P. Rajurkar, "Cryogenic Machining of Hard-to-Cut Materials," Wear vol. 239 2000 pp168–175

[21] H.Z. Li, H. Zeng, X.Q. Chen, "An experimental study of tool wear and cutting force variation in the end milling of Inconel 718 with coated carbide inserts" Journal of Materials Processing Technology vol. 180 (2006) pp. 296–304

II EXPERIMENTAL INVESTIGATION OF THE EFFECTS OF COOLING STRATEGIES AND CUTTING PARAMETERS ON SURFACE ROUGHNESS AND RESIDUAL STRESSES IN END-MILLING OF TITANIUM ALLOY, TI-6AL-4V, USING DESIGN OF EXPERIMENTS

A. Chukwujekwu Okafor and Emenike Chukwuma
Laboratory for Industrial Automation and Flexible Manufacturing
Department of Mechanical and Aerospace Engineering
Missouri University of Science and Technology
327 Toomey Hall, 1870 Miner Circle, Rolla, MO 65409-0050, USA
E-mails: okafor@mst.edu, encwdf@mst.edu

ABSTRACT

This paper presents the results of experimental investigation of the effects of cutting parameters (spindle speed and feed rate) and cooling strategies (emulsion cooling, Minimum Quantity Lubrication MQL and Liquid Nitrogen LN_2 Cooling) on surface roughness and residual stresses in endmilling of titanium alloy Ti-6Al-4V using fractional factorial design of experiments (DOE). STATISTICA was used to study and analyze the surface roughness data measured in the feed direction and vertical to the feed direction while residual stresses measured on the ribs were also studied with the same software. Endmilling experiments were conducted using four-flute 0.5 inch diameter uncoated solid carbide endmill on Cincinnati Milacron, Sabre 750 vertical machining center equipped with Acramatic 2100 controller. Surface roughness was measured at three points using a portable Brown & Sharpe Pocket Surf profilometer which uses a piezoelectric probe for measurement, the measurements were 1 inch apart on the ribs, and the average values were taken. Optimum cutting and cooling parameters were identified from the minimum surface roughness and residual stresses using analysis of variance ANOVA at a significance level of 0.05. Pareto charts and marginal mean plots showing the individual effects of each factor and their levels on surface roughness and residual

stresses are also presented. From the analyses, it was observed that surface roughness on the web increased with increase in feed while MQL was found as the optimal cooling condition on the web. On the rib, surface roughness increased with increase in speed but dropped at maximum speed while high and low feed rates were identified as the optimal feed rate for surface roughness on the rib. Therefore, with focused attention on surface roughness on the rib, it can be concluded that the optimum cooling condition of the combination of MQL and LN_2 and cutting parameters of low feed rate and high spindle speed helps to reduce surface roughness. The combination of MQL and LN_2 was the best in producing the most compressive residual stresses on the surface of the left rib after slot-end-milling of titanium alloy while LN_2 cooling strategy alone was the worst with high tensile residual stress on the surface of the left rib after slot end-milling of titanium alloy. All the cooling strategies were tensile in the subsurface of the left rib with MQL as the least tensile on the subsurface.

Keywords: Minimum Quantity Lubrication, Cryogenic Machining, end-milling, fractional factorial design of experiment, residual stresses, surface roughness, Titanium alloy Ti-6Al-4V

1. INTRODUCTION/LITERATURE REVIEW

The fast improvement in today's high-speed milling industry, particularly in the aerospace industries, the surface roughness of machined parts and residual stress analyses are very important in evaluating parts overall quality. The adoption of the end milling process in manufacturing is because of its versatility and efficiency and also because it may be used for the rough and finish machining of such features as slots, pockets, peripheries, and faces of components. Cutter breakage, generation of finished part surface which does not conform to product design specifications and process instability are some of the problems which may arise from end milling process. It may result to shank or tool breakage if the level of cutting force applied is in excess. The stability of the end milling process is also dependent on the cutting force system and its interaction with the dynamics of the machining system.

However, it could be worse with the machining of titanium and its alloys because of several inherent properties of the material. Titanium is very chemically reactive therefore has the tendency of welding to the cutting tool during machining thus, leading to premature tool failure. Its low thermal conductivity increases the temperature at the tool-work interface thus, affecting the tool life adversely.

In CNC industrial machining process, milling is a basic machining operation with end-milling as the most commonly used metal removal operation process encountered. Because of its wide use in machining delicate to machine parts, such as found in aerospace and automotive sectors, the quality cannot be over-emphasized. Surface roughness plays a very important role in functional attributes of parts such as; reduction of surface friction, wearing, light reflection, heat transmission, ability to distribute and

hold lubricants, coating and resistance to fatigue. Residual stresses also play important roles in the performance of machined components in engineering applications. The effects of residual stresses in metals and alloys include but not limited to fatigue life, corrosion resistance, and part distortion. The performance of machined components can be enhanced or impaired by residual stresses. Because of this, understanding the residual stress imparted by machining is essential in understanding machining general part quality. Therefore, there's the need for a perfectly finished part with highly compressive residual stress which could be achieved by selection of appropriate processes and strategies. Tool geometry, depth of cut, spindle speed and feed rate are some of the few factors that may influence the final surface roughness after a CNC milling operation [1]. Also, natural surface roughness as a result of irregularities in cutting operation and in the occurrence of chatter or vibration of the machine tool, or irregularities of chip formation contributes to the surface damage in practice during machining.

Lou et al. [2] developed a one-surface prediction technique for surface roughness and evaluated the prediction ability. Multiple regression analysis was used to determine the correlation between the criterion variables and a combination of predictor/independent variables (feed rate, spindle speed, or depth of cut). A four-flute high speed steel cutter was used for experimental verification while a 1 inch (25.4 mm) 6061 Aluminum cubic block was the workpiece. Percentage deviation of actual surface roughness was measured using an offline profilometer resulting to an average percentage deviation of 9.71% for training data set and 9.97% for testing data set. Therefore statistical model was used to predict surface roughness with about 90.29% accuracy of training data set and approximately 90.03% accuracy of testing data set.

Thamizhmnaii et al [3] proposed a cold working plastic deformation process called burnishing by pressing a rotating roller hard and freely on a horizontal axis against a square titanium alloy material to produce smooth surface. A low surface roughness value was obtained at spindle speed of 1400 inch/min and feed rate of 300mm/min with a depth of cut of 0.35mm. Therefore, with an increase in these parameters, there was a significant improvement in surface roughness and hardness values, ability to impart compressive stress, and also, improved fatigue life of cutting tool. The limitation of this research was that the experiment could not produce a glassy surface due to poor machinability of material. This approach may induce fatigue in the machined workpiece, therefore fatigue analysis testing after burnishing is recommended for further research. Their findings had limitations in increasing the operating parameters due to the possibilities of flaw and micro cracks development on the machined surface. Ab. Rashid and M.R. Abdul Lani [4] inquired into the effective way of predicting surface roughness in CNC end-milling, a mathematical model was developed using multiple regression method with spindle speed, feed rate, and depth of cut as the input variables and surface roughness as the output variables. An artificial neural network model for artificial intelligent method with an input-output intelligence was used along with end-milling and four-flute high speed steel of 10mm diameter as machining operation and cutting tool respectively to model surface. Spindle speed (1000, 1250, and 1500rpm), feed rate (152, 380, and 588mm/min) and depth of cut (0.25, 076, and 1.27) were all varied at 3 levels. Full factorial experiment was used by generating all the possible combination levels of factors. The surface roughness for each experiment was measured using portable surface tester, Perthometer S2. The artificial neural model gave a reliable result of 93.58%

accuracy. In circular end milling of 4140 steel, the individual effects of training parameters: learning rate, momentum rate, number of hidden layer nodes, and processing element's transfer function, on the performance of back propagation networks were evaluated in predicting quality characteristics of end milled parts using multi-sensor signatures (acoustic emission, spindle vibration, and cutting force components) acquired. The corresponding measured quality characteristics (surface roughness and bore tolerance) were used to train the network with hyperbolic tangent transfer function giving a better performance than the sigmoid and sine functions respectively [5]. Nagi et al [6] investigated the effects of cutting parameters on the titanium machinability characteristics in terms of tool life with the design of experiment statistical approach. They carried out a slot milling experiment on a Sabre 750 Cincinnati vertical machining center which was controlled by Acramatic 850 sx-controller. The work piece was a 100 x 100 x 160 mm Titanium-Ti-6Al-4V block. The factors considered were axial and radial depth of cut, cutting speed and feed rate using dry cooling. The high and low values of the design matrix factors were estimated by several trial experiments. The experiment was stopped at the occurrence of tool wear. Their result was presented for just coated carbide tool due to its observed higher tool life compared to uncoated carbide tool. The flank wear on the tool and surface finish of the workpiece material was measured by setting cutting tool deterioration criterion using a tool marker microscope and mpi Mahr perthometer respectively. The R_a values of the machined surface were obtained by measuring at three locations and finding the average. The experiment showed a strong relationship between cutting speed and tool life as high tool life was obtained at lower values of feed rate. It was also identified that the depth of cut did not have any significant effects on the life of

the tool. An increase in cutting speed showed a significant decrease in surface roughness values. Surface hardness improved due to increased cutting speed and feed rate at the best record time. Therefore, cutting speed and feed rate are the dominant factors in controlling tool life, the flank wear, adhesion and that thermal crack at high cutting speed are the dominant failure modes when machining Ti64 with PVD carbide tool.

Zhang et al [7] examined the Taguchi design approach on surface roughness optimization in end milling operation with the aim of determining efficiently, the optimal face milling parameters to achieve smallest surface roughness value for aluminum part under varying conditions. The controlled factors were spindle speed, feed rate, depth of cut, type of end milling tool, and noise factors. This method is similar to design of experiment, but conducted orthogonal experimental combinations. The procedure in the Taguchi method analysis was in three stages; system design, parameter design, tolerance design. This parameter design was further analyzed in steps as thus; selecting the proper orthogonal array (OA) according to the parameters considered, running experiments based on the OA, analyzing the data, identifying the optimum cutting conditions and conducting confirmation runs with optimal levels of all the parameters. The experimental design was carried out on Fadal VMC 40 vertical milling center and surface roughness was measured with a federal pocket surf stylus profilometer. Space heater (Honey well quick heat ceramic heater) and thermometer was used to measure temperature. Ingersoll coated cutting tool on a Fadal 3-insert mill tool holder was used for milling. A polished granite surface table was used to ensure stability and accurate surface roughness measurement. The optimal cutting conditions were established by working with the smallest surface roughness value and the largest signal-noise ratio. The effects of spindle

speed, feed rate, noise factor (tool wear) on surface roughness were more convincing than depth of cut.

Turnad et al [8] developed a model for surface roughness based on cutting speed, depth of cut and feed rate using response surface methodology and a design expert software. The produced surface roughness was investigated in terms of these independent variables using multiplicative models. A vertical milling center (VMC ZPS, Model: MLR 542 with full immersion cutting) was used for the end milling test under dry cutting condition with one uncoated WC-Co insert fitted on a 20mm diameter endmill tool holder. The independent variables were coded by taking into account, the limitation and capacity of the milling machine from the lowest to the highest values ranging from ($-\sqrt{2}$ to $\sqrt{2}$). A design of experiment and design expert 6.0 package, a small central composite design and the analysis of variance were respectively used to develop the first and second order models at 95% confidence. The result of the experiment was used to develop empirical equations for surface roughness prediction with varying conditions of the significant parameters involved. From the first order, the linear graphs showed a direct proportion of feed versus surface roughness and speed. The second order model developed by RSM was more significant than the linear models with an insignificant noise factor leading to development of central composite model. Range of cutting speed v, axial depth of cut a, and feed f were $30.59 \leq v \leq 126$, $0.5 \leq a \leq 2.03$, and $0.05 \leq f \leq 0.15$ respectively. This study proved that a small central composite design is a successful technique to predict the surface roughness in end-milling of titanium alloy using uncoated inserts under dry conditions and that the feed was the most dominant cutting condition on surface roughness followed by cutting speed and axial depth of cut.

Yang et al [9] investigated the effects of milling speed and cooling methods on surface integrity in high-speed milling of titanium alloy TC11. The machining experiments were carried out on a three-axis Mikron HSM 800 high speed milling center with an ITNC 530 controller and a 10 mm uncoated cemented carbide milling cutter of four teeth were used. Cutting tool rake angle was 14^{o}, relief angle was 10^{o} and helix angle was 30^{o}. The milling mode was down milling. The investigation of the resultant effect of cutting condition on surface integrity was by the single factor experiments, maintaining constant values of feed, depth and width of cut of respectively; (0.05mm/tooth, 0.2mm and 10mm). The cooling method varied from emulsion liquid to oil mist, then dry cutting. The residual stresses were measured by X-ray diffraction method with measurement taken at three locations in feed and step over direction, and then, take the average. Surface roughness was measured after each test using a contact type profilometer instrument (Taylor Hobson Form Talysurf 120). The machined workpiece were further cut along the feed direction and prepared as metallographic specimens. The sections were grinded, polished and tested for corrosion. It yielded a 1:1:10 ratios for metric acid, hydrofluoric acid and water. Leica DMI 5000M inversion metallographic microscope was used to observe the micro structure of the cross-sections. The result showed that all the surface residual stresses were compressive both in feed and step-over directions as compressive surface residual stresses give longer fatigue life at the reduction in the peak tensile load of workpiece. The highest compressive stress on the surface in both directions appeared under dry cutting condition while the lowest was with the use of emulsion as cooling method. Also increased milling speed caused increased surface roughness and when oil mist cooling method was used with the highest surface roughness

seen with this cooling condition. Residual stress, surface roughness and microstructure show that emulsion liquid cooling is the best method of cooling in high speed milling of titanium in this research.

X-ray diffraction technologies are well developed, which makes it is possible to use experimental approaches for measuring the residual stress distribution of machined parts. However, on a practical level, the high cost of residual stress tests highly discourages residual stress study.

Turnad et al [10] developed a method to determine models for the optimization of tool life and surface roughness in end milling of titanium alloy Ti-6Al-4V using 20 mm-diameter uncoated WC-co inserts at dry cutting conditions. Vertical Machining center (VMC ZPS, model: MLR 542) was used for all machining. Mituoyo SURFTEST SV-50 was used for surface roughness measurement and a Histomet II toolmaker's microscope for measuring tool wear. The input parameters were of 5 levels: cutting speed (30.59-160.6 m/min); axial depth of cut (0.5-2.03 mm), and feed rate (0.05-0.15 mm/tooth). RSM and CCD were used to develop the tool life and surface roughness models in relation to the cutting parameters. A fit and summary test suggests that the 1^{st} and 2^{nd} order models are the most suitable for tool life prediction and a perturbation plot was used on the 2^{nd} order model to obtain the most suitable prediction for surface roughness. Feed has the most significant effect on surface roughness, followed by cutting speed and axial depth of cut.

Geng et al [11] carried out experimental studies on the milling of a high strength titanium alloy with the aim of optimizing the effects of cutting speed, feed rate, axial depth of cut, and radial depth of cut on its machinability. Their areas of interest were tool

wear, milling force, temperature and surface integrity. Normal and high speed milling were carried out on XS 5040 with a spindle speed range of 50-2500 rpm, a feed rate range of 40-2000 mm/min and a maximum spindle power of 19KW. High speed milling was on a TH 5660A CNC machining center with a variable speed of 0-6000 rpm, a feed rate of up to 8000 mm/min and maximum spindle power of 8KW. 4 different types of cutting tools, (indexable carbide of 32mm diameter, solid carbide of 20 mm diameter, SWT HSS of 20mm diameter, and Hanita HSS of 20 mm diameter) were used. A microscope with a digital camera was used to measure tool wear. Cutting forces were measured in 3 axes with a Kistler 9265B piezoelectric dynamometer, Kistler 5019A charge amplifiers and a data acquisition and analysis system. Teflon-coated constantan wire was used to measure the cutting temperature. Surface roughness was measured using a Marh M1 surface roughness tester, the work piece samples were examined with an MM-6 metallographic microscope, a HXS-1000 digital micro hardness tester was used for hardness measurement and residual stress was measured using Y3 X-ray diffraction meter. Their experiment showed that: cutting speed has the greatest effect on tool life; higher milling speed reduces the deformation of the work piece; compressive residual stress is beneficial to the improvement of the fatigue property of the finished product, the surface quality of the machined surface is fairly good from the viewpoint of surface roughness and residual stress. The values of Ra are commonly less than 0.60μm and the residual stresses are compressive under cutting speed from 30m/min to 20m/min.

Tensile residual stress created from machining processes is the primary cause a reduction of the fatigue life of the parts [12] X-ray diffraction (XRD) is very important for failure analysis and are commonly applied when failure analyses is completed. They

are sometimes the only viable way of residual stress data acquisition. Residual stress measurement is important in manufacturing to determine inappropriate machining process and can be used to evaluate corrective measures while optimizing production parameters needed to extend the service life of machined parts used in engineering applications [13]. Residual stresses are the reason for post-processing of machined parts in order to remove tensile residual stresses. Due to the lofty requirements of the efficiency and the quality of the parts, it is very critical to find exact and realistic solutions to predict distribution of residual stress in a machined component. Generally, high-speed machining and cryogenic cooling are used to improve compressive residual stress in aero engine alloys [14, 15]. Therefore, having a better comprehension on how the residual stress distributes with high-speed machining approach helps engineers to choose and recommend the appropriate cutting conditions in future machining operation. The experimental data of residual stress in feed direction and perpendicular to feed direction is validated with finite element (FE) simulation, which resulted in the finding that residual stress distribution is non-uniform in varied machined circular areas while stresses in different directions at tool tip are developed based on two different coordinate systems. The distribution of residual stresses is significantly influenced by uncut chip thickness, as well as the type of machining sequence i.e. “up or down milling”. The magnitude of residual radial stress decreased or smaller feed rate, and also its variation trend of complete radius milling are in proportion with the uncut chip thickness. Proper choice of feed rate, cutting speed, and the uncut chip thickness, are important in order to obtain ideal residual stress distribution [16]. The effects of material hardness, cutting edge geometry, feed rate and cutting speed on surface roughness are statistically

significant. The effects of two-factor interactions of the edge geometry and the workpiece hardness, the edge geometry and the feed rate, and the cutting speed and feed rate also appeared to be significant. Honed edge geometry and lower workpiece surface hardness resulted in better surface roughness. Cutting-edge geometry, workpiece hardness and cutting speed are found to be affecting force components. The lower workpiece surface hardness and honed edge geometry resulted in lower tangential and radial forces [17]. Surface and subsurface residual stress model from slot and face milling was developed from using process conditions as inputs with geometric transformation and location effects considered. The model uses cutting forces and cutting temperature predictions to define the thermo mechanical loading on the workpiece. It also considered the effects of cutting fluid during prediction. The model concurred with experimental data. The measured subsurface residual stress profiles were more compressive than the ones on the surface [18].

2. THE OVERVIEW OF CURRENT RESEARCH

2.1 CRYOGENIC COOLING (LN_2) AND MINIMUM QUANTITY LUBRICATION STRATEGIES

The overview of current research plan for investigating the effects of cooling/lubrication strategies for high-speed machining of difficult-to-cut metals (nickel alloy, titanium alloy, and Hastelloy) is shown in Figure 1.

Conventional emulsion cooling, MQL, Cryogenic cooling (LN_2), and LN_2 + MQL are investigated under varying machining parameters of cutting speed and feed rate using solid carbide endmills.

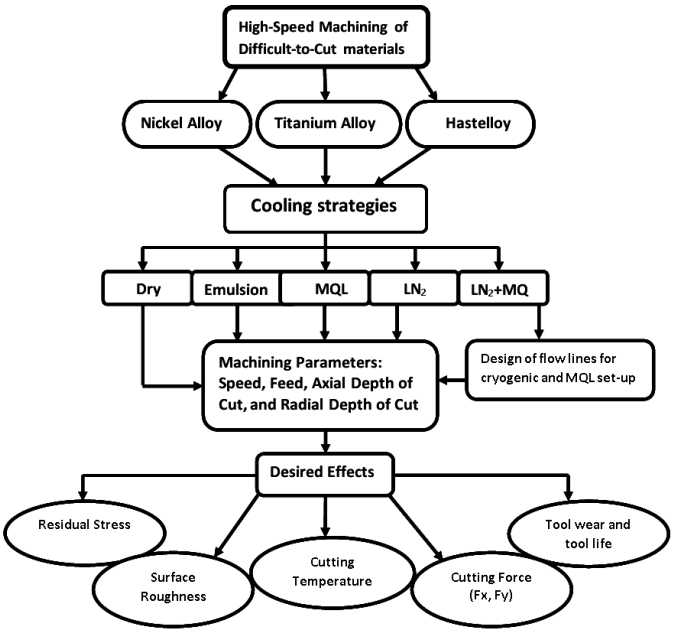

Fig 1. Overview of Current Research Plan for Investigating the Effects of Cooling/Lubrication Strategies for High-Speed Machining of Difficult-to-Cut Metals

2.1.1 DESIGN AND ASSEMBLY OF CRYOGENIC FLOW LINE

This is required to control a super chilled liquid nitrogen (LN_2) temperature of -196^{o}C to a temperature in the range of 0^{o}C to -15^{o}C (cold air). This was done using pipe couplings, valves and flexible cryogenic hose to connect the LN_2 tank to an in-house designed and fabricated nozzle for mixing LN_2 with shop air to supply cold air at a predetermined temperature to the cutting zone; and also mixing this controlled LN_2 with MQL and simultaneously flowing both through their different nozzles to the cutting zone. The pressure of LN2 flowing from the cryogenic (LN_2) cylinder was determined using a pressure gage, however, this pressure gage measured LN2 pressure indirectly using a 0.25 inch Swagelok pipe fitting which was connected to 0.25 inch Tee and linked up to a 0.25 inch pigtail pipe as shown in Figure 2: Schematic diagram of experimental set-up showing cutting force data acquisition system, cryogenic and MQL flow lines. This design was to prevent the flowing LN2 from getting in contact with the pressure gauge in order not to destroy it. A 1.5 inch outer diameter (OD) and 1.375 inch inner diameter (ID) nozzles with an orifice of 1/16 inch was designed to help increase LN2 temperature from cryogenic temperature value of -196 ^{o}C to -15^{o}C. A 230 psi pressure relief valve was used on the cryogenic flow line to take care of pressure build up due to flow control of liquid nitrogen which expands at a very high rate when it changes from liquid to gas.

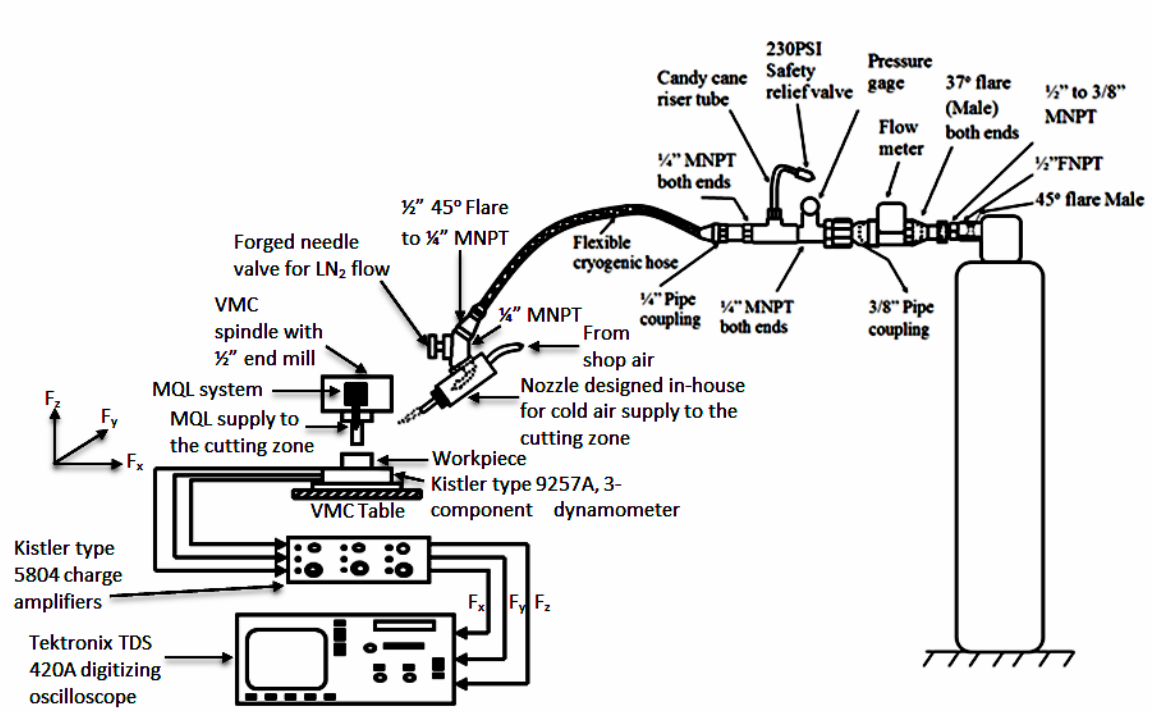

2a. VMC Data Acquisition System and Cryogenic Flow Line

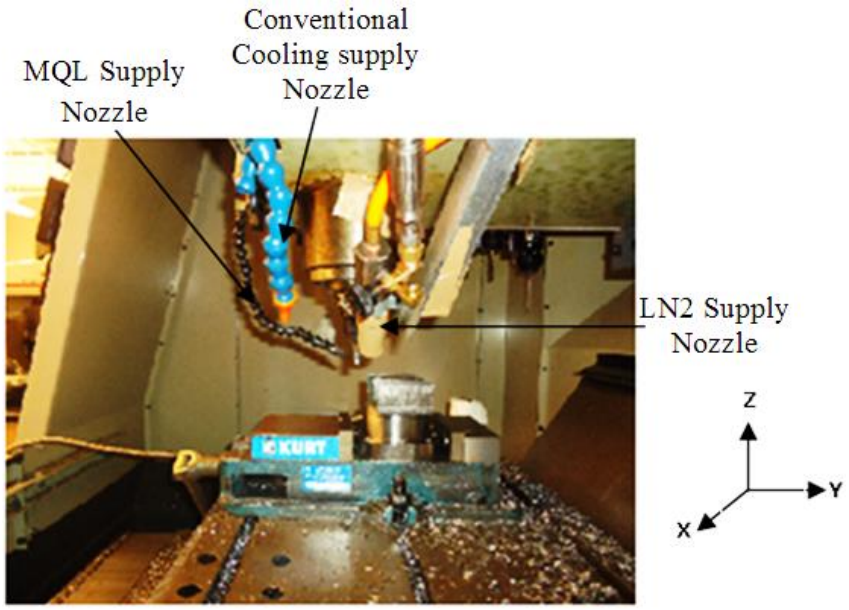

2b. MQL, LN2 and Conventional cooling supplied to the cutting zone

Figure 2. Schematic Diagram of Experimental Set-Up Showing Cutting Force Data Acquisition System, Cryogenic and MQL Flow Lines

2.1.2 CRYOGENIC FLOW LINE CALIBRATION

In an experiment, when two or more variables are related, it is of interest to model the relationship between these variables. In regression analyses, models have both dependent or response variables and independent or regressor variables. The relationship between the dependent and independent variables is called a regression model. Regression analysis is mostly used to analyze data from experiments that might arise from observation of uncontrolled phenomena. Multiple regression analysis is a flexible method of data analysis that may be appropriate whenever the dependent variable is to be examined in correlation to the independent variables in linear or nonlinear relationships. These analyses were conducted at a significance level of 0.05. Below are some of the results from analyzing 1 dependent variable of temperature and 2 independent variables of LN2 pressure and shop air pressure.

The general regression model is given below as:

$$Y = \beta_0 + X_1\beta_1 + X_2\beta_2 + \varepsilon \qquad 1$$

Where Y is the dependent variable (nozzle temperature) and X_1 & X_2 are the LN_2 pressure and air pressure respectively and β_1 and β_2 are the regression coefficients, ε is the error.

Experimental tests were conducted with combination of LN2 and shop air supplied to the cutting zone at varying flow pressure. The flow pressure for shop air and LN2 were independently recorded and STATSTICA^{TM} software from STATSOFT^{R} was used to obtain a regression model used for the calibration of the cryogenic flow line in order to accurately get a -15^{o}C cooling air temperature at the cutting zone. The calibration process was conducted by placing the thermocouple inside the nozzle for cold

air supply housing and taped in place, and flowing liquid nitrogen from the liquid nozzle of the LN_2 cylinder at a pressure of 70 psi for about 15 minutes until the whole length of the flow line is completely chilled up to the point where you can observe the white ice formed on the periphery of the entire length of the flow line, ensuring that Nitrogen in liquid phase is maintained in the line. At this point, LN2 pressure remained steady, then the pressure of LN2 is gradually reduced to 50 psi, and at that point it was still steady even without turning on the shop air pressure. Shop air of 5 psi is gradually added, but the rate at which it takes to attain steady state seemed too slow and may waste a lot of LN_2, so the shop air pressure is increased until the temperature slope/gradient on the computer was approximately zero. The point where the slope was almost zero was at 20 psi shop air, at this point, the temperature measured by the thermocouple probe is recorded. Table 1 shows the cryogenic flow line calibration data. The first nozzle temperature recorded, -10.5 ^{o}C, as described was for the combination of LN2 temperature at 50 psi and shop air temperature at 20 psi. The next nozzle temperature value recorded -20.5^{o} C, as described above was for combination of LN2 temperature at 60 psi and shop air temperature at 27.5 psi, for the next nozzle temperature of -52.5 ^{o} C, the pressure of shop air was kept constant while LN2 pressure was varied. This process continued with the rest of the other nozzle temperature data acquired, keeping LN_2 pressure constant at one point and varying shop air pressure and at another point; varying LN_2 pressure and keeping shop air pressure constant as can be seen from the 5th and 6th data points for constant LN_2 pressure and the 7th and 8th data points. The reason for this approach was that at continuous flow of about an hour of LN_2 flow through the cryogenic flow line at a temperature not low enough to chill the entire length of the flow line, there's fluctuation

of LN_2 pressure in the flow line and the thermocouple temperature recorded from the computer, this makes one always on the watch to monitor the pressure of LN_2 flowing through the line thereby making the process a flaw. It initially was very difficult to set LN_2 pressure at a predetermined value, but success was achieved following the above stated procedure and the flow line was successfully calibrated and used to run the experiments with confidence that it will remain at a set pressure point until it is changed.

Table 1. Cryogenic flow line calibration data

Calibration #	LN2 Pressure (psi)	Shop Air Pressure (psi)	Temperature (Deg C)
1	50	20	-10.5
2	60	27.5	-20.5
3	72.5	27.5	-52.5
4	75	35	-44.3
5	85	35	-56.5
6	85	45	-47.5
7	100	45	-70.5
8	100	50	-64.8

A simple least square model fitting technique was applied to the calibration data of Table 1 using the STATISTICA^{TM} software from STATSOFT^{R}

Table 2 shows the regression analysis summary for nozzle cold air supply temperature; the embedded table shows an R^2 value of 0.96744821 with a P-level of <0.00019. The P-level which is the probability of obtaining a test statistic at least as extreme as the one that was actually observed when the null hypothesis is true. One often rejects the null hypothesis when the p-value is less than the significance level α which is 0.05 in this case. Since 0.00019 is less than 0.05, the null hypothesis is rejected, the result

is therefore said to be statistically significant. From Table 2 it can be seen that the p-level of the intercept, LN2 pressure, and shop air pressure shows that the analysis was statistically significant. The regression model can be seen on the B column where 51.91926 is the intercept of the model, while -1.89403 and 1.42473 are the coefficients of X_1 (LN_2 pressure) and X_2 (shop air pressure) respectively.

Table 2. Regression summary for dependent variable: Temperature, T

N=8	Regression Summary for Dependent Variable: Temperature (Deg C) R= .98358945 R²= .96744821 Adjusted R²= .95442749 F(2,5)=74.301 p<.00019 Std.Error of estimate: 4.4354					
	Beta	Std.Err. of Beta	B	Std.Err. of B	t(5)	p-level
Intercept			51.91926	8.298837	6.25621	0.001530
LN2 Pressure (PSI)	-1.62041	0.230626	-1.89403	0.269570	-7.02610	0.000901
Air Pressure (PSI)	0.71422	0.230626	1.42473	0.460054	3.09688	0.026948

This therefore yields a regression equation as shown in equation 2;

$$T = Y = 51.91926 - 1.89403X_1 + 1.42473\ X_2, \qquad R^2 = 0.96744821 \qquad 2$$

Forward stepwise regression was used in order to have the independent variables of LN2 pressure X_1 and shop air pressure X_2 to be added or removed from the model at 57.16415 and 9.959068 respectively until the best regression was obtained as shown in Table 3. Table 3 is the ANOVA table with the all the sums of squares, mean squares, degrees of freedom, F-ratio and P-level represented. As stated earlier, this regression analysis based on 0.05 significant level shows that the data collected from the calibration test is statistically significant.

Table 3. Summary of stepwise regression

Variable	Summary of Stepwise Regression; DV: Temperature (Deg C) (Spreadsheet1)						
	Step +in/-out	Multiple R	Multiple R-square	R-square change	F - to entr/rem	p-level	Variables included
LN2 Pressure (PSI)	1	0.951320	0.905009	0.905009	57.16415	0.000278	1
Air Pressure (PSI)	2	0.983589	0.967448	0.062439	9.59068	0.026948	2

The graph in Figure 3a below shows a 3D surface plot for the 3 variables with shop air pressure and LN2 pressure are along the y and x axes respectively while the z axis is the response variable, i.e. temperature in degree centigrade. From the surface plot, it can be seen that as the pressure of LN2 increases with a decrease in shop air pressure, the temperature response decreases, while as the shop air pressure increases and the LN2 pressure decreases the temperature response increases.

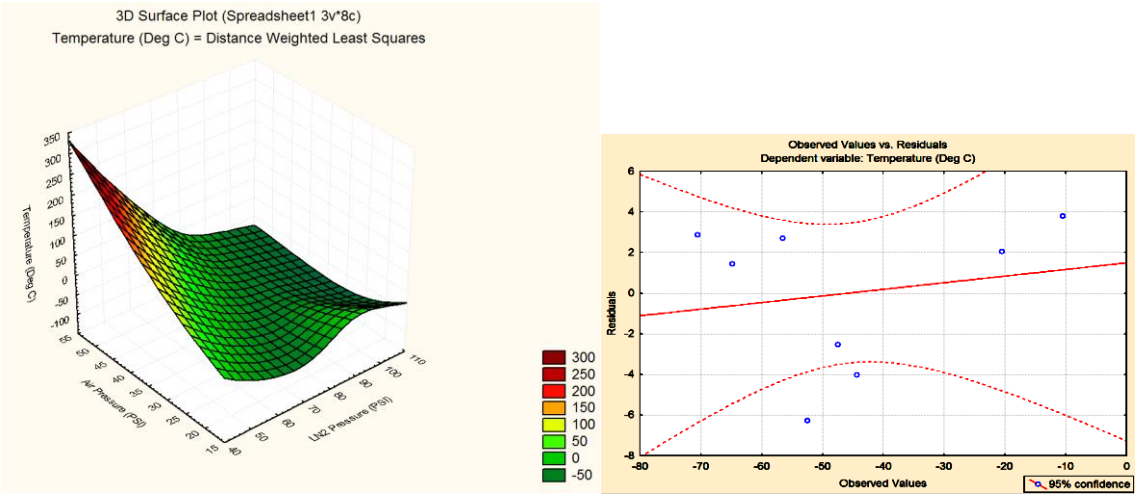

3a. Surface Plot for Nozzle Cold Air Temp 3b Plot of observed values vs residuals

Figure 3. Surface plot of response variable-Temperature vs LN2 and shop air pressure

Figure 3b shows the plot of observed values vs residuals which can be used to detect the outliers or group of observations that are consistently over predicted or under predicted which confirms the adequacy of the regression model. It is used to display how

well the entire set of observed values for observation points ties with the solution data. The values of desired output nozzle cold temperature and LN2 pressure were entered in the derived regression equation 2 to generate the values of shop air pressure to be used for the cryogenic slot end-milling experiments as seen in Table 4. This explains the reason why the resolution of the values in the shop air pressure column is very low, up to 8 decimal places.

Table 4. Table of obtained values using regression model of equation 2

Y (Temp in Deg C)	**Intercept**	**LN2 (PSI)**	**Shop Air (PSI)**
-10	51.91926	50	23.00944039
-15	**51.91926**	**55**	**26.14698224**
-20	51.91926	60	29.28452409

2.1.3 MQL COOLING/LUBRICATION STRATEGY-SET-UP

Acculube MQL Box precision pump box applicator automatic on/off with 18 inch copper nozzle was used. The applicator is a positive displacement lubrication system for MQL that regulates the amount of lubricant applied to the tool cutting edge in exact quantities. When the unit is switched on, it is supplied with compressed air at (80psi) and lubricant at 0.5 bars. The lubricant is supplied from the reservoir, flowing through the base to the volumetric pneumatic micro pumps. The delivery frequency of the micro pump used was four strokes per second and can be adjusted anytime with the pneumatic pulse generator, which is controlled via the control unit on the system. The flow rate of the micro pump was set with a thumb wheel. The micro pump delivers a metered quantity

of lubricant, which goes through the inner channel of the base to the coaxial outlet port then into the capillary tube of the coaxial line. Air was supplied from a compressed shop air network. The air inlet is controlled with a solenoid valve. The compressed air also flows through the base and is divided in two ways. Some compressed air is supplied to the micro pump to actuate it and the other part of the compressed air (called carrier air) is supplied to the coaxial outlet port and goes through the outer tube of the hose. The carrier air pressure of the outlet can be adjusted with a pressure regulator. The low-pressure carrier air and the lubricant are simultaneously transported via the coaxial hose to the nozzle. The carrier air is swirled in the nozzle. As a result, the metered quantity of lubricant is broken down into micro droplets, which are transported by the carrier air to the friction point without causing any mist. The micro droplet size (200 – 600 μm) ensures a perfect lubricant coating without atomization.

2.2 DESIGN OF EXPERIMENT

2.2.1 FRACTIONAL FACTORIAL DESIGN OF EXPERIMENT

A fraction of the total set of all treatment combinations is selected for the experiment. A three factor at three level, 3^3, full factorial experimental design requires that 27 experimental runs be conducted. With replication, this full factorial design will require 54 experimental runs. Therefore, the number of runs required may outgrow the resources required to carry out the experiment. In fractional factorial design, it is assumed that certain higher order interactions are negligible. This statistical method becomes necessary when there are insufficient resources to conduct experiments, as higher order experimental interactions reproduce initial results. Therefore a fraction of a complete factorial design of experiment will suffice. In this study, 1/3 fractional factorial design of experiment is used to reduce the number of experimental runs and cost, which requires 9 experimental runs or treatment combinations, each run was replicated resulting to 18 total runs in order to minimize the noise effect in the data obtained and allow the estimation of experimental error. Each replicate is divided into 3 blocks of 9 treatment combinations.

2.2.2 SELECTION OF PARAMETER AND THEIR LEVELS

The objectives of this experiment are to investigate the effects of cooling strategies and machining parameters on cutting forces, cutting temperature, and tool wear in slot end-milling and detect optimum machining parameters and cooling strategies to reduce cutting forces generated during end-milling of titanium alloy, reduce cutting tool-workpiece temperature, tool wear, improve residual stresses and surface finish during end-milling of Ti-6Al-4V using uncoated solid carbide endmill. Spindle speed at three levels of (1000, 1500, and 2000 rpm), feed rate at 3 levels (6, 12 and 18 ipm) and cooling

strategies at three levels (conventional emulsion, MQL and LN_2) were the three factors (parameters) selected for evaluation as shown in Table 5. Axial and radial depths of cut are kept constant at 0.125 inch and 0.5 inch respectively, also corner radius of 0.3 inch was kept constant for all the bull-nosed end-mills used throughout the experiments. These machining parameters chosen are based on optimum machining conditions in a previous work done by Okafor and Aramalla [21].

TABLE 5: SELECTION OF PARAMETERS AND THEIR LEVELS

Table 5a: Experimental factors and levels

Level	Factors		
	Cooling Methods	Speed (RPM)	Feed (IPM)
0	Emulsion	1000	6
1	MQL	1500	12
2	LN2	2000	18

Table 5b. Design of experimental runs for the principal block

1	**000**	4	101	+	101	**202**	7	101	+	021	**122**
2	**012**	5	012	+	012	**021**	8	012	+	202	**211**
3	**101**	6	101	+	012	**110**	9	021	+	202	**220**

Each factor is investigated at three levels to determine the optimum setting for the end-milling process. A 3^3 full factorial experiment requires 27 treatment combinations. In this experimental case, higher order interaction is aligned with the mean; this higher order

interaction together with blocks is used to obtain $1/3^k$ fraction of a S^n experiment, where (n) is the number of factors and (S) is the level of each factor. This case uses $K = 1$, $S = 3$ and $n = 3$, which allows the construction of three blocks with each block having $3^{3-1} = 9$ treatment. The treatment combination (1, 1, 1) is chosen for higher order interactions. Let AB^2C^2 be the generator of the fraction that will be confounded with blocks.

The defining contrast is given in equation 3;

$$L = X_1 + 2X_2 + 2X_3 \qquad 3$$

From the defining contrast above, it is easy to verify that the treatment combinations, 000, 012, and 101 belong to the principal block and the remaining experimental runs in the principal block generated as shown in Table 5b. In Table 5b, the figures in bold prints are the runs generated for the principal block and it is this principal block that is chosen as the one-third fraction of the 27 treatment combinations as shown in Table 6.

In Table 6, the column designated as treatment combination is the runs generated for the principal block and it is the one-third fraction of the 27 treatment combinations.

Table 6: 1/3 Fractional Factorial Experimental Design

Experimental Runs	Treatment combination	3 Factors at 3 Levels		
		Cooling Methods	Speed (RPM)	Feed (IPM)
1	(0,0,0)	Emulsion	1000	6
2	(0,1,2)	Emulsion	1500	18
3	(1,0,1)	MQL	1000	12
4	(2,0,2)	LN2	1000	18
5	(0,2,1)	Emulsion	2000	12
6	(1,1,0)	MQL	1500	6
7	(1,2,2)	MQL	2000	18
8	(2,1,1)	LN2	1500	12
9	(2,2,0)	LN2	2000	6

2.2.3 ANALYSIS OF VARIANCE

Analysis of variance (ANOVA) was used to test the significant differences between the means for each factor. ANOVA can determine if the variation in the result of the variable is due to the changing of each factor from one level to another, or if the variation is attributed to random error. It can also quantify the contribution of each cutting parameter to the total variation in the dependent variable quality characteristics. The columns of the ANOVA tables are the sources (factors), degrees of freedom (df), sum of square (SS), means square (MS), variance factor (F), and the P-values for the factors. The variance can be separated into effect or error, by analyzing the sum of squares of the variation (SS). Taking into account, the SS for each factor, interaction, and error, and dividing by the number of degrees of freedom, the mean square effect and mean square error are obtained. The variance ratio, F, is the variance ratio of the mean square effect to the mean square error. The larger the variance ratio for a given factor, the more significant that factor's effect is on the total variance. P-values are the significance level of the test. A factor is said to have significant effect on the response variable if the P-value for that factor is less than the significance (α) level of the test.

2.2.4 MARGINAL MEANS

Marginal means plots in this experimental runs were used to visually represent the effects of each factor on the dependent variable: cutting force components, tool wear, and cutting temperature. The marginal means of a factor at a particular level are calculated as the mean of the dependent variable with the factor set at that level. The marginal means presented in the results are for all three levels and are calculated as shown in equation 4 below;

$$\bar{X}_1 = \frac{\sum_{i=1}^{N1} X1}{N_1} \quad 4$$

Where $\bar{X}$ = Marginal mean for every level

X_1 = value of dependent variable at level 1

N_1 = Number of measurements at level 1

2.2.5 PARETO CHART

Pareto chart of effects is a visual representation of the main effects and interaction that are calculated using ANOVA. The magnitude of each effect is represented by a shaded column and the dotted line crossing the column indicates the magnitude of each effect required for that effect to be statistically significant. The Pareto chart lists each effect in the order of significance.

3 EXPERIMENTAL SET-UP AND PROCEDURE

3.1 MACHINE TOOL, WORKPIECE MATERIAL, CUTTING TOOL AND CONDITIONS

A schematic diagram of the experimental set-up is shown in Figure 2. The slot end-milling experiments were conducted on Cincinnati Milacron, Sabre 750 Vertical Machining Center (VMC) with Acramatic 2100 controller. The workpiece material used are two rectangular blocks of Titanium alloy Ti-6Al-4V, 6 inches (152.4 mm) long x 3 inches (76.2 mm) wide x 1.5 inches (38.1 mm) thick.

Two sets of experiments were conducted on each block. For the first block, Block A, all the experimental runs using conventional emulsion and MQL cooling strategies were carried out on it with 3 slots on one half of the block for conventional emulsion cooling (experimental runs 1, 2 and 5) and another 3 slots on the second half of the block for MQL cooling strategy (experimental runs 3, 6 and 7) all at different combinations of machining parameters as shown in Table 6. The second block, Block B, has the experimental runs (slots) for LN_2 cooling strategy (experimental runs 4, 8 and 9) on one half of the block and on the second half of the block 3 slots were machined for a comparative evaluation of MQL, LN_2 and MQL + LN_2 cooling strategies using the identified optimum machining parameters from the analysis of variance of fractional factorial design of experiments.

The cutting tool used is a 4-flute uncoated solid carbide endmill of 0.5 inch (12.7 mm) diameter, 0.5 inch (12.7 mm) shank diameter, 1 inch (25.4 mm) flute length, 3 inch (76.2 mm) overall length, and 0.3 inch (0.76 mm) corner radius. A corner radius of 0.3 inch was chosen to give minimum cutting force values as reported by Okafor, Aramalla

[9]. A new endmill was used for each experimental run (slot) to eliminate the effect for tool wear and a total of 12 endmills were used for all experiments.

The range of cutting speed and feed rate were selected with the aim of suitably covering the recommended ranges of machining conditions for Titanium alloy while cooling strategies and cryogenic temperature of -15^{o}C were selected from recommendations from published literatures.

The cutting conditions chosen for the experiments were; cutting speed 1000 rpm (39.9 m/min), 1500 rpm (59.85 m/min), 2000 rpm (79.8 m/min), feed rate 6 ipm (152.4 mm/min), 12 ipm (304.8 mm/min) 18 ipm (457.2 mm/min), axial depth of cut was 0.125 inch (3.175 mm) and radial depth of cut was 0.5 inch (12.7 mm).

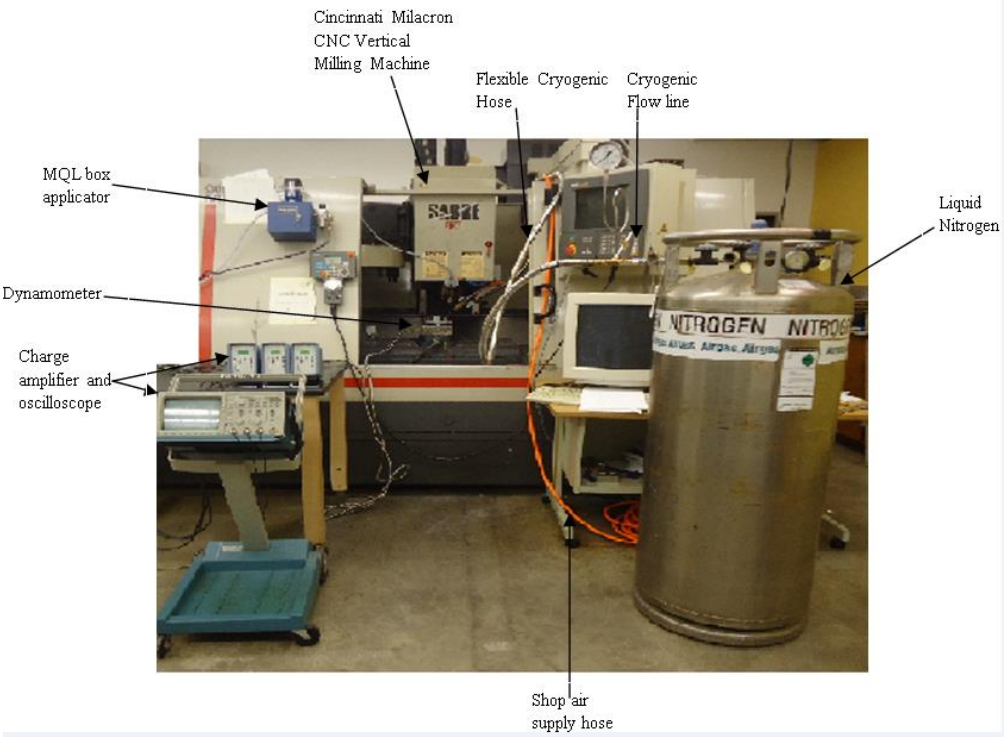

Figure 4. PHOTOGRAPH OF COMPLETE EXPERIMENTAL SET-UP SHOWING VMC, FORCE DATA ACQUISITION SYSTEM, MQL AND LN_2 COOLING SYSTEMS

Figure 4 shows a pictorial view of the entire set-up with all the components labeled.

The set-up for the cooling strategies investigated was made up of cryogenic liquid nitrogen (LN_2) flow line built in-house at Missouri University of Science and Technology for liquid nitrogen (LN_2) cooling, conventional emulsion coolant supplied from the VMC, and Acculube Minimum Quantity Lubricant precision box applicator for MQL cooling. The set-up for the comparative evaluation of MQL + LN_2 with MQL, LN_2 and conventional emulsion cooling strategies as shown in Figures 2 a, b and Figure 4, was used for comparison with the original three levels of cooling strategies. The cryogenic (LN_2) flow line is a nozzle designed to regulate the flow and temperature of both liquid nitrogen and a mixture of liquid nitrogen and shop air when flown directly on the cutting zone.

Before the slot endmilling tests, the workpiece materials were prepared by drilling two holes with two counter bores. The holes were tapped to allow tight clamping of the workpiece to the KISTLER force dynamometer with threaded bolts, and the dynamometer was tightened on the vice of the CNC machine bed. Clamping the workpiece on the dynamometer through threaded holes on the workpiece will prevent play and extraneous noise effects being superimposed on the acquired force and temperature signals.

3.2. EXPERIMENTAL PROCEDURE

The slot end-milling experimental runs were performed at cutting speeds of 1000 rpm, 1500 rpm, and 2000 rpm, feed rates at 6 ipm, 12 ipm and 18 ipm, and cooling strategies were emulsion cooling, cryogenic cooling at -15^{o}C, and minimum quantity lubrication at constant axial and radial depths of cut of 0.125" (3.175 mm) and 0.5" (12.7 mm) respectively were maintained. The feed direction of the workpiece/table was along the negative y-axis of the workpiece/table applying right-hand rule. A total of 8 machining passes were made for each machined slot, for the 1 inch (25.4 mm) deep slots. The CNC program containing the G & M codes for machining test run #1 (slot #1) in inch unit is given below;

```
:100 T1 M6
N10 G01 X0.375 Y-1 Z1 F50
N20 Z-0.25
N30 S1000 M03
N40 G01 Y3.7 F18
N50 G01 Z1 F50
N60 G01 X0.375 Y-1 F50
N70 G01 Z-0.375
N80 G01 Y3.7 F18
N90 G01 Z1 F50
N100 G01 X0.375 Y-1 F50
N110 G01 Z-0.5
N120 G01 Y3.7 F18
N130 G01 Z1 F50
N140 G01 X0.375 Y-1 F50
N150 G01 Z-0.625
N160 G01 Y3.7 F18
N170 G01 Z1 F50
N180 G01 X0.375 Y-1 F50
N190 G01 Z-0.75
N200 G01 Y3.7 F18
N210 G01 Z1 F50
N220 G01 X0.375 Y-1 F50
N230 G01 Z-0.875
N240 G01 Y3.7 F18
N250 G01 Z1 F50
N260 G01 X0.375 Y-1 F50
N270 G01 Z-1
N280 G01 Y3.7 F18
N290 G01 Z1 F50
N300 G01 X0.375 Y-1 F50
N310 M02
N320 M30
```

The 3-D and 2-D drawings of the machined titanium alloy blocks showing the slots, 8 thermocouple holes, 2 drilled and counter bored holed threaded for clamping the block on the dynamometer and also, the section of the block where surface roughness and residual stresses were measured are shown in Figures 5a, b and 6.

3.2.1 SURFACE ROUGHNESS MEASUREMENT

Surface roughness was measured with a portable Brown and Sharpe pocket surf of a measuring range of 0.3 µm – 6.35 µm. This portable profilometer uses a piezoelectric probe for measurements. Measurements were made for a tracing length of 5 mm at a

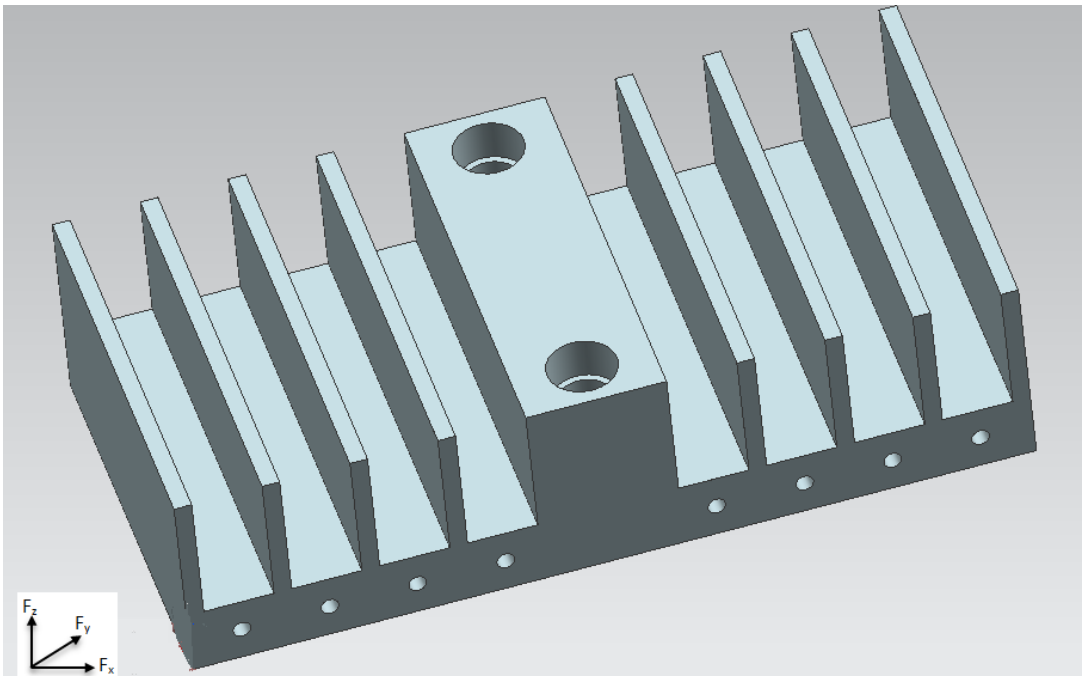

5a. 3D VIEW OF MACHINED WORKPIECE WITH 8 SLOTS AND DRILLED THERMOCOUPLE HOLES

speed of 5.08 mm/sec. Surface roughness was measured on the web and rib of the slots at three different locations that are 1 inch apart each experimental run/slot. For the rib, the measurements were made perpendicular to the feed direction, while on the web, the measurements were made at the mid-plane of the slot, at three different locations parallel to the feed direction also 1 inch apart. The averages of the three measured surface roughness values were analyzed by ANOVA.

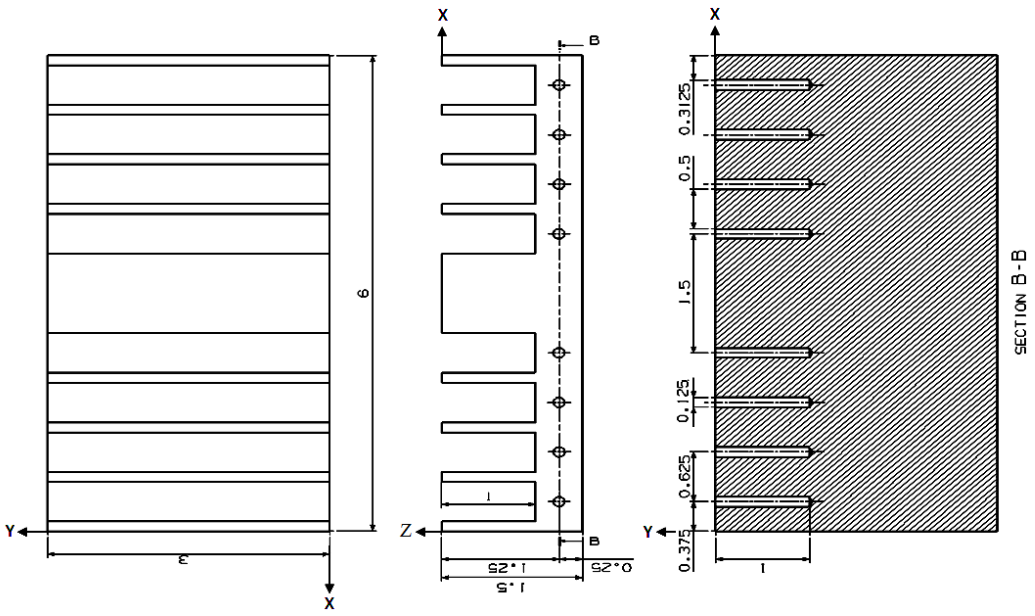

5b. Workpiece drawing of top and side view of workpiece with hatched section

Figure 5. WORKPIECE DESIGN FOR SLOT END-MILLING EXPERIMENTS

The geometry of the workpiece design is shown in Figure 5.

3.2.2 RESIDUAL STRESS MEASUREMENT

Residual stresses induced in machined parts can build up at any major step during machining process. These machining-induced residual stresses affect the fatigue life, corrosion resistance and distortion of engineering structures. Machining parameters and cooling/lubrication strategies, and cutting tool geometry and characteristics affect residual stresses in machined parts. Experiments and proper measurement approach can be used to evaluate the effects of machining parameters and cooling strategies on residual stresses on the surface and sub-surface of machined parts. Proto Manufacturing of Ontario, Canada was contracted for the measurement of residual stress on the left ribs of all the machined slots at different experimental conditions using non-destructive X-ray diffraction. The purpose of the investigation is to determine the best machining parameter

and cooling strategies that minimizes RS. Measurements were on the left ribs of all the identified machined slots in the direction parallel to the feed direction. Wire EDM of 0.012 inch (0.30480 mm) was used on a Hitachi Model 8Q EDM machine to cut off the identified left ribs for residual stress measurements. The wire EDM can remove the ribs without causing any residual stresses on the workpiece.

The X-Ray diffraction theory is used to determine the points where residual stresses are either more compressive or more tensile. These residual stresses technique are measured using the distance between crystallographic planes, i.e. d-spacing as a strain gage. When the material is in tension, d-spacing increases and decreases when in compression. The directions and depths of measurement were selected by measuring stress in six directions during characterization in order to expose potentially beneficial or harmful subsurface residual stresses in the material. The number of subsurface is not limited; therefore measurement depths are generally selected to view the full shape of the stress versus depth profile to depths where stress gradients tend to level off [13]. Also, the direction perpendicular to the feed direction which was located on the rib is of interest since the surface roughness values measured on the ribs have higher values when compared with the ones measured on the web. This gave the clue to focus attention on measuring RS on the ribs, and also to minimize the residual stresses measurements. Table 7 shows the residual stress measurement locations on block A, these measurements were used for design of experiments and Analysis of Variance (ANOVA). Table 8 shows the table for residual stress measurement locations on block B for comparative analysis and parameters optimization.

Table7. RESIDUAL STRESS MEASUREMENT LOCATION ON BLOCK A FOR DESIGN OF EXPERIMENTS

Slot	Measurement Location\Depth (mm)	0	0.01	0.015	0.05
1	Web	N/A			
	Rib	* *			
2	Web	N/A			
	Rib	* *			
3	Web	N/A			
	Rib	* *			
4	Web	N/M			
	Rib	N/M			
5	Web	N/A			
	Rib	* *			
6	Web	N/A			
	Rib	* *			
7	Web	N/A			
	Rib	* *			
8	Web	N/M			
	Rib	N/M			

Table 8. RESIDUAL STRESS MEASUREMENT LOCATION ON BLOCK B FOR COMPARATIVE ANALYSIS AND PARAMETERS OPTIMIZATION

Slot	Measurement Location\Depth (mm)	0	0.01	0.015	0.05
1	Web	N/A			
	Rib	* *			
2	Web	N/A			
	Rib	* *			
3	Web	N/A			
	Rib	* *	*	*	*
4	Web	N/M			
	Rib	N/M			
5	Web	N/M			
	Rib	N/M			
6	Web	N/M			
	Rib	N/M			
7	Web				
	Rib	*	*	*	*
8	Web				
	Rib	*	*	*	*

Figure 5a and b represent 2 rectangular Titanium Alloy Workpiece blocks (Block A and Block B) with 8 slots machined on each block on which measurement for residual stresses was carried out on. The measurements were on the left rib walls (looking from the side of the drilled holes for thermocouple probes. Residual stresses were measured at two points on each identified left rib wall as shown in Figure 6

3.2.3 DESIGN OF EXPERIMENT APPROACH

Residual stresses were measured on slots # 1, 2, 3, 5, 6 and 7 (which represent experimental runs 1, 2, 5, 3, 6, and 7 respectively) of Figure 1 (block A) and slots # 1, 2 & 3 (which represents experimental runs 4, 8 and 9 respectively) of (block B). For each

of the identified slot, two-point measurements of 0.5 inch (12.7 mm) apart were made on the surface (i.e. at 0 mm depth) of the rib at a total number of measurements of 18 points. These measurements were used to perform design of experiment analysis in order to generate ANOVA table, plots Pareto charts and marginal mean of effects plot.

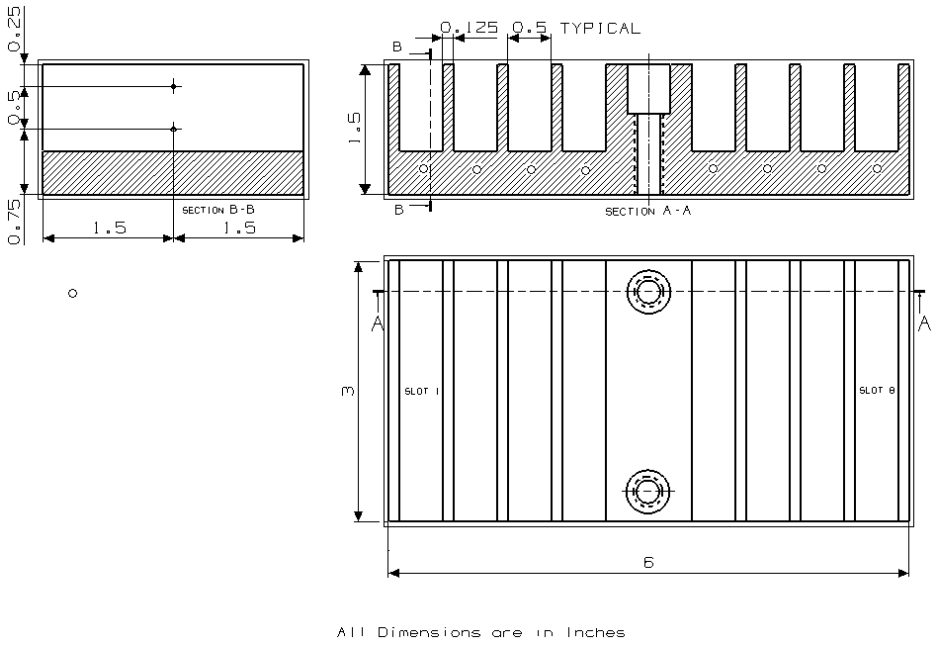

Figure 6. MACHINED SLOTS IN TITANIUM ALLOY WORKPIECE (TI-6AL-4V) WITH RESIDUAL STRESS MEASUREMENT POINTS LOCATIONS

3.2.4 COMPARATIVE ANALYSIS APPROACH

Residual stresses were measured on slot # 3 of Block B, at depths of 0.01 mm, 0.015 mm, 0.05 mm, one point each on the rib, total points measured were 3 points. Also, residual stresses were measured on slots 7 & 8 of Block B, 1 point each on the rib at 0.0 mm, 0.01 mm, 0.015 mm, and 0.05 mm for a total number of 8 points to measure. Therefore, the total numbers of measurements on the rib were eleven. These

measurements were made for comparative analysis of the effects of the optimum cooling strategies (MQL and LN_2) and machining parameters (spindle speed of 2000 rpm and feed rate of 6 ipm) on residual stresses on the surface and subsurface.

4. RESULTS AND DISCUSSION

4.1 SURFACE ROUGHNESS

The average surface roughness of the machined workpiece was analyzed using fractional design of experiment to obtain optimum conditions for producing better surface finish.

The results of the fractional design of experiment and comparative analysis of the optimum machining parameters and cooling strategies are presented.

4.1.1 EFFECTS OF COOLING STRATEGIES AND MACHINING PARAMETERS ON SURFACE ROUGHNESS ON THE RIB AND ON THE WEB

In this study, surface roughness was measured on the ribs and on the webs. The average surface rough values on the ribs were found to be significantly higher than on the web, for this reason, attention was focused on the rib to find the best way to improve surface finish on the rib using ANOVA table, Pareto charts and marginal means of effects plot from fractional factorial design of experiment for slot end-milling of titanium alloy Ti-6Al-4V. In table 9, the ANOVA tables for surface roughness values are shown

TABLE 9: ANOVA TABLE FOR SURFACE ROUGHNESS VALUES

Table 9a. ANOVA TABLE FOR SURFACE ROUGHNESS VALUES ON THE WEB

	ANOVA; Var.:Ra Web; R-sqr=.99689; Adj:.99413 3 3-level factors, 1 Blocks, 18 Runs; MS Residual=.0021 DV: Ra Web				
Factor	SS	df	MS	F	p
(1)Cooling L+Q	3.193378	2	1.596689	760.3280	0.000000
(2)Speed L+Q	0.217078	2	0.108539	51.6852	0.000012
(3)Feed L+Q	0.543239	2	0.271619	129.3426	0.000000
1*2	0.758678	2	0.379339	180.6376	0.000000
Error	0.018900	9	0.002100		
Total SS	6.079711	17			

Table 9b. ANOVA TABLE FOR SURFACE ROUGHNESS VALUES ON THE RIB

	ANOVA; Var.:Ra Rib; R-sqr=.97137; Adj:.94592 3 3-level factors, 1 Blocks, 18 Runs; MS Residual=.0227556 DV: Ra Rib				
Factor	SS	df	MS	F	p
(1)Cooling L+Q	2.854433	2	1.427217	62.71948	0.000005
(2)Speed L+Q	1.663033	2	0.831517	36.54126	0.000048
(3)Feed L+Q	1.388317	2	0.694158	30.50500	0.000098
1*2	1.779100	2	0.889550	39.09155	0.000036
Error	0.204800	9	0.022756		
Total SS	7.153400	17			

Table 9. ANOVA Table for surface roughness values on the web and on the rib

The ANOVA table in Table 9 represents the linear and quadratic effects of the factors considered in this experiment and also the linear and quadratic effects of the factors interactions.

In the ANOVA table, Table 9a, the linear and quadratic effects of cooling strategy, feed rate and the interaction of cooling strategy and spindle speed were 0.000000. This therefore means that the differences observed are statistically significant. So the differences are real differences and not random fluctuations caused by sampling error. For confidence levels, it would be the same as saying the differences are significant

to the 99.999999% confidence level. In essence, since the p-value is less than the chosen level of significance 0.05, the null hypothesis is rejected. The quadratic effect of spindle speed is the next statistically significant effect on surface roughness on the web while the linear effect of spindle speed and linear effect of cooling are the next statistically significant factors. The linear effect of speed and the quadratic effect of feed are both not statistically significant. The second ANOVA table of Table 9 shows that the linear and quadratic effect of cooling is the dominant and statistically significant main effects on surface roughness average on the rib and on the web, while the interaction of cooling strategy and spindle speed is next statistically significant factors for better surface finish on the rib. The linear and quadratic effects of spindle speed are the next statistically significant factors while linear effect of feed rate is the least statistically significant factor.

The surface plot in Figure 7 shows the 3-dimensional plots of surface roughness on the vertical scale (Z plane) versus 2 factors on the horizontal (X-Y plane) scale.

From the Pareto chart of Figure 8 the visual representation of the main effects of the different factors and their interactions effects are seen on horizontal bars with a vertical red line to mark the point of statistical significance.

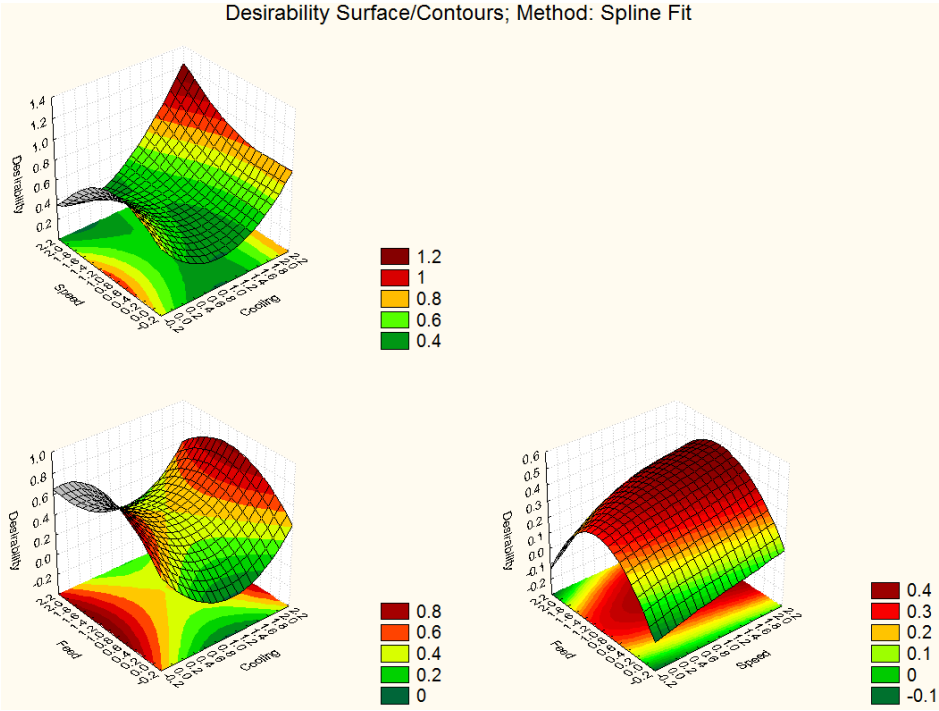

Figure 7. SURFACE ROUGHNESS DESIRABILITY SURFACE/CONTOUR PLOTS

From the desirability surface contour plot of Figure 7, the first plot shows the combined effects of spindle speed and cooling strategies on average surface roughness values measured on the web and on the rib. From the first plot, MQL cooling is the best cooling strategy at all spindle speed levels considered for this experiment. The best spindle speed level using MQL cooling as seen from the plot is high spindle speed of 2000 rpm. Worst combination is the use of LN_2 at high spindle speed of 2000 rpm. The second plot on Figure 7 shows the effects of the use of different levels of cooling strategies and feed rate on surface roughness on the web and on the rib. From the plot, MQL cooling strategy and low feed rate of 6 ipm gave the best surface finish, next was MQL cooling strategy at high feed rate of 18 ipm. Emulsion cooling and LN_2 cooling at medium feed rate of 12 ipm are the worst combinations. The third plot shows that low feed rate of 6 ipm at both low and high spindle speed of 1000 rpm and 2000 rpm

respectively are the best combination for best surface finish on slot end-milling of Ti-6Al-4V. Also, high feed of 18 ipm at low speed gave a better surface finish. Medium feed rate of 12 ipm at all speed levels gave the worst surface finish on slot end-milling of titanium alloy.

4.1.1.1 EFFECTS OF COOLING STRATEGIES ON SURFACE ROUGHNESS ON THE RIB AND WEB

From the Pareto charts of Figure 8, the linear effect of cooling strategy is the dominant and statistically significant main effect on average surface roughness on the rib while the quadratic effect of cooling strategy is the dominant and statistically significant factor on the web.

On the rib, linear effect of cooling strategy has an increasing effect on surface roughness while a decreasing effect on the web is seen from the quadratic effect of cooling strategy. The marginal mean effects plot of Figure 9 shows the effects of the different cooling strategy levels on average surface roughness on the rib and on the web.

The first plot on the first column shows that conventional emulsion cooling strategy which is the 0 cooling strategy level gave the average highest surface roughness value on the web while MQL which is the mid cooling strategy level (level 1) gave the lowest average surface roughness value on the web. LN_2 which is the highest cooling strategy level (level 2) was the next best cooling strategy on average surface roughness value produced on the web during slot end-milling of titanium alloy, Ti-6Al-4V. On the rib, the same trend was followed with MQL cooling strategy as the best over LN_2 and emulsion cooling, but the variation in the average surface roughness values on the rib

using the different cooling strategies are not much as can be seen from the second plot of the first column of Figure 9.

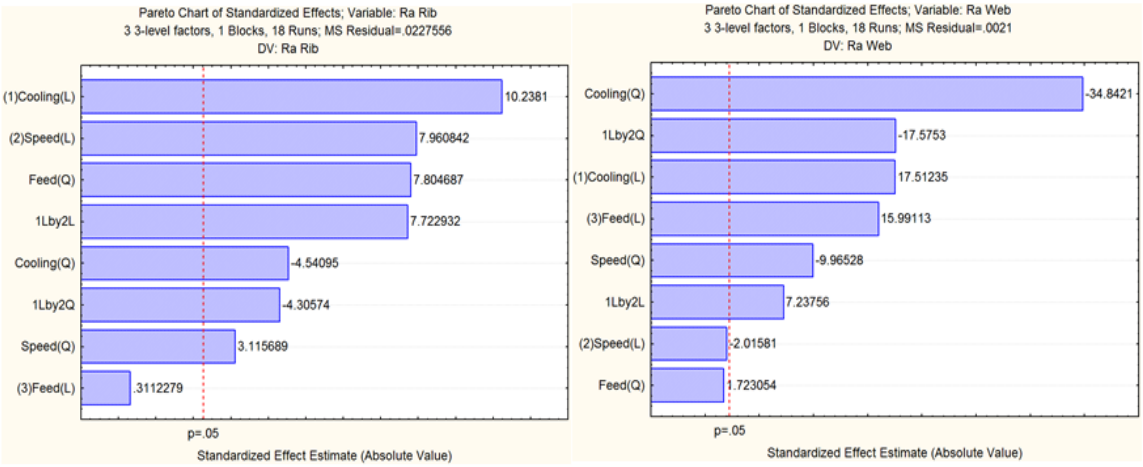

Figure 8. PARETO CHART OF THE EFFECTS OF EACH FACTOR AND INTERACTIONS ON SURFACE ROUGHNESS ON THE RIB AND ON THE WEB

4.1.1.2 EFFECTS OF SPINDLE SPEED ON SURFACE ROUGHNESS ON THE RIB AND WEB

From the Pareto chart of Figure 8, the first chart shows that the linear effect of spindle speed is the second dominant and statistically significant factor on average surface roughness on the rib with an increasing effect while the quadratic effect of spindle speed is the fifth dominant and statistically significant effect with a decreasing effect on average surface roughness values on the web.

On the first plot on the second column of the marginal mean plot, Figure 9, it can be seen that medium and high spindle speed of 1500 rpm and 2000 rpm respectively are the preferred spindle speed levels for low surface roughness values on the web while low speed of 1000 rpm gave the highest/worst average surface roughness values on the web. On the second plot in the second column, low speed of 1000 rpm produced the lowest

average surface roughness value on the rib while medium speed and high speed of 1500 and 2000 rpm respectively are the worst for improving surface roughness on the rib.

4.1.1.3 EFFECTS OF FEED RATE ON SURFACE ROUGHNESS ON THE RIB AND WEB

From the Pareto chart of Figure 8, the quadratic effect of feed rate is the third dominant and statistically significant factor with an increasing effect on average surface roughness on the rib while linear effect of feed is the fourth dominant and statistically significant factor with also an increasing effect on average surface roughness values on the web.

The marginal mean plot of Figure 9 shows that low feed of 6 ipm is the best feed rate level for reducing average surface roughness on the web while medium feed rate level of 12 ipm is the next best. High feed rate of 18 ipm is the worst level of feed rate for better surface finish on the web during slot end-milling of titanium alloy, Ti-6Al-4V.

The second plot on the third column shows that low feed rate of 6 ipm and high feed rate of 18 ipm are the best feed rate levels for reducing surface finish on the rib while medium feed rate level of 12 ipm is the worst feed rate level for a better surface finish on the rib during slot end-milling of Ti-6Al-4V.

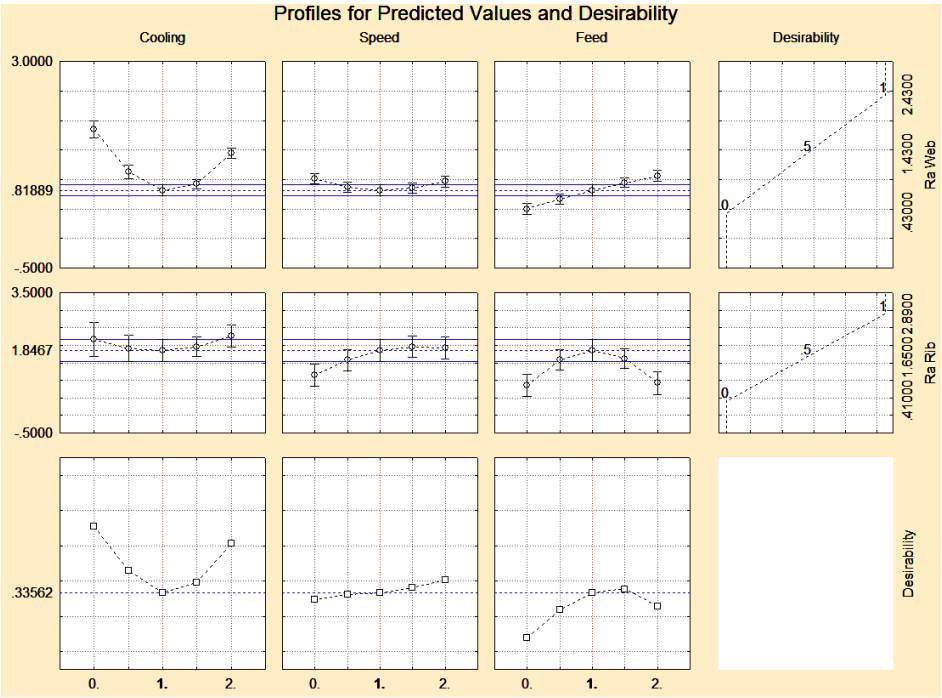

Figure 9. MARGINAL MEAN PLOT FOR AVERAGE SURFACE ROUGHNESS VALUES ON THE WEB AND THE RIB

4.1.2 COMPARATIVE EFFECTS OF OPTIMUM COOLING STRATEGIES, FEED RATE, AND SPINDLE SPEED ON SURFACE ROUGHNESS

Table 10 contains the surface roughness data obtained in our machine center using Brown and Sharpe pocket surf profilometer.

TABLE 10. SURFACE ROUGHNESS DATA FROM SLOT END-MILLING TI-6AL-4V FROM THE OPTIMAL EXPERIMENTAL CONDITIONS

Cooling Methods	Speed (RPM)	Feed (IPM)	Ra Web(µm)			Ra Average (µm)	Ra Rib (µm)			Ra Average (µm)
MQL	2000	6	2.08	2.14	2.12	2.11333	2.33	2.89	2.52	2.58
LN2	2000	6	1.04	0.67	0.84	0.85	1.23	0.88	1.83	1.313
MQL+LN2	2000	6	0.4	0.5	0.45	0.45	1.54	0.98	1.14	1.22
Emulsion@ 2000 rpm & 12 ipm	2000	12	1.09	0.88	1.07	1.0133	0.78	1.27	1.42	1.157

The table is for surface roughness values for MQL, LN_2, combination of MQL and LN_2 all at a constant spindle speed and feed rate. The fourth row contains values acquired when emulsion cooling was used at the same spindle speed as was with the MQL and LN_2 but with a feed rate of 12 ipm instead of 6 ipm. This is because fractional factorial design of experiment did not give us the opportunity to obtain an experimental run with emulsion cooling at 2000 rpm and 6 ipm therefore the need to use the closest to this.

Figure 10 shows a bar chart of the average surface roughness values measured at constant speed and feed for MQL, LN2 and the combination of LN2 and MQL. A fourth plot is with emulsion but using a feed rate of 12 ipm. Because fractional factorial design of experiment was used, this experiment does not have the experimental run of low level of cooling using high level of speed and low level of feed rate, the closest in the list of experimental run in this experimental design is low level of cooling (emulsion) at medium feed rate and high spindle speed. We have plotted this chart to compare the effects of different cooling strategies on the surface roughness values of end-milled Titanium Alloy block Ti-6Al-4V using constant cutting speed and feed rate.

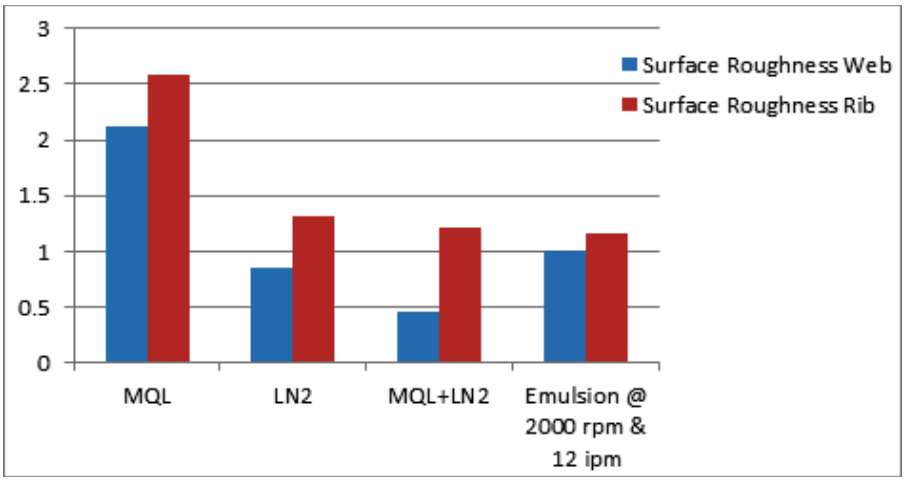

Figure 10. AVERAGE SURFACE ROUGHNESS VALUES FOR OPTIMIZED CUTTING AND COOLING CONDITIONS

The bar charts show that the combination of MQL and LN2 (MQL+LN_2) gave the best surface finish both on the web and on the rib. MQL resulted in the poorest surface finish both on the ribs and webs; next to MQL was LN_2 which resulted to a significantly low surface roughness average both on the web and on the ribs compared to MQL. From the chart, it can be seen that the value of surface roughness using LN2 on the rib is less than 1.5 µm while it's less than 1 µm on the web. On the web, average surface roughness was less than 0.5 µm. On the rib, the average surface roughness values measured is slightly lower when compared with the value from LN_2 cooling. When the average surface roughness values of the optimized cutting and cooling conditions were compared with cutting conditions of 12 ipm and 2000 rpm using emulsion cooling, the surface roughness average on the web was higher than both LN_2 and MQL+LN_2 but appeared to give a good surface finish on the rib.

Therefore it may be safe to focus attention on surface roughness on the rib for improvement on finish as the experiment has indicated that there's significant increase in surface roughness average on the rib for all conditions. This also indicates the rib as the part of the slot with possible high induced residual stresses.

4.2 RESIDUAL STRESS

The enormous impact of manufacturing processes on residual stresses of engineering materials has led to the investigation of the effects of machining parameters and cooling strategies used in this experiment on residual stresses. X-ray diffraction is used to measure residual stresses on the left ribs of slots in the direction perpendicular to the feed direction (X).

Residual stresses vary from surface to subsurface, therefore the reason for characterization of residual stresses from surface through subsurface is to identify the stress gradients generated from the effects of machining parameters and cooling strategies used. Residual stresses measurements were performed on the left ribs of all the slots end-milled with different cooling strategies and machining parameters using the set up shown in Figure 11. Optimum machining parameters and cooling strategies were identified from fractional factorial design of experiment analysis and comparative analyses were performed and presented.

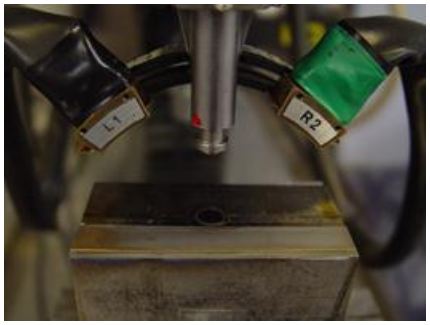

Figure 11. RESIDUAL STRESS MEASUREMENT SETUP

Table 11 shows the acquired residual stresses values used to perform analysis of variance to determine the optimum combination of cooling strategies and machining

parameters for slot end-milling of titanium alloy. This table was also used for the Pareto charts and for identifying the marginal means effects seen from the marginal mean plots.

In table 11, the table of values for residual stress measurement data for fractional design of experiment analysis is shown.

Table 11. TABLE OF VALUES FOR RESIDUAL STRESS MEASUREMENT DATA FOR FRACTIONAL DESIGN OF EXPERIMENT ANALYSIS

	Surface Residual Stress (ksi)											
	Block A											
Location	Rib 1		Rib 2		Rib 3		Rib 5		Rib 6		Rib 7	
0.25"	-39	± 1	-32	±2	-47	±2	-38	±2	-38	±2	-0	±2
0.75"	-45	± 2	-14	±2	-34	±2	-48	±2	-47	±4	-6	±1
	Surface Residual Stress (ksi)											
	Block B											
Location	Rib 1		Rib 2		Rib 3		Rib 7		Rib 8			
0.25"	-39	± 1	-32	±2	-8	±1	N/A		N/A			
0.75"	-45	± 2	-14	±2	3	±1	-3	±2	-15	±1		

Table 12 shows the parameters for the measurement set-up of the x-ray diffraction equipment used for non-destructive residual stress measurement. Before residual stress measurements were made, surface topography was first inspected using scanning electron microscope to check for cracking uniformly distribution of the deformation features. The average depth of oscillations in the surface was measured using a calibrated optical metallographic microscope.

Residual stresses and line profiles were measured at the identified locations on the left rib, and then the specimen surface was electro-polished to expose deeper layers to the X-ray beam. The entire specimen, except the region in the gauge section where electro-polishing was desired (1.8 cm^2), was masked (with Microstop) from the polishing solution as this minimized polishing time and stress relaxation due to material removal.

The electro-polishing conditions were selected so that etching of the phases was minimized.

Table 12. RESIDUAL STRESSES MEASUREMENT SETUP/PARAMETERS

Setup Parameters - Residual Stress:	
Target: Cu (Ka_{avg} 1.542 Angstroms)	Oscillation(s): Beta 5°
Target Power: 25 kV, 30 mA	Collection Time: 4 seconds x 20 exposures
Gain Material: glass	Total Collection Time: 16 minutes
Gain Power: 20 kV, 30 mA	Peak Fit: Gaussian at 85%
Filters: Ni	Two Peak Model: No
Material:Ti-6-4	LPA Correction On: Yes
X-Ray Elastic Constant: 12200 ksi	Gain Correction: P/G
Crystallographic Plane: {213}	Background Subtraction: Linear
Bragg Angle (2q): 142°	Peak Shift Method: Absolute Peak
Aperture: 2 mm Round	Psi Zero Assignment: Curve Fit Linear
Powder Correction: No	Instrument: Lab001
Autoremove Bad Points: No	Software Version: 2.0 Build 71
Psi Tilts: 22	Goniometer Configuration: Psi
Tilts: (0, ±25.00, ±19.00, ±13.55, ±7.06, ±0.90)	

4.2.1 EFFECTS OF COOLING STRATEGIES AND MACHINING PARAMETERS ON RESIDUAL STRESSES ON THE LEFT RIB OF END-MILLED SLOTS

This study presents the experimental results of the effects of machining parameters and cooling strategies on residual stresses on the left rib using fractional factorial design of experiments. ANOVA table, Pareto charts and marginal means of effects from the fractional factorial design of experiment for slot end-milling of titanium alloy Ti-6Al-4V are used for this analysis.

The ANOVA table of Table 13 presents the linear and quadratic effects of machining parameters and cooling strategies (main effects) considered in this experiment and also the linear and quadratic effects of the factors interactions. This table shows the statistically calculated linear and quadratic effects of the parameters (factors) used in this experiment.

The linear and quadratic effects of spindle speed, and feed rate are found to be the main effects that are statistically significant with P-values of 0.001075 and 0.014311 respectively. The interaction effect of cooling strategies and spindle speed is also statistically significant with a P-value of 0.004437.

Table 13. ANOVA TABLE FOR RESIDUAL STRESSES ON THE LEFT RIB OF END-MILLED SLOTS

	ANOVA; Var.:R.Stress; R-sqr=.88227; Adj:.77762 3 3-level factors, 1 Blocks, 18 Runs; MS Residual=68.16667 DV: R.Stress				
Factor	SS	df	MS	F	p
(1)Cooling L+Q	483.111	2	241.556	3.54360	0.073270
(2)Speed L+Q	2188.778	2	1094.389	16.05460	0.001075
(3)Feed L+Q	962.889	2	481.444	7.06275	0.014311
1*2	1431.444	2	715.722	10.49959	0.004437
Error	613.500	9	68.167		
Total SS	5210.944	17			

From the Pareto chart of Figure 12 the visual representation of the main effects of the different factors and their interactions effects are presented on horizontal bars with a vertical red line to mark the point of statistical significance.

The Pareto chart shows that linear effect of spindle speed is the dominant and statistically significant factor with an increasing effect on residual stresses on the rib while the linear interaction of cooling strategies and spindle speed is the next statistically significant effects. The linear interaction of spindle speed and cooling strategies has an increasing effect on residual stresses on the rib. Linear effect of feed rate and the linear effect of cooling strategies are the third and fourth dominant and statistically significant factors both with increasing effects on residual stresses.

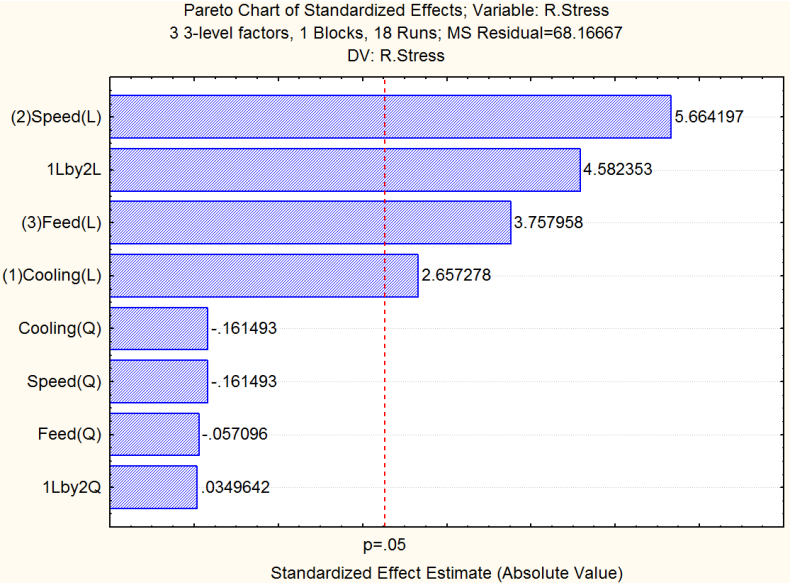

Figure 12. PARETO CHART FOR RESIDUAL STRESSES ON THE RIB

From the surface contour plot of Figure 13, the first plot shows that the combination of low spindle speed of 1000 rpm and LN_2 cooling strategy reduces residual stresses on the rib best while the combination of emulsion cooling strategy at high spindle speed of 2000 rpm is the next best combination of spindle speed and cooling strategies. The worst combination for the first plot is the use of LN_2 cooling strategy at high spindle speed of 2000 rpm, with the tendencies of producing highly tensile residual stresses during slot end-milling of Ti-6Al-4V. The second plot of Figure 13 shows that the combination of emulsion cooling at low feed rate of 6 ipm is best in producing a more compressive residual stress during slot end-milling of titanium alloy. The use of LN_2 cooling at high feed rate of 18 ipm is the worst combination of cooling strategy and feed rate for this experiment. The third plot shows that low spindle speed of 1000 rpm and low feed rate of 6 ipm is the best in producing compressive residual stresses during slot end-milling of titanium alloy. The worst combination is end-milling of titanium alloy using

2000 rpm spindle speed and 18 ipm feed rate as the plot shows there's the tendencies of high residual stresses with this spindle speed and feed rate combination.

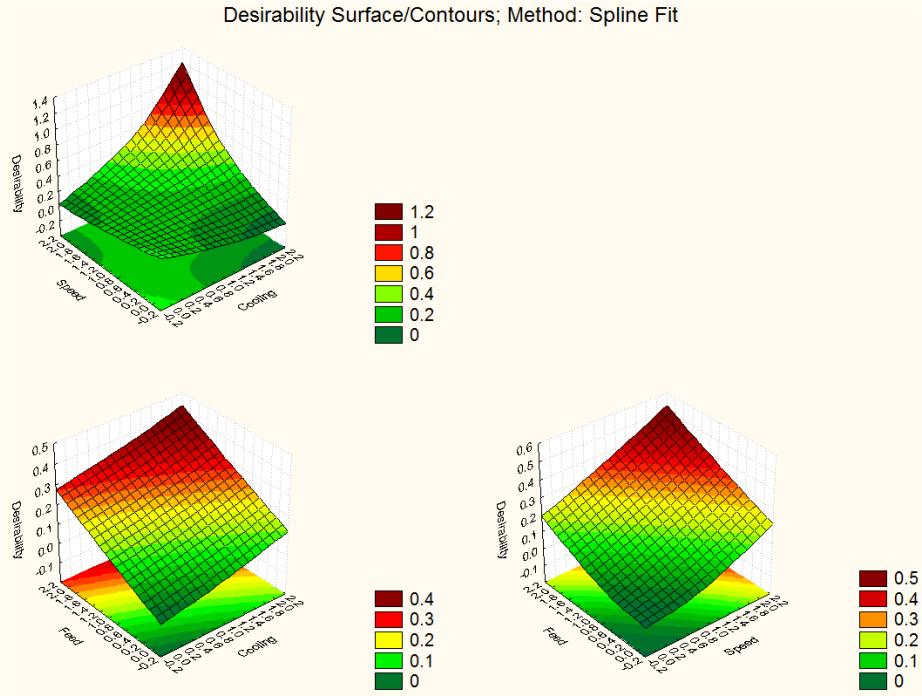

Figure 13. RESIDUAL STRESS DESIRABILITY SURFACE/CONTOUR PLOTS

4.2.1.1 EFFECTS OF COOLING STRATEGIES ON RESIDUAL STRESSES ON THE LEFT RIB OF END-MILLED SLOTS

The first plot on the first column of the marginal mean of effects plot of Figure 14 shows how cooling strategies affect residual stresses on the left rib in slot-end-milling titanium alloy block. From the plot, emulsion cooling is best in reducing residual stresses while MQL is next best.

LN_2 is the worst cooling strategy because it has the tendency of increasing tensile residual stresses on the left rib of a Ti-6Al-4V as can be seen from the high residual stresses generated.

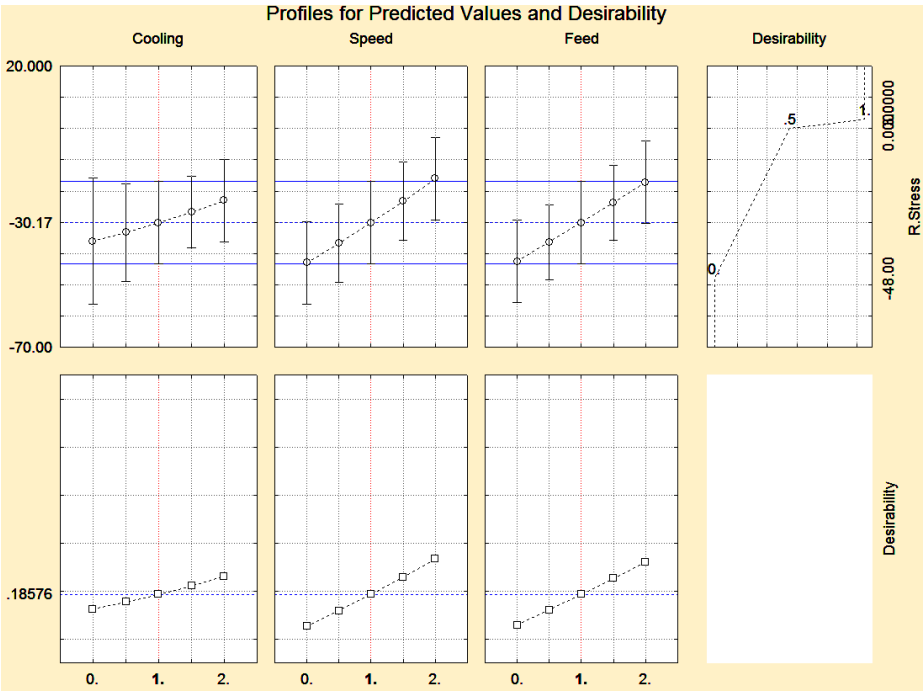

Figure 14. MARGINAL MEAN PLOT FOR RESIDUAL STRESSES ON THE RIB

4.2.1.2 EFFECTS OF SPINDLE SPEED ON RESIDUAL STRESSES ON THE LEFT RIB OF END-MILLED SLOTS

The second plot on the first row of Figure 14 shows the effects of the different levels of spindle speed on residual stresses on the left rib of end-milled slots of titanium alloy block. The plot shows that low spindle speed of 1000 rpm is the best in reducing tensile residual stresses on left ribs of the slots while medium spindle speed of 1500 rpm is the next best. The worst is high speed of 2000 rpm which gives more tensile stress than compressive.

4.2.1.3 EFFECTS OF FEED RATE ON RESIDUAL STRESSES ON THE LEFT RIB OF END-MILLED SLOTS

The third plot on the first row of Figure 14 shows the effects of the different levels of feed rate on residual stresses.

This plot shows that low feed rate of 6 ipm is the best in reducing tensile residual stresses on left ribs of the slots while medium feed rate of 12 ipm is the next. The worst is high feed rate of 18 ipm which gives more tensile stress than compressive.

4.2.2 COMPARATIVE EFFECTS OF OPTIMUM COOLING STRATEGIES, FEED RATE, AND SPINDLE SPEED ON RESIDUAL STRESSES ON THE LEFT RIB OF END-MILLED SLOTS

Figure 15 is the plots of the residual stresses measured on the left rib of end-milled titanium alloy Block B. The plot represents the values of the measurements made on the surface and subsurface of the identified points of measure.

As described earlier, rib 3 represents machining parameter of 2000 rpm spindle speed and 6 ipm feed rate and cooling strategy as LN_2 cooling while rib 7 represents end-milling process with the same machining parameter as rib 3 but with MQL as cooling strategy, rib 8 is with machining parameters as in rib 3 and 7 but with combination of LN_2 and MQL as cooling strategy. These slots are end-milled using optimum cutting parameters (spindle speed of 2000 rpm, and feed rate of 6 ipm), optimum cooling strategy (MQL and LN_2) and combination of MQL and LN_2 to a depth of 1 inch (25.4 mm). The combination of MQL and LN_2 was the best in producing the most compressive residual stresses on the surface of the left rib after slot-end-milling of titanium alloy. MQL was next best while LN_2 cooling strategy alone was the worst with high tensile residual stress on the surface of the left rib after slot end-milling of titanium alloy.

In Table 14, the table of values from comparative residual stress measurement is shown.

Table 14. TABLE OF VALUES FROM COMPARATIVE RESIDUAL STRESS MEASUREMENT

Block B - Location at 0.75" From Top						
Depth (mm)	Rib 3					
	Measured		Gradient Corrected		Grad. & Depth	
	Stress (ksi)		Stress (ksi)		Corr. Stress (ksi)	
0.000	+3	± 1	+2	± 2	+2	± 2
0.012	+3	± 1	-1	± 2	-1	± 2
0.017	+8	± 1	+2	± 1	+2	± 1
0.055	+2	± 1	+3	± 1	+3	± 1
Depth (mm)	Rib 7					
	Measured		Gradient Corrected		Grad. & Depth	
	Stress (ksi)		Stress (ksi)		Corr. Stress (ksi)	
0.000	-3	± 2	-5	± 2	-5	± 2
0.009	+2	± 2	+2	± 2	+2	± 2
0.015	-1	± 1	+2	± 2	+2	± 2
0.050	+1	± 1	+1	± 1	+1	± 1
Depth (mm)	Rib 8					
	Measured		Gradient Corrected		Grad. & Depth	
	Stress (ksi)		Stress (ksi)		Corr. Stress (ksi)	
0.000	-15	± 1	-21	± 2	-21	± 2
0.011	-3	± 1	-7	± 2	-7	± 2
0.018	+1	± 1	-1	± 1	-1	± 1
0.053	+5	± 1	+5	± 1	+5	± 1

"-" indicates compressive residual stress, “+" indicates tensile residual stress

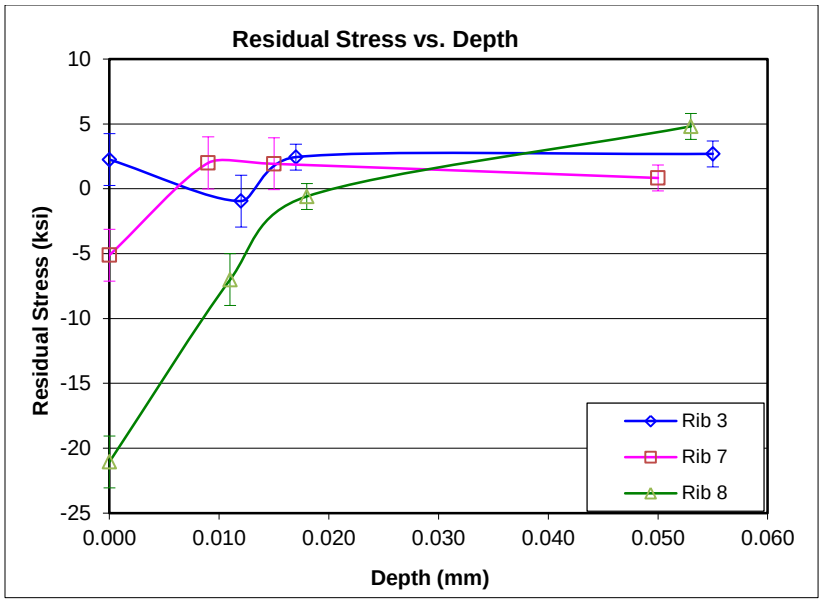

Figure 15. PLOTS OF RESIDUAL STRESSES VS. DEPTH ON THE LEFT RIB OF END-MILLED SLOTS

The plot shows that LN_2 cooling strategy at 0.012 mm depth was compressive but going down the subsurface in to the thickness of left rib of the slot, the residual stresses change from compressive to tensile and stays at approximately 2.5 ksi (17.24 MPa) till the depth of 0.055 on the subsurface. MQL cooling strategy represented by rib 7 became tensile on the subsurface as can be seen from the measurement taken at 0.009 mm depth.

The residual stress plot from 0.009 mm point to 0.050 mm point in the subsurface was a negative slope, meaning that with MQL cooling, residual stress tends towards being compressive on the subsurface.

The combination of MQL and LN_2 which was best on the surface with high compressive stress tends towards tensile on the subsurface giving 5 ksi (34.48 MPa) at 0.053 mm point in the subsurface.

5. CONCLUSION

1. Emulsion cooling which is the 0 cooling level gave the average highest surface roughness value on the web while MQL which is the mid cooling level (level 1) gave the lowest average surface roughness value on the web. LN_2 which is the highest cooling level (level 2) was the next best cooling strategy on average surface roughness value produced on the web during slot end-milling of titanium alloy, Ti-6Al-4V. On the rib, the same trend was followed with MQL preferred over LN_2 and emulsion cooling, but the differences between the average surface roughness values measured on the rib using the different cooling strategies are not much.

2. Low speed of 1000 rpm gave the highest average surface roughness values on the web while medium speed and high speed of 1500 rpm and 2000 rpm respectively are the best spindle speed levels for low surface roughness values on the web. On the rib, low speed of 1000 rpm produced the lowest average surface roughness value while medium speed and high speed of 1500 and 2000 rpm respectively are the worst for improving surface roughness on the rib.

3. Low feed rate of 6 ipm is the best feed rate level for reducing average surface roughness on the web. High feed rate of 18 ipm is the worst level of feed rate on surface finish on the web during slot end-milling of titanium alloy, Ti-6Al-4V. On the rib, low feed rate of 6 ipm and high feed rate of 18 ipm are the best feed rate levels on surface finish while medium feed rate level of 12 ipm is the worst feed rate level on surface finish on the rib during slot end-milling of Ti-6Al-4V.

4. The combination of MQL and LN2 (MQL+LN_2) gave the best surface finish both on the web and on the rib. On the web, average surface roughness was less than 0.5 µm. On the rib, the average surface roughness values measured is slightly lower when compared with the value from both MQL and LN_2 cooling strategies. Attention should be on surface roughness on the rib for improvement on the finish on this part of the slot as the experiment has indicated that there's significant increase in surface roughness average on the rib for all conditions.

5. Low speed of 1000 rpm is the best in reducing tensile residual stresses on left ribs of the slots while medium spindle speed of 1500 rpm is the next best spindle speed level. The worst is high speed of 2000 rpm which gives more tensile stress than compressive.

6. Low feed rate of 6 ipm is the best in reducing tensile residual stresses on left ribs of the slots while medium feed rate of 12 ipm is the next best feed rate level. The worst is high feed rate of 18 ipm which gives more tensile stress than compressive.

7. Low feed rate of 6 ipm is the best in reducing tensile residual stresses on left ribs of the slots while medium feed rate of 12 ipm is the next preferred feed level. The worst is high feed rate of 18 ipm which gives more tensile stress than compressive.

8. The combination of MQL and LN_2 was the best in producing the most compressive residual stresses on the surface of the left rib after slot-end-milling of titanium alloy. MQL was next best while LN_2 cooling strategy alone was the

worst with high tensile residual stress on the surface of the left rib after slot end-milling of titanium alloy.

9. All the cooling strategies were tensile in the subsurface of the left rib with MQL as the least tensile on the subsurface.

6. ACKNOWLEDGEMENTS

The financial support from the National Science Foundation (NSF) under grant no. CMMI 800871 and Intelligent Systems Center (ISC) of Missouri University of Science and Technology are gratefully acknowledged. The financial assistance provided in the form of Graduate Teaching Assistantship by the Department of Mechanical and Aerospace Engineering at Missouri University of Science and Technology is also gratefully acknowledged.

7. REFERENCES

[1] Okafor A. C, Matthews Ryan. "Effects of Machining Parameters on Workpiece Temperature and Surface Roughness in End-Milling of Hastelloy C-2000 using Design of Experiments and Response Surface Methodology" Thesis presented to Mechanical and Aerospace Engineering Department of Missouri University of Science and Technology. (2011)

[2]. Mike Lou, Joseph Chen, and Caleb Li, (1999). **"**Surface Roughness Prediction Technique for CNC End-Milling," Journal of Industrial Technology Volume 15, Number 1 pp2-6

[3]. Thamizhmnaii S., Bin Omar, Saparudin S. and Hassan S., (2008) "Surface Roughness Investigation and Hardness by Burnishing on Titanium Alloy" Journal of achievements in materials and manufacturing engineering, volume 28, Issue 2 of, pp 139-142.

[4]. Rashid Ab. and Abdul Lani M.R., (2010) "Surface Roughness Prediction for CNC Milling Process Using Artificial Neural Network." Proceedings of the World Congress on Engineering 2010 Vol III

[5]. Okafor A. and Adetona O., (1995). "Predicting quality characteristics of end-milled parts based on multi-sensor integration using neural networks: individual effects of learning parameter and rules." Journal of Intelligent Manufacturing, pp 389-400.

[6] Nagi Elmagrabi, Che Hassan, Jaharah A., F Shuaeib, (2008). "High Speed Milling of Ti-6Al-4V Using Coated Carbide Tool" European Journal of Scientific Research: pp 153-162.

[7] Zhang Julie, Joseph Chen, and Daniel Kirby, (2007). "Surface roughness optimization in end-milling operation using the taguchi design method" Journal of Material Processing Technology: pp 233-239

[8] Turnad Ginta, Nurul Amin, Mohd Radzi, Mohd Lajis, (2009). "Development of surface roughness models in end milling titanium alloy Ti6Al-4V using uncoated tungsten carbide". European Journal of Scientific Research, pp 542-551.

[9] Yang Z, Dinghua Zhang, Changfeng Yao, Junxue Ren, Xinchun Huang, (2008) National Science and Technology Planning Project 2008BAF32B10.

[10] Turnad L Ginta, A.K.M. Nurul Amin, A.N.M Karim, Anayet Patwari, M.A. Lajis, (2008) "Modeling and Optimization of Tool Life and Surface Roughness for End Milling Titanium Alloy Ti-6Al-4V Using Uncoated WC-Co Inserts" CUTSE International conference

[11] Geng G.S., Xu J.H., Ge Y.F., and Fu Y.C., (2004) "Experimental Study on the Milling of a High Strength Titanium Alloy," Material Science Forum Vols 471-472, pp 731-735.

[12] Sasahara H (2005) The effect on fatigue life of residual stress and surface hardness resulting from different cutting conditions of 0.45 %C steel. Int J Mach Tools Manuf 45:131–136

[13] Pinault J.A., Belassel M., and Brauss M.E., "X-Ray Diffraction Residual Stress Measurement in Failure Analysis" Proto Manufacturing Ltd. 485-497

[14] Schulz H, Moriwaki T (1992) High-speed machining. Annal CIRP 41:637–643

[15] Ezugwu EO (2004) High-speed machining of aero-engine alloys. J Braz Soc Mech Sci Eng XXVI:1–11

[16] Xiaohui Jiang & Beizhi Li & Jianguo Yang & XiaoYan Zuo & Kang Li "An approach for analyzing and controlling residual stress generation during high-speed circular milling" Int J Adv Manuf Technol DOI 10.1007/s00170-012-4421-8. July 2012

[17] Tugrul O¨ zel · Tsu-Kong Hsu · Erol Zeren "Effects of cutting edge geometry, workpiece hardness, feed rate and cutting speed on surface roughness and forces in finish turning of hardened AISI H13 steel" Int. J Adv Manuf. Technol. (2005) 25: 262–269

[18] Jiann-Cherng Su & Keith A. Young & Kong Ma & Shesh Srivatsa & John B. Morehouse & Steven Y. Liang "Modeling of residual stresses in milling" Int J Adv Manuf Technol (2012). DOI 10.1007/s00170-012-4211-3

SECTION
2. THESIS CONCLUSION

Cryogenic Liquid Nitrogen (LN_2) cooling, low spindle speed of 1000 rpm and high feed rate of 18 ipm are the optimum cooling strategy and machining parameter gave the lowest maximum workpiece/cutting temperature.

The cutting force component in the feed direction F_y (feed force) is more sensitive to tool wear and increases more rapidly than the other cutting force components F_x and F_z, thus this is recommended to be used for indirect monitoring of tool wear.

Cryogenic Liquid Nitrogen (LN_2) cooling, high spindle speed of 2000 rpm, and low feed rate of 6 ipm are the optimum cooling strategy and machining parameters that gave the lowest tool wear results.

Comparative evaluation of MQL, LN_2 and MQL+LN_2 cooling strategies at optimum machining parameters of 2000 rpm and 6 ipm show that combination of MQL and LN_2 gave the lowest cutting force components for the first and last passes. The combination of MQL and LN2 (MQL+LN_2) gave the best surface finish both on the web and on the rib. On the web, average surface roughness was less than 0.5 μm. On the rib, the average surface roughness values measured is slightly lower when compared with the value from both MQL and LN_2 cooling strategies. Attention should be on surface roughness on the rib for improvement on the finish on this part of the slot as the experiment has indicated that there's significant increase in surface roughness average on the rib for all conditions. Low speed of 1000 rpm is the best in reducing tensile residual stresses on left ribs of the slots while medium spindle speed of 1500 rpm is the next best

spindle speed level. The worst is high speed of 2000 rpm which gives more tensile stress than compressive.

Low feed rate of 6 ipm is the best in reducing tensile residual stresses on left ribs of the slots while medium feed rate of 12 ipm is the next best feed rate level. The worst is high feed rate of 18 ipm which gives more tensile stress than compressive.

Low feed rate of 6 ipm is the best in reducing tensile residual stresses on left ribs of the slots while medium feed rate of 12 ipm is the next preferred feed level. The worst is high feed rate of 18 ipm which gives more tensile stress than compressive.

The combination of MQL and LN_2 was the best in producing the most compressive residual stresses on the surface of the left rib after slot-end-milling of titanium alloy. MQL was next best while LN_2 cooling strategy alone was the worst with high tensile residual stress on the surface of the left rib after slot end-milling of titanium alloy.

All the cooling strategies were tensile in the subsurface of the left rib with MQL as the least tensile on the subsurface.

BIBLIOGRAPHY

PAPER
I

[1] A. Devillez, F. Schneider, S. Dominiak, D. Dudzinski, D. Larrouquere, "Cutting forces and wear in dry machining of Inconel 718 with coated carbide tools," Wear, 2007, Vol.262, pp.931-942

[2] A. Jawaid, S. Koksal, S. Sharif, "Cutting performance and wear characteristics of PVD coated and uncoated carbide tools in face milling Inconel 718 aerospace alloy," Journal of Materials Processing Technology, 2001, Vol.116, pp.2-9

[3] Raul B.Rebak, "Effects of Metallurgical Variables on the corrosion of High-Nickel Alloys," ASM Handbook, 2005, Vol.13A, pp.279

[4] Z.Y. Wang, K.P. Rajurkar, J. Fan, S. Lei, Y.C. Shin, G. Petrescu, "Hybrid machining of Inconel 718, International Journal of Machine Tools & Manufacture," 2003, Vol.43, pp.1391-1396

[5] M. Alauddin, M.A. Mazid, M.A. El Baradi, M.S.J. Hashmi, "Cutting forces in the end milling of Inconel 718," Journal of Materials Processing Technology, 1998, Vol.77, pp.153-159

[6] P.K Wright, J.G. Chow, 1982, "Deformation Characteristics of Nickel Alloys during Machining," Transaction of ASME, Journal of Engineering Materials Technology. Vol. 104, 85-93

[7] Hanasaki, S., Fujiwara, J., 1994, "Ceramic Coated Cutting Tools. Key Engineering Materials," Vol. 96, pp 197-220

[8] A. Chukwujekwu Okafor, B. Oguejiofor, 2007, "Investigating the effects of cutting parameters on temperature in high speed end-milling of thin-walled titanium structure," Proceedings of the 10th CIRP international workshop on modeling of machining operations, Regio-Calabria, Italia pp 381-388

[9] A. Chukwujekwu Okafor, S. Aramalla, 2006," Modeling of Cutting Forces in High Speed End Milling of Titanium Alloys using Finite Element Analysis and Mechanistic Model," Proceedings of the 9th CIRP international workshop on modeling of machining operations, Ljubljana Slovenia, pp.219-226

[10] A. Chukwujekwu Okafor, Development of Virtual Computer Numerical Control Machine Tools and Web-based Machining Process Simulation and Learning – NSF Annual Report Year 3, May 31, 2011

[11] Yuan S.M., Yan L.T, Liu W.D. Liu Q., "Effects of Cooling Air Temperature on Cryogenic Machining of Ti-6Al-4V Alloy," Journal of Material Processing Technology (2010)

[12] Abele E. & Frohlich B., "High Speed Milling of Titanium Alloys" Advances in Production Engineering & Management 3 (2008) 3, 131-140

[13] Turnad L Ginta, A.K.M. Nurul Amin, A.N.M Karim, Anayet Patwari, M.A. Lajis, (2008), "Modeling and Optimization of Tool Life and Surface Roughness for End Milling Titanium Alloy Ti-6Al-4V Using Uncoated WC-Co Inserts," Curtin University of Technology Science and Engineering International Conference

[14] G.S.Geng, J.H. Xu, Y.F. Ge and Y.C. Fu, (2004),"Experimental Study on the Milling of a High Strength Titanium Alloy," Material Science Forum Vols 471-472, pp 731-735

[15] Xiaoqin Wang, Xing Ai, Jun Zhao and Tiantian Li, "Experimental Investigation on Cutting Force and Tool Wear of Carbide Tools in Ti6Al4V Turning" *Key Engineering Materials Vols. 375-376 (2008) pp 231-235*

[16] S. Zhang & J. F. Li & J. Sun & F. Jiang, "Tool wear and cutting forces variation in high-speed endmilling Ti-6Al-4V alloy" *International Journal of Advanced Manufacturing Technology (2010) vol. 46 pp 69–78*

[17] Shane Hong, Irel Markus, Woo-cheol Jeong, (2001), "New Cooling Approach and Tool Life Improvement in Cryogenic Machining of Titanium Alloy Ti-6Al-4V", International Journal of Machine Tools & Manufacture, 41, pp 2245-2260

[18] Ke Ying-lin, Dong Hui-yue, Liu Gang, Zhang Ming, "Use of Nitrogen Gas in High-Speed Milling of Ti-6Al-4V," *Trans Nonferrous Met Soc China vol. 19 (2009) pp 530-534*

[19] E.O. Ezugwu, J. Bonney, Y. Yamane, "An Overview of the Machinability of Aeroengine Alloys", Journal of Material Processing 134 (2004) pp 233-253

[20] Z.Y. Wang, K.P. Rajurkar, "Cryogenic Machining of Hard-to-Cut Materials," Wear vol. 239 2000 pp168–175

[21] H.Z. Li, H. Zeng, X.Q. Chen, "An experimental study of tool wear and cutting force variation in the end milling of Inconel 718 with coated carbide inserts" Journal of Materials Processing Technology vol. 180 (2006) pp. 296–304

II

[1] Okafor A. C, Matthews Ryan. "Effects of Machining Parameters on Workpiece Temperature and Surface Roughness in End-Milling of Hastelloy C-2000 using Design of Experiments and Response Surface Methodology" Thesis presented to Mechanical and Aerospace Engineering Department of Missouri University of Science and Technology. (2011)

[2]. Mike Lou, Joseph Chen, and Caleb Li, (1999). **"**Surface Roughness Prediction Technique for CNC End-Milling," Journal of Industrial Technology Volume 15, Number 1 pp2-6

[3]. Thamizhmnaii S., Bin Omar, Saparudin S. and Hassan S., (2008) "Surface Roughness Investigation and Hardness by Burnishing on Titanium Alloy" Journal of achievements in materials and manufacturing engineering, volume 28, Issue 2 of, pp 139-142

[4]. Rashid Ab. and Abdul Lani M.R., (2010) "Surface Roughness Prediction for CNC Milling Process Using Artificial Neural Network." Proceedings of the World Congress on Engineering 2010 Vol III

[5]. Okafor A. and Adetona O., (1995). "Predicting quality characteristics of end-milled parts based on multi-sensor integration using neural networks: individual effects of learning parameter and rules." Journal of Intelligent Manufacturing, pp 389-400

[6] Nagi Elmagrabi, Che Hassan, Jaharah A., F Shuaeib, (2008). "High Speed Milling of Ti-6Al-4V Using Coated Carbide Tool" European Journal of Scientific Research: pp 153-162

[7] Zhang Julie, Joseph Chen, and Daniel Kirby, (2007). "Surface roughness optimization in end-milling operation using the taguchi design method" Journal of Material Processing Technology: pp 233-239

[8] Turnad Ginta, Nurul Amin, Mohd Radzi, Mohd Lajis, (2009). "Development of surface roughness models in end milling titanium alloy Ti6Al-4V using uncoated tungsten carbide". European Journal of Scientific Research, pp 542-551

[9] Yang Z, Dinghua Zhang, Changfeng Yao, Junxue Ren, Xinchun Huang, (2008) National Science and Technology Planning Project 2008BAF32B10

[10] Turnad L Ginta, A.K.M. Nurul Amin, A.N.M Karim, Anayet Patwari, M.A. Lajis, (2008) "Modeling and Optimization of Tool Life and Surface Roughness for End Milling Titanium Alloy Ti-6Al-4V Using Uncoated WC-Co Inserts" CUTSE International conference

[11] Geng G.S., Xu J.H., Ge Y.F., and Fu Y.C., (2004) "Experimental Study on the Milling of a High Strength Titanium Alloy," Material Science Forum Vols 471-472, pp 731-735

[12] Sasahara H (2005) The effect on fatigue life of residual stress and surface hardness resulting from different cutting conditions of 0.45 %C steel. Int J Mach Tools Manuf 45:131–136

[13] Pinault J.A., Belassel M., and Brauss M.E., "X-Ray Diffraction Residual Stress Measurement in Failure Analysis" Proto Manufacturing Ltd. 485-497

[14] Schulz H, Moriwaki T (1992) High-speed machining. Annal CIRP 41:637–643

[15] Ezugwu EO (2004) High-speed machining of aero-engine alloys. J Braz Soc Mech Sci Eng XXVI:1–11

[16] Xiaohui Jiang & Beizhi Li & Jianguo Yang & XiaoYan Zuo & Kang Li "An approach for analyzing and controlling residual stress generation during high-speed circular milling" Int J Adv Manuf Technol DOI 10.1007/s00170-012-4421-8. July 2012

[17] Tugrul O¨ zel · Tsu-Kong Hsu · Erol Zeren "Effects of cutting edge geometry, workpiece hardness, feed rate and cutting speed on surface roughness and forces in finish turning of hardened AISI H13 steel" Int. J Adv Manuf. Technol. (2005) 25: 262–269

[18] Jiann-Cherng Su & Keith A. Young & Kong Ma & Shesh Srivatsa & John B. Morehouse & Steven Y. Liang "Modeling of residual stresses in milling" Int J Adv Manuf Technol (2012). DOI 10.1007/s00170-012-4211-3

VITA

Emenike Nick Chukwuma was born in Enugu, Nigeria. He received his primary and secondary education from Federal Government College Staff School, Enugu and Federal Government College, Enugu respectively. Mr. Emenike Chukwuma received his Bachelor of Engineering degree, Honors in Mechanical and Production Engineering in 2008 from Nnamdi Azikiwe University of Nigeria, Awka. He worked as a Facilities Graduate Engineer with Chevron Nigeria Ltd from July 2009 until he joined Dr. Okafor's research team in August 2010 to pursue his Master of Science degree program in Mechanical Engineering. He was inducted into the Society of Manufacturing Engineers and American Society of Mechanical Engineers in 2011 and 2013 respectively. He held a Graduate Research Assistantship position from start to finish of his MS pursuit. He was also a Graduate Teaching Assistant in the Department of Mechanical and Aerospace Engineering of Missouri University of Science and Technology, Missouri-Rolla. He received his MS degree in Mechanical Engineering from Missouri University of Science and Technology, Missouri-Rolla in May 2013.